REPORT DOCUMENTATION PAGE

Public reporting burden for this collection of information is estimated to average 1 hour per response, including the time for reviewing instructions, searching existing data sources, gathering and maintaining the data needed, and completing and reviewing the collection of information. Send comments regarding this burden estimate or any other aspect of this collection of information, including suggestions for reducing this burden, to Washington Headquarters Services, Directorate for Information Operations and Reports, 1215 Jefferson Davis Highway, Suite 1204, Arlington, VA 22202-4302, and to the Office of Management and Budget, Paperwork Reduction Project (0704-0188), Washington, DC 20503.

1. AGENCY USE ONLY (Leave blank)	2. REPORT DATE 10 Sep 95	3. REPORT TYPE AND DATES COVERED

4. TITLE AND SUBTITLE
Aerosol Analysis With The Coastal Zone Collor Scanner (CZCS): The Australasian Region

5. FUNDING NUMBERS

6. AUTHOR(S)
Gregory Michael Giondomenica

95-113

7. PERFORMING ORGANIZATION NAME(S) AND ADDRESS(ES)
AFIT Students Attending:

Texas A&M University

8. PERFORMING ORGANIZATION REPORT NUMBER

95-113

9. SPONSORING/MONITORING AGENCY NAME(S) AND ADDRESS(ES)
DEPARTMENT OF THE AIR FORCE
AFIT/CI
2950 P STREET, BLDG 125
WRIGHT-PATTERSON AFB OH 45433-7765

10. SPONSORING/MONITORING AGENCY REPORT NUMBER

11. SUPPLEMENTARY NOTES

12a. DISTRIBUTION/AVAILABILITY STATEMENT
Approved for Public Release IAW AFR 190-1
Distribution Unlimited
BRIAN D. GAUTHIER, MSgt, USAF
Chief of Administration

12b. DISTRIBUTION CODE

13. ABSTRACT (Maximum 200 words)

19951017 159

DTIC
SELECTED
OCL 1 8 1995
B

DTIC QUALITY INSPECTED 5

14. SUBJECT TERMS			15. NUMBER OF PAGES 98
			16. PRICE CODE

17. SECURITY CLASSIFICATION OF REPORT	18. SECURITY CLASSIFICATION OF THIS PAGE	19. SECURITY CLASSIFICATION OF ABSTRACT	20. LIMITATION OF ABSTRACT

NSN 7540-01-280-5500

Standard Form 298 (Rev. 2-89)

AEROSOL ANALYSIS WITH THE COASTAL ZONE COLOR

SCANNER (CZCS): THE AUSTRALASIAN REGION

A Thesis

by

GREGORY MICHAEL GIONDOMENICA

Submitted to the Office of Graduate Studies of
Texas A&M University
in partial fulfillment of the requirements for the degree of

MASTER OF SCIENCE

August 1995

Major Subject: Meteorology

AEROSOL ANALYSIS WITH THE COASTAL ZONE COLOR

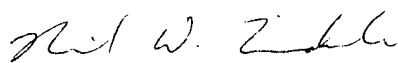# SCANNER (CZCS): THE AUSTRALASIAN REGION

A Thesis

by
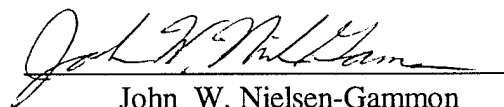
GREGORY MICHAEL GIONDOMENICA

Submitted to Texas A&M University
in partial fulfillment of the requirements
for the degree of

MASTER OF SCIENCE

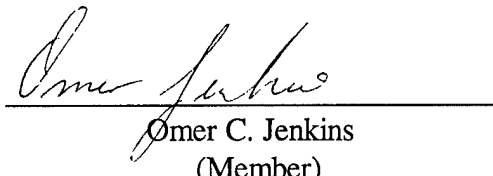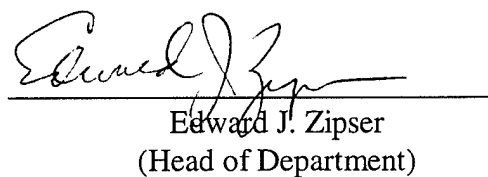Approved as to style and content by:

Neil W. Tindale	John W. Nielsen-Gammon
(Chair of Committee)	(Member)
Ømer C. Jenkins	Edward J. Zipser
(Member)	(Head of Department)

August 1995

Major Subject: Meteorology

ABSTRACT

Aerosol Analysis with the Coastal Zone Color

Scanner (CZCS): The Australasian Region. (August 1995)

Gregory Michael Giondomenica,

B.S., United States Air Force Academy; B.S., Texas A&M University

Chair of Advisory Committee: Dr. Neil W. Tindale

The Channel 4 data from the Coastal Zone Color Scanner (CZCS), a space-borne radiometer, was analyzed to infer aerosol distributions in the Australasian region for 1979.

Monthly, seasonal, and annual composites of the Channel 4 data were created. An accompanying data density image was created for each composite to indicate the degree of data coverage. Australian climatological data and 1000mb and 850mb monthly mean wind fields were used to interpret the dominant features in the composites.

Because the primary source of the measured radiances in the Channel 4 data was thought to be suspended dust, it was theorized that the dominant aerosol features would be located downwind of regions with high dust storm activity.

Elevated $670nm$ radiances were observed throughout 1979 within the portion of study region located between ~15°S and the equator. However, the wind field data and rainfall climatology did not support dust transport to this region. Although biomass burning and biogenic hydrocarbon production were likely aerosol sources, the Channel 4 data suggested that they were not likely to be the primary source for the elevated radiances in the region.

The low level wind fields and climatological data supported the feasibility of dust transport off the northwest coast of Australia over the Indian Ocean. The 1979 CZCS data indicated elevated $670nm$ radiances did occur in this region. However, the pattern of the signal suggested these radiances may not have been due to dust transport. The daily $670nm$ images indicated sun glint and faulty cloud-masking were probable sources for the observed radiances.

The fallout of dust over New Zealand and mineral-rich deposits in sea floor sediments support the established theory of aeolian dust transport over the Tasman Sea. Elevated $670nm$ radiances were observed during the 1979 summer season, corroborating the existing empirical evidence. The seasonal climatology, dust storm activity, and wind field data further supported the theory of aeolian dust transport over the region during the summer months. Furthermore, due to fewer clouds and less sun glint, the potential problems with the CZCS algorithm were also thought to be reduced.

DEDICATION

I dedicate this thesis to by beautiful wife, Brenda, and my lovely children, Kendra and Cameron. If it were not for their endless patience and understanding over the past two years, this body of work would not have been possible. I am truly grateful for their sacrifices.

I also dedicate this thesis to my parents, William and Renate Giondomenica, for their unconditional love and consistent support over the years.

ACKNOWLEDGMENTS

I acknowledge and thank the members of my committee for their input and guidance. I especially want to express my thanks to the chair of my committee, Dr. Neil Tindale, for his assistance, understanding, and inspiration. In addition, I thank Dr. John Nielsen-Gammon for his valuable insight concerning interpretation of the CZCS imagery.

I thank the United States Air Force for providing me with a golden opportunity to continue my education in the best of circumstances. I also thank Dr. Petra Stegmann for her friendship and relentless efforts in providing me with the CZCS data. Finally, I thank my fellow graduate students for their friendship and advise.

TABLE OF CONTENTS

TABLE OF CONTENTS (continued)

LIST OF FIGURES

LIST OF FIGURES (continued)

LIST OF TABLES

CHAPTER I

INTRODUCTION

Aerosols have long been the focus of scientific research, but more recently, their potentially significant role in climate change has made them a subject of hot debate (Penner *et al.*, 1994; Taylor and Penner, 1994). Due to the growth of humanity, both in numbers and technology, the anthropogenic inputs into our environment are steadily increasing. Consequently, there is growing interest in predicting the impact of these inputs on our climate. Recent developments in global climate models (GCMs) have resulted from a need to account for many chemical and physical processes which comprise the earth's evolving and complex climate. It has been determined that aerosols are important players in both the global energy budget and biogeochemical cycles (Charlson and Pilat, 1969; Weiss *et al.*, 1976; Patterson *et al*, 1980). In part, the success of GCMs hinges on resolving the relationship between aerosols and climate change. Historically, this task has been hampered by an inability to accurately characterize and quantify global aerosol distributions. Fortunately, remote sensing, specifically that from earth-orbiting satellites, provides the scientific community with the potential to accomplish just that.

The Coastal Zone Color Scanner (CZCS), a multi-spectral radiometer, was operational on the National Aeronautics and Space Administration's (NASA) Nimbus-7 platform from late 1978 through mid-1986 (Feldman *et al.*, 1989). The CZCS mission was of an exploratory nature. The goal was to test the concept of an ocean color sensor which could map the phytoplankton productivity of the world's oceans, as this information would prove valuable to marine biologists and the fishing industry alike. The CZCS had six channels: four in the visible spectrum, one in the near infrared (NIR), and the last in the infrared (IR). Aside from measuring ocean color, the CZCS Channel 4 data, largely used for atmospheric correction in the CZCS algorithms, is thought to be

---

The style is that of the *Monthly Weather Review.*

ideal for studying aerosols due to its high radiometric sensitivity and excellent calibration (Gordon and Castaño, 1989). In addition, aerosol analysis with the CZCS data set is computationally inexpensive since the desired quantity (radiance due to aerosol scattering) is calculated in the first steps of the atmospheric correction procedure within the CZCS algorithm necessary for deriving ocean color.

It has been postulated that the concentrations of aerosols in the Southern Hemisphere (SH) are less than those in the Northern Hemisphere (NH) (Patterson *et al.*, 1980). This is mainly due to there being more aerosol sources in the NH where the amount of land mass and number of population centers are considerably greater than that for the SH (Warneck, 1988). Since aerosol concentrations over land tend to be greater than those over water, many of the enhanced aerosol events which occur over water are a result of the input of continental material. Therefore, in many cases, these events can be related to the synoptic weather patterns governing tropospheric transport (Patterson *et al.*, 1980).

The immediate goal of this research is to characterize the aerosol distribution in the Australasian region. Primarily due to a combination of demographics and politics, the wealth of scientific research has focused on the NH. The existing literature, albeit sparse, suggests there are plumes of mineral-rich material in the sea floor sediments of the Tasman Sea, located between Australia and New Zealand (Glasby, 1971; Glasby, 1991). It has been hypothesized that these plumes are the result of aeolian dust transport from Australia (Healy, 1970). To date the research which corroborates this hypothesis has resulted from case studies of single events. In addition, because of the predominantly easterly wind flow off the northwest coast of Australia, elevated aerosol concentrations over this region of the Indian Ocean might be expected (Pye, 1987). The research in this study could potentially provide further support for these arguments over significantly larger temporal and spatial scales.

The secondary goal is to further investigate the use of space-borne ocean color sensors to conduct large scale aerosol analysis. While Durkee *et al.* (1991) has used the Advanced Very High Resolution Radiometer (AVHRR) data set to show space-borne

radiometry is a viable approach, the use of ocean color sensors is relatively new and is still in the developmental stages.

In this research, climatological averages of relative aerosol distributions were mapped using the CZCS data set. Together with synoptic wind fields generated from the Australian National Meteorology Research Centre (ANMRC) forecast model, an attempt was made to correlate the large scale aerosol features with the synoptic wind fields. In particular, it is hoped that the aerosol analysis over the Tasman Sea will verify the existence of aerosol plumes, corroborating the empirical evidence of mineral-rich ocean sediments and thereby further validating the use of space-borne remote sensing for aerosol analysis.

Chapter II provides background information. It includes a review of the theory and previous work involving aerosol analysis through the use of space-borne remote sensing as well as discussions of the CZCS, its atmospheric correction algorithm, and the nature of aerosol variability. The objectives of this research and the procedures used to achieve them are outlined in Chapter III. Chapter IV details the data sets used in this research: the CZCS data set and the ANMRC model output. It also addresses some of the limitations of the CZCS data set. Emphasizing wind and precipitation, Chapter V describes the pertinent features of Australian climate. Chapter VI discusses the results of this research. It describes the seasonal aerosol analyses developed from the two data sets mentioned above. Finally, a summary of the research and the conclusions which can be drawn from it are included in Chapter VII.

CHAPTER II

BACKGROUND

Until recently the vast majority of available data on global aerosol distributions have been the result of direct measurements (Abbott and Chelton, 1991). Typical means for gathering data have been stationary collection sites, ships, balloons and aircraft. In heavily populated regions and over commonly used ship routes, the volume of these measurements can be appreciable. However, over remote regions of land and ocean, data availability is often sparse, if existent at all. This is because time and expense make the use of these traditional methods of data collection prohibitive when looking at global scales. Due to its ability to cover large spatial and temporal scales, remote sensing can provide the versatility necessary for global coverage. Satellite monitoring, in particular, allows for analysis over large areas in a relatively short period of time.

The impact of aerosols on the earth's radiation budget is thought to be significant. Charlson *et al.* (1992) have estimated that regional climate forcing due to anthropogenic sulfate aerosols is -1 to -2 watts per square meter annually, a magnitude that is comparable but opposite in sign to the forcing by anthropogenic greenhouse gases. This cooling effect is primarily due to the aerosols scattering incoming solar radiation, increasing the earth's albedo. However, Charlson *et al.* (1992) concede that aerosols, unlike greenhouse gases, are short-lived in the atmosphere, meaning their effects on the radiation budget are erratic and non-uniform. Their work does not address the potential impact of non-anthropogenic aerosols. These issues complicate efforts to arrive at globally representative aerosol distributions and, in turn, inhibit a clear understanding of the impact of aerosols on our climate. This and similar work suggest further research in this area is warranted (Taylor and Penner, 1994). Simply stated by Charlson *et al.* (1992), "The large uncertainties in the magnitude and geographical distribution of aerosol forcing, much larger than those associated with greenhouse forcing, indicate the need for substantial research to improve the description of aerosol forcing."

Of the climate models which attempt to account for the effect of aerosols, most have simply incorporated some globally averaged offset due to aerosol forcing (Hansen and Lacis, 1990). While this may be sufficient when accounting for background aerosol concentrations, which are believed to be less variable, it does not satisfactorily account for the potential effects of the ever-increasing anthropogenic inputs, a very dynamic and geographically dependent source (Charlson *et al.*, 1992). Consequently, while GCMs attempt to predict the impact of humanity on our climate, representing aerosols with a forcing function effectively negates their influence on the predictive nature of the model. In other words, without the necessary physics and chemistry, a computational model's ability to forecast climate can be significantly impeded. As a result, because the complexity and variability of the influences of aerosols on our climate is great, there must be an attempt to explicitly incorporate these processes into GCMs. However, many believe we must first be able to quantify current aerosol concentrations on a global scale before we can hope to predict their long-term climatic effect (Charlson and Pilat, 1969; Patterson *et al.*, 1980; Penner *et al.*, 1994). Once this is achieved, the science community will then have an aerosol climatology at its disposal, significantly enhancing the prospect of understanding the processes by which aerosols affect the climate and, ultimately, incorporating them into GCMs.

As mentioned previously, remote sensing from space provides a promising method to achieve this. Unfortunately, because the CZCS was experimental in nature, there are limitations to the work which can be derived from its data set. On the other hand, for now, it is one of only two global tropospheric aerosol data sets available (the second being the Advanced Very High Resolution Radiometer data). While use of these data sets is unlikely to provide a complete picture of global aerosol distributions, the methods and implications which result may be used as stepping stones for future data sets which promise to be more accurate as well as extensive (Hooker *et al.*, 1993).

Theory

Much of the remote sensing done from space is passive; the instruments orbiting the

earth simply record natural signals. Over the past two decades, many passive remote sensing experiments have involved space-borne radiometers which register the earth's upwelling radiance. Scientific algorithms can then be used to interpret this information, revealing something about the physical properties of the volume being measured. Because this method involves indirect measurements, there are inherent errors that must be recognized and when possible, corrected (Abbot and Chelton, 1991). More specifically, passive remote sensing from space involves a signal originating at the earth's surface (and/or its atmosphere) which must penetrate the atmosphere before being detected at the satellite. As a result, correcting the signal for the effect of the atmosphere is often a critical step (Gordon *et al.*, 1983a; Durkee *et al.*, 1991). In the case of the CZCS, the radiance received at the satellite is a combination of the attenuated water-leaving radiance and the backscattered solar radiance resulting from the atmospheric constituents. In order to determine a true water-leaving radiance and, in turn, ocean color, the degree of attenuation must be added to the measured signal while the backscatter must be subtracted from it. Aerosol analysis, using CZCS data, has evolved from this need for atmospheric correction of the sensor's raw data.

According to Gordon *et al.* (1983a), atmospheric attenuation is largely due to scattering by aerosols and air molecules. The degree of attenuation due to absorption varies with the makeup of the atmosphere but is considered to be negligible. This is especially true for the visible spectrum in which atmospheric scattering often accounts for 80 to 90% of the upwelling signal at the top of the atmosphere. Therefore, for each of the CZCS channels, the signal received at the satellite (L) is said to be entirely due to the water-leaving radiance (L_w) and the aerosol and Rayleigh upwelling radiances, L_a and L_r respectively (Gordon and Castaño, 1989):

$$L = L_w + L_a + L_r \ . \qquad (1)$$

However, in the red portion of the spectrum (620-760nm), the ocean is essentially black, meaning it absorbs nearly all the incoming radiation. This means L_w can be assumed to be zero for the Channel 4 data, removing an unknown from Eqn (1):

$$L(670nm) = L_a(670nm) + L_r \ . \qquad (2)$$

Hence, those sensors requiring atmospheric correction typically have a channel in the red region of the visible spectrum.

Since the contribution due to Rayleigh scattering can be theoretically derived, the aerosol scattering contribution can be determined by rewriting Eqn (2) as:

$$L_a(670nm) = L(670nm) - L_r \ . \tag{3}$$

The resulting equation defines the upwelling radiance due to aerosol scattering with two known quantities, the radiance measured by the sensor and the *a priori* Rayleigh radiance.

Aerosol Analysis with the AVHRR

The National Oceanographic and Atmospheric Administration's (NOAA) Advanced Very High Resolution Radiometer (AVHRR) has been used for aerosol analysis for several years (Durkee *et al.*, 1991). The respective algorithms convert the radiance received by the AVHRR aerosol channel (Channel 1, 580-680*nm)* into an aerosol optical thickness (δ_a) and a size parameter (S_{12}). Being defined as the "sum of the extinction by aerosol particles over some path length", δ_a is representative of the concentration of aerosols in the viewed volume (Durkee *et al.*, 1986). Griggs (1975) and Durkee *et al.* (1986) showed the relationship between the upwelled radiance measured by the sensor (L) and the atmosphere's optical thickness (δ) is nearly linear:

$$L \propto \frac{\omega_o F_o}{4\cos\theta} p(\Theta)\delta \ , \tag{4}$$

where πF_o is the incoming solar radiative flux and θ is the satellite zenith angle. Note that ω_o is the single-scattering albedo which is assumed to be ~1 for aerosols, i.e. no absorption. $p(\Theta)$ is the scattering phase function where Θ is the single-scattering angle. While Eqn (4) accounts for both Rayleigh and aerosol scattering, it can be rewritten specifically for aerosols:

$$\delta_a \propto \frac{4\cos\theta}{\omega_o F_o} \frac{1}{p(\Theta)} L_a \ . \tag{5}$$

This means the aerosol optical depth can be determined from the derived aerosol radiance in Eqn (3).

However, if Eqn (5) is to represent a "nearly" linear relationship between δ_a and L_a, two basic assumptions must be made:

a) Assume a single-scattering atmosphere

b) Assume a constant aerosol size distribution.

First, due to relatively small aerosol concentrations over the ocean (compared to those over land), the AVHRR algorithm assumes a single-scattering atmosphere. According to Deschamps *et al.* (1983), this is probably an acceptable assumption when dealing with aerosol scattering but is probably inadequate for Rayleigh scattering. [This issue will be discussed later.] The second assumption concerns $p(\Theta)$. Because it is a function of aerosol size distribution, $n(r)$, analysis is only accurate on small scales in which $n(r)$ does not vary greatly. For large scale studies, an assumption must be made concerning the size distribution. Durkee *et al.* (1991) assumed a global size distribution which was developed by Griggs (1975) using Landsat 2 images off the coast of California.

The method used to determine the size parameter, S_{12}, took advantage of the AVHRR's Channel 2 which had a spectral band of $725nm$ to $1100nm$. Durkee *et al.*, (1990) suggested that the size parameter could be expressed as a simple ratio:

$$S_{12} = \frac{(L_a)_1}{(L_a)_2} , \tag{6}$$

where the subscripts refer to Channels 1 and 2. Since Eqn (6) uses aerosol upwelling radiances derived from Eqn (3), the assumption of single-scattering atmosphere applies, incorporating the associated errors into the size calculations as well.

Another potentially significant error in the AVHRR aerosol algorithm results from there being no internal calibration for Channels 1 and 2. Staylor (1990) estimated there was 3.5% degradation per year of the AVHRR sensors. Because of the lack of regular calibration information, there is no effective way to account for this error (Durkee *et al.*, 1991).

Coastal Zone Color Scanner (CZCS)

As was previously mentioned, the CZCS was an experimental instrument mounted aboard the Nimbus-7 spacecraft. Launched in October 1978, the Nimbus-7 had a sun-synchronous orbit with a nominal altitude of 955*km*. As described by Feldman *et al.* (1989), the CZCS was a six channel spectrometer used to measure the surface productivity of the world's oceans. The first three channels (443, 520, and 550*nm*), ranging from dark blue to green, were intended to spectrally classify the concentration of chlorophyll in the ocean while the fourth channel (670*nm*) was used for atmospheric correction. Channels 1-4 all had a narrow bandwidth of 20*nm*. Channel 5 (700-800*nm*) was initially designed to distinguish between organic and inorganic material in the ocean water. It was also found to be effective in performing cloud- and land-masking for all the CZCS channels. Failing early in the mission, Channel 6 was in the infrared and was intended for estimation of sea surface temperatures.

Based on comparisons with ship measurements over the Middle Atlantic Bight, Gordon *et al.* (1983a) showed the water-leaving radiance from Channels 1-4 could be calculated from the CZCS data to within 10%. This demonstrates the CZCS algorithm was able to effectively account for atmospheric correction. From this, it can be concluded that the upwelling radiance due to aerosol scattering (L_a) derived from the atmospheric correction algorithm was also accurate within these limits. Of course, the atmospheric correction algorithm was only the first step in the primary objective of the CZCS, deriving chlorophyll concentrations in the world's oceans. Because the process was significantly more complicated than that of atmospheric correction alone, the error in the final chlorophyll estimates was 30-40% (Gordon *et al.*, 1983a).

There are several design features which make the CZCS unique among earth-orbiting radiometers and deserve mention (Feldman *et al.*, 1989). One that has already been mentioned is its high spectral response. The 20*nm* bandwidth for the CZCS's aerosol channel, compared to 100*nm* for the AVHRR's, allowed for analysts to more clearly define the content of the measured volume. In essence, if the radiometric window is narrower, the degree of variability of constituents being measured is also

narrower. Furthermore, the instantaneous field of view (IFOV) was only 826m at nadir. Allowing for more detailed analyses, this resolution surpasses the AVHRR's IFOV of 1100m at nadir (Richards, 1986). Moreover, because the first five channels all used the same field stop for the incoming radiation signal, they were inherently "perfectly" coregistered. Although precise geolocation has historically been problematic for those working with satellite imagery, the fact that the CZCS channels are consistently registered should significantly reduce the associated errors. In addition, to avoid sun glint problems, the CZCS was equipped with the ability to tilt the scan viewing angle +20° from nadir. This removed one unknown from the CZCS correction algorithm's governing equation. As a result, it was possible to salvage many images which would have otherwise been saturated in the visible channels due to specular radiance from the ocean surface. Finally, where the AVHRR had no internal calibration for Channels 1 and 2, the CZCS had two internal lamps (the second being a backup) which calibrated the instrument after each scan. Unfortunately, like the AVHRR, the CZCS showed signs of degradation early in the mission due to declining intensity of the calibration lamps (Gordon *et al.*, 1983b). However, the calibration record made it possible for Gordon (1983b) to attempt to correct for the error by quantifying the lamps' degradation. As will be discussed later, the ability to correct for the lamps' degradation has been refuted by some scientists (Carder *et al.*, 1991; Simpson, 1993).

When compared to the AVHRR, the high radiometric sensitivity and continuous calibration of the CZCS provided a high degree of precision for the measured radiance counts. This is significant since the radiance backscattered by the atmosphere is approximately one order of magnitude greater than the ocean color signal (Gordon and Castaño, 1989). Although instruments like the AVHRR are suitable for aerosol analysis, Gordon and Castaño (1989) contend the CZCS has the potential to yield more representative results. In addition to the radiometric sensitivity and calibration differences mentioned above, this suggested superiority was made possible by eliminating some of the error resulting from the two assumptions in the AVHRR algorithm addressed in the previous section.

The first atmospheric correction algorithm for the CZCS also assumed an universally single-scattering atmosphere (Gordon *et al.*, 1983a). However, Deschamps *et al.* (1983) revealed while this assumption may be acceptable for aerosol scattering, it was only marginally acceptable for Rayleigh scattering. Remember, single-scattering theory was adopted due to relatively low aerosol concentrations over the ocean. No analogous statement can be made for the air molecules responsible for Rayleigh scattering. Consequently, Gordon and Castaño (1987) developed a subsequent algorithm that accounted for multiple Rayleigh scattering.

Given the spacecraft and solar zenith angles, the upwelling radiance due to Rayleigh scattering (L_r) can be theoretically derived using single-scattering radiative transfer theory together with information about atmospheric pressure and ozone concentrations. Therefore, the ability to accurately calculate L_r using single-scattering theory was limited by the accuracy of the pressure and ozone data available. Early on, a standard atmosphere and average ozone concentrations were assumed. In the most recent algorithm, data from the Total Ozone Mapping Spectrometer (TOMS), also mounted on the Nimbus-7, has been used. To date, the variation in pressure fields has been ignored, as it has been determined that the resulting error is below the sensitivity limit of the CZCS (André and Morel, 1989). Once the single-scattering Rayleigh radiance was determined, Gordon and Castaño (1989) demonstrated, for optical thickness (δ_a) $\leq$ 0.6, the L_a derived from single-scattering theory is linearly related to that derived from multiple-scattering theory. In this way, while avoiding the complexities of multiple scattering theory, the CZCS algorithm indirectly accounted for multiple-scattering effects.

Nature of Aerosol Variability

There are a multitude of processes which generate aerosols. These processes can be separated into two categories: natural sources and anthropogenic sources. According to Patterson *et al.* (1980), in the Southern Hemisphere, it is believed the natural sources far exceed the anthropogenic sources due to a relatively small number of population

centers. The natural sources can be further divided into continental inputs and marine inputs. Maritime aerosol inputs at the larger end of the size spectrum ($>1\mu$m) are not expected to be spectral (Carder, 1991). The submicron particles may exhibit a blue-rich scatter but exist in relatively smaller concentrations. Moreover, aerosol concentrations over the continents are usually significantly higher than those over the oceans (Patterson *et al.*, 1980). As a result, marine aerosols do not contribute significantly to measured radiances, meaning the aerosol signal detected by the CZCS is primarily of continental origin (Gordon, 1993). Furthermore, because the CZCS's aerosol channel has a bandwidth of 660*nm* to 680*nm* (placing it in the red end of the visible spectrum), the detected aerosols are most likely dust particles which are typically a reddish-brown color (Carder *et al.*, 1991).

The generation of dust particles is primarily dependent on two factors. First, there must be a dust source. Naturally, the availability of dust in a given region is largely dependent on the local precipitation cycle. The second requirement for generating dust aerosols is a force to lift and suspend the particle from the earth's surface. Consequently, dust particles are commonly generated in arid and semi-arid regions disrupted by the event of a wind storm (Pye, 1987). Because the top soil layer in these regions is often exposed to the atmosphere due to a lack of vegetation, low level turbulence generated by the storm can serve as a mechanism to lift loose dry soil from the surface. Additionally, it is worth noting human intervention can play a critical role in this process. Left undisturbed, the earth's surface often forms a crustal layer which may inhibit aerosol generation. In many cases, however, agricultural processes and the presence of livestock serve to break this crustal layer, thereby enhancing the likelihood of aerosol generation. These human influences may also strip the land of vegetation which otherwise serves as a natural barrier against wind erosion.

Synoptic weather patterns usually have time scales on the order of three to five days (Wallace and Hobbs, 1977). On the other hand, the high surface winds often associated with dust storms may only last for several hours during this period. The elevated aerosol concentrations resulting from dust generation during a storm will typically peak

during these high winds. In spite of this, due to the longevity of the weather system after the 'dust storm', a transport mechanism exists which may carry the dust for several days, resulting in a 'dust event' (Healy, 1970). Naturally, due to atmospheric turbulence and diffusion, the cloud of dust particles will gradually disperse as the dust event ages (Houghton, 1985).

Once the dust is suspended in the atmosphere, there are two primary removal processes: settling due to gravity and removal due to precipitation (Houghton, 1985). Settling is largely dependent on the size distribution of the aerosols. Naturally, the larger particles are expected to fall out first. The size distribution of particles resulting from a dust storm is mainly a function of the degree of turbulence generated at the surface, i.e. the higher the wind speed, the larger the size distribution. If settling were the only removal mechanism, one would expect to find an aerosol plume downwind of a dust storm which gradually decreases in both size and concentration with distance from the source.

On the other hand, in the event of significant rain, a dust event is swiftly terminated within the regions of rainfall. This results from two separate mechanisms: nucleation and diffusion processes within clouds as well as scavenging by falling raindrops (Rogers and Yau, 1976). First, aerosol particles greater than $0.1\mu m$ may serve as cloud condensation nuclei (CCN). When conditions in the cloud sufficiently promote droplet growth, these cloud droplets may coalesce by diffusion and eventually form a raindrop, effectively removing the CCN. Naturally, not all CCN are removed from the atmosphere as many clouds form and dissipate without producing rain. Second, the scavenging effect of the falling water droplet will remove nearly all suspended dust particles in its path. While smaller aerosols may be swept around the falling drop, the inertia of a typical dust particle is large enough to prevent it from escaping the collision. Although the nucleation process may potentially remove a single aerosol, a raindrop consists of many cloud droplets and can be responsible for scavenging a large number of aerosols on its descent to the earth's surface.

Thus, it has been established that the production and transport of dust particles is largely dependent on two climatic factors: low level wind and precipitation. From this, the concept of a dust event and its longevity is particularly important when doing aerosol analysis. When focusing on possible transport mechanisms within the atmosphere or wishing to explain oceanic sediment cores through aeolian transport, the extreme dust events which usually leave a clear signature are of particular interest. However, when determining the impact of global aerosol concentrations on the earth's radiation budget, these extreme events become less important. In this case, it is the daily average concentrations which would most likely better represent the global impact of aerosols. And finally, for the sparse CZCS data set, this issue of longevity is critical. There is a significant possibility that individual dust events were not recorded which would bias the composite towards low values. Conversely, extreme events may have been recorded in regions with low data coverage biasing the composites towards high values.

CHAPTER III

OBJECTIVES AND PROCEDURES

The primary goal of this research is to characterize the aerosol distribution in the Australasian region. The secondary goal is to further investigate the feasibility of using space-borne ocean color sensors to conduct large scale aerosol analysis. To achieve these goals, there are four specific objectives which must be met. Below is a list of the objectives followed by the procedures necessary for their completion:

Objective (a): Archive the entire CZCS data set for the Australasian region.

The data was retrieved via electronic transfer from the University of Rhode Island. Although only the aerosol data was used in this research, three types of images were collected: aerosol, chlorophyll, and cloud/land images. Although the entire seven year CZCS data set is available, the analysis in this research will only include the period between November 1978 and December 1979, which accounts for 4668 images or 1.25 Gb of data.

Objective (b): Composite the Channel 4 data creating monthly, seasonal and annual averages.

The composites were created on a Silicon Graphics platform using the Interactive Data Language (IDL®) software. Monthly composites were first created for the months November 1978 through December 1979. The seasonal and annual composites were then created from these monthly composites.

Fundamentally, the monthly composites were simply averages of all the CZCS Channel 4 images which occurred within the target month. Because most of the 262,144 pixels for any given image were null data points, it was necessary to flag these pixel locations and not include them in the averaging process. Obviously, failing to do this would result in averages biased towards the low end of the spectrum. After creating the composite, the image was mapped as a Mercator projection. In this process, the mapped images were converted to 640x512 grids. IDL® was used to warp

the pixel size of the original 512x512 data grid. Avoiding the need for interpolation, this procedure stretches the pixels in the original 512x512 grid to fit within the larger 640x512 grid. The result was then saved as an IEEE format file in order that it may be viewed with Spyglass® Transform. After adjusting the color table and generating an appropriately scaled legend for the composite image with Spyglass® Transform, the image was captured and edited for final output using Showcase.

Objective (c): Discuss the representativeness of these composites based on the degree of regional coverage the data provides.

Due to the experimental nature of the CZCS mission, it is important to outline the representativeness of the data set. A general discussion of limitations of the data is included in Chapter III. The specific impacts of these limitations on this research is addressed in Chapter VI.

As part of the study of the limitations of the CZCS data, an attempt was made to graphically represent the degree of data coverage. For each composite image, an accompanying 512x512 array was created using IDL®. The new array contains the number of data points averaged for each pixel providing an indication of the density of the sampling for any given location. In other words, these images highlight the areas which are relatively well represented and those which are not. The data density images were then mapped and edited similar to the aerosol images.

Objective (d): Look for trends in the Channel 4 data which may be explained by Australasian synoptic climatology.

For those regions with adequate temporal and spatial coverage by the CZCS, the composites were analyzed for predominant aerosol features. These features were then correlated with the synoptic meteorology of this region. The wind charts were derived from the ANMRC data using GrADS (Gridded Analysis and Display System). The average monthly low level wind field was computed using 1000mb and 850mb levels. From this, wind vector and streamline plots were created for the months November

1978 through December 1979. Annual and seasonal plots were created in the same manner.

The resulting plots mirrored the aerosol composites in time and space. This provided a convenient way to compare and contrast the observed aerosol distributions with the low level wind climatology for the region. Note the climatology is based on model forecast analysis and not actual observations. This approach was used because the meteorological observation network in Australia and over the Southern Ocean is arguably insufficient to create meaningful wind charts based on observations alone.

CHAPTER IV

DATA

CZCS Data Set

During its life span, the CZCS acquired nearly 66,000 images, some covering up to 2 million square kilometers (Feldman *et al.*, 1989). The radiance counts for each of the six channels were calibrated and digitized with eight bit resolution. This Level 1 data has approximately 1-*km* resolution (.826*km*) and is earth-gridded as a Mercator projection. The University of Miami developed Level 2 data which has been corrected for atmospheric attenuation (Gordon and Castaño, 1987). This is a condensed form of Level 1 data with about a 4-*km* resolution. Although Level 3 data, which contains daily, monthly and annual composites, is available, it is limited to selective regions and times and has a 20-*km* resolution.

This research will make use of Level 2 data. Having been corrected for Rayleigh multiple-scattering effects, the Channel 4 data (660-680*nm*) is considered to be a good measure of aerosols (Gordon and Castaño, 1989). The entire data set consists of all the images in the Australasian region of interest from the complete seven and a half year life span of the CZCS. However, due to the degradation problems with the CZCS mentioned earlier, the analysis in this research is limited to the first fourteen months of data (November 1978 - December 1979). The study region is contained within a box which is approximately bordered by 90° East, 150° West, 75° South, and the equator. This equates to approximately 85 million square kilometers or roughly a third of the Southern Hemisphere. A map of the study region is included in Figure 1.

A typical CZCS image is the result of a two minute earth scan and has been masked for both clouds and land (Feldman *et al.*, 1989). Each file is the result of an individual image (Figure 2). The actual image data is preceded by three lines (1536 bytes) of header which includes information like the image type, the time of the scan, and the location and scan angle of the satellite. The header is followed by a 512x512 grid of unitless values ranging from 0 to 255. The values are a measure of the relative
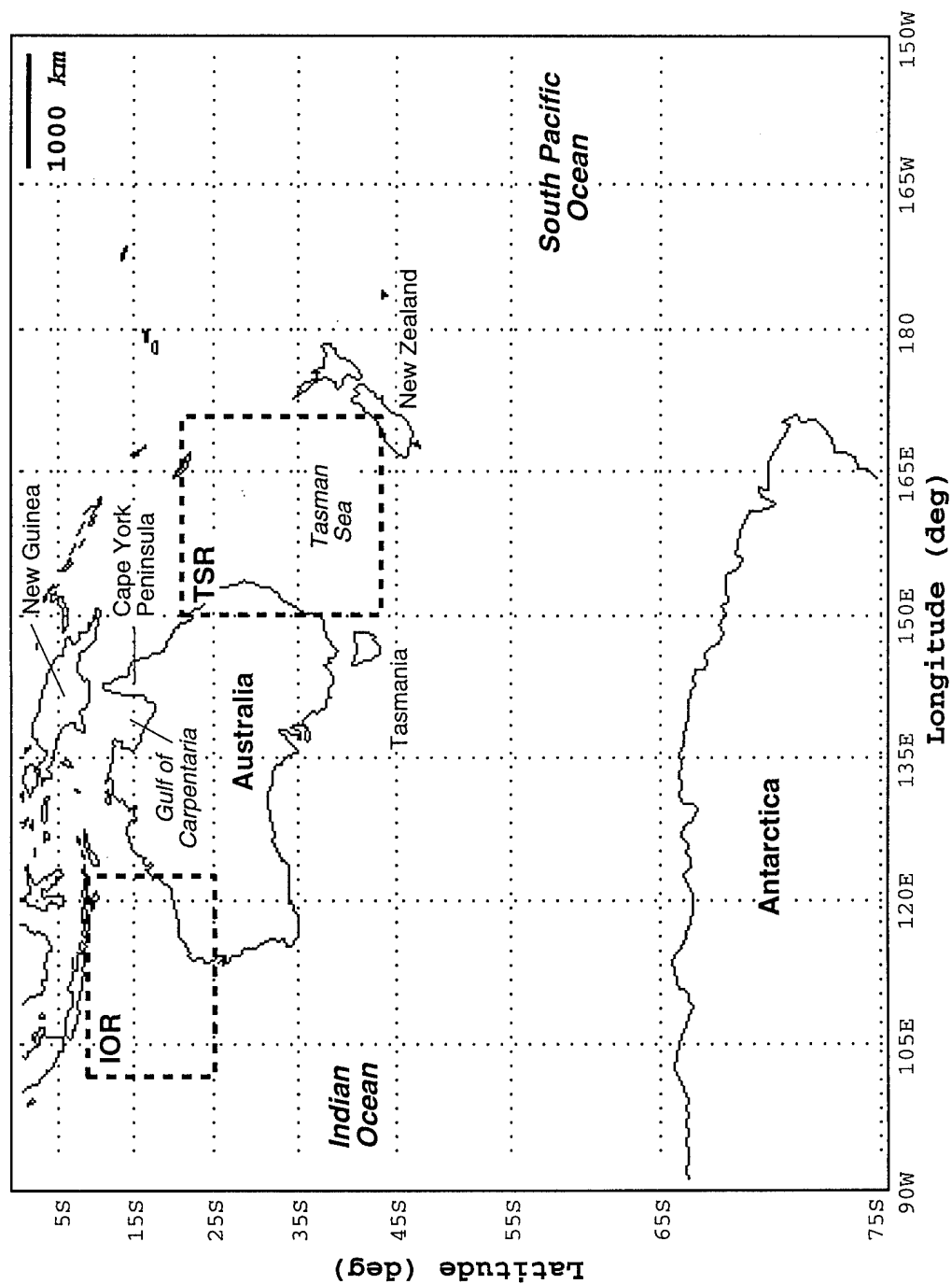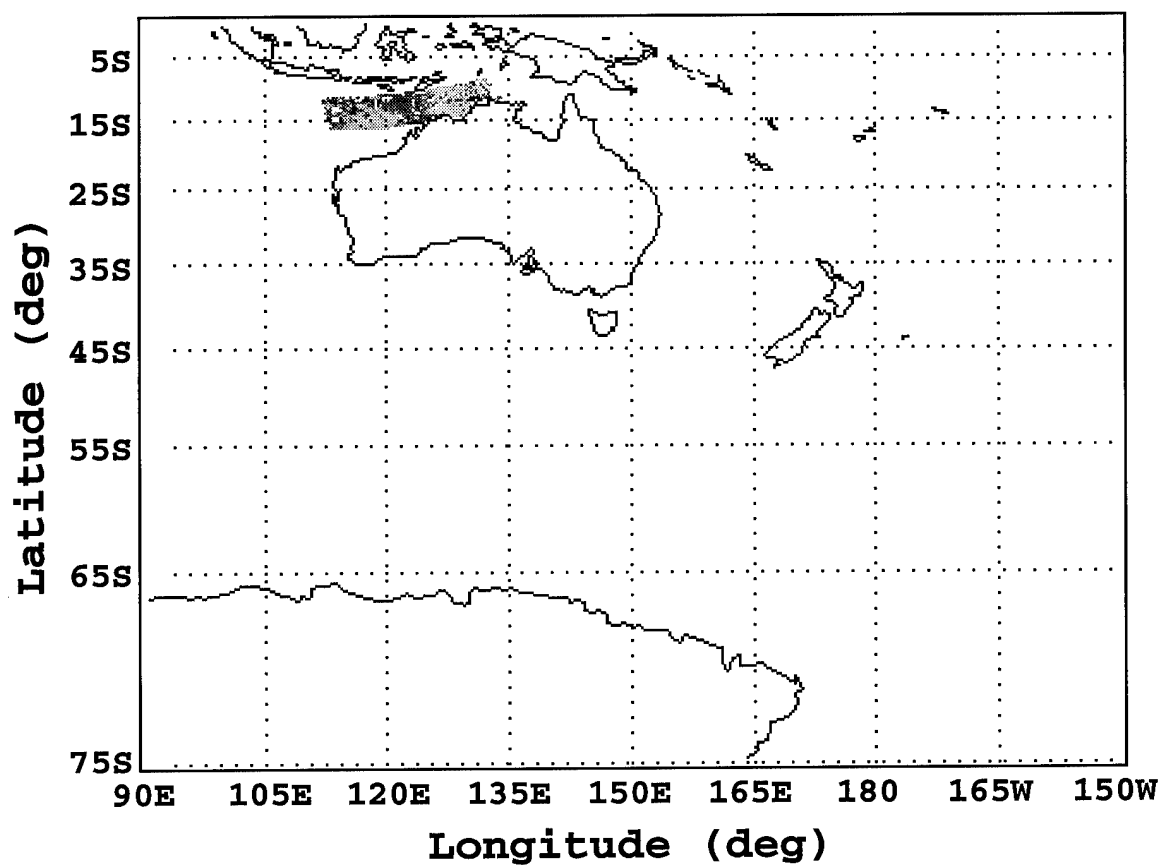
Figure 1. Map of the study region. The boxed areas are particular regions of interest which will be addressed in Chapter VI. They are the Indian Ocean Region (IOR) and the Tasman Sea Region (TSR) as labeled.

CZCS Aerosol Image
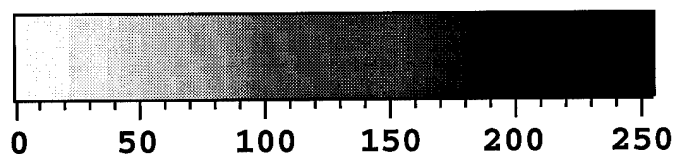## (5Nov79)

Corrected 670nm Radiance
(unitless)

Figure 2. Example CZCS image. This image was the result of a single scan taken November 5, 1979. Derived from the CZCS Channel 4 data, the values represent relative aerosol distributions.

distribution of aerosols which scatter light with wavelengths between 660*nm* and 680*nm*. Because the spectral properties of various aerosol types can differ significantly and due to the lack of *in situ* measurements during the CZCS's operation, it is difficult to infer physical characteristics of the sampled aerosols.

In order to simplify the compositing process, the satellite image (the swath of data north of Australia in Figure 2) has been remapped within the study region. Of the 262,144 pixels in each grid, there are typically only a few hundred data values. As a result, the vast majority of the array elements are zero. These zero values mean one of three things:

1) The pixel was not part of the scanned swath and therefore was not measured by the sensor. As mentioned above, this often accounted for > 99% of the total grid points.

2) The pixel was over land and therefore eliminated. Although there was a small degree of error due to geolocation problems, this remained fairly consistent for all the images.

3) The pixel was masked for clouds and therefore eliminated. This varied with the location and season.

The CZCS data in its raw form is a National Aeronautics Space Administration (NASA) product. The Level 2 data, a product of the University of Miami, used in this research was received from the CZCS archive at the University of Rhode Island.

Limitations of the CZCS Data

When attempting to create an aerosol climatology as in this research, the most significant problem with the CZCS data set stems from its lack of continuity. This is evident in Figure 3 which shows the Channel 4 data availability for 1979. The Nimbus-7 mission was purely experimental, and there was only a limited power supply on board the satellite platform. As a result, the CZCS was only allotted an average of two hours of scanning time per day (Feldman *et al.*, 1989). Naturally, this lack of coverage can pose a problem when attempting to do a study on large temporal and spatial scales.
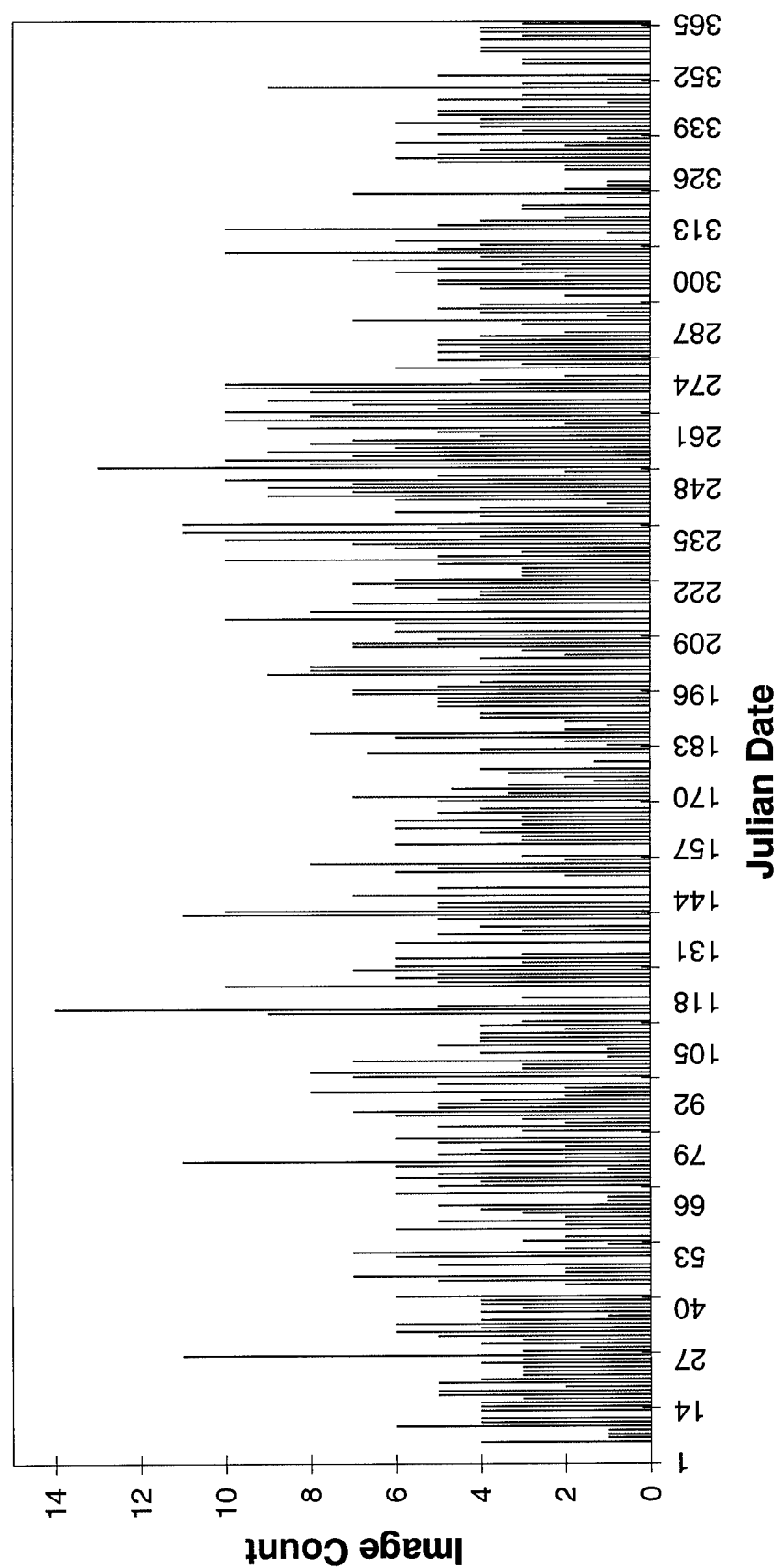
Figure 3. Daily image count for 1979.

Carder *et al.* (1991) successfully used the CZCS imagery to track a major influx of Saharan dust across the Florida coast on 27-29 July 1980. They developed a *two-component* algorithm which calculated chlorophyll concentrations to within 6% of observed values which was considerably more accurate than the 30-40% error estimated for the algorithm used to process the CZCS Type 2 data. Carder *et al.* (1991) used the term *two-component* to describe their algorithm and refer to the algorithm developed by Gordon *et al.* (1983a) as the *single-component* algorithm. [This should not be confused with "single-scattering" theory mentioned in Chapter II.] In their 1991 paper, Carder *et al.* contend there are two significant limitations to the CZCS data set:

1) Due to the *single-component* atmospheric correction algorithm, the CZCS data is best suited for analyzing regions of the atmosphere dominated by a single aerosol type.

2) Due to the CZCS's degradation with time, only the first couple of years of data is thought to be accurate to the degree mentioned above.

From Eqn (3), the Channel 4 wavelengths (660-680nm) were used to derive L_a which limits the aerosols represented to those scattering in this portion of the visible spectrum. Therefore, while the narrow bandwidth allows analysts to more clearly define the components being measured, it also can be a limiting factor if other channels are not used to account for the aerosol components which do not scatter within the given bandwidth.

Due to this perceived limitation with the *single-component* atmospheric correction algorithm, Carder *et al.* (1991) developed a *two-component* algorithm which allowed them to simultaneously correct for Saharan dust and bluish haze. The Saharan dust contained rather large particles (4-8 μm) which absorb strongly in the blue spectrum resulting in a reddish-brown color. The bluish haze, however, is a maritime haze which usually occurs near land. These aerosols are generally submicron and exhibit blue-rich scatter. The *two-component* algorithm made use of all the CZCS channels in the visible

spectrum (Channels 1-4), therefore, allowing it to detect aerosols in the blue end of the spectrum as well as in the red. Carder *et al.* (1991) conclude that "the chlorophyll fields appeared confounded in imagery derived using single-component methods when multiple aerosol types were present, but no confounding was observed for imagery generated by the *two-component* method."

Ideally, when using remote sensing to monitor global aerosol distributions, the sensors would be capable of detecting *all* the aerosol types one might find in the earth's atmosphere. Unfortunately, this is a complex issue since there is a trade-off. Accounting for more of the potential aerosol types can also lead to measuring radiances which are from non-aerosol sources. The solution will most likely be a combination of more sensor channels with greater precision and highly advanced algorithms which, together, will create a more accurate and complete picture of sampled aerosol distributions (Hooker *et al.*, 1993).

However, because Carder *et al.* (1991) were dealing with a single event confined to a relatively small area of the globe, they were afforded two circumstances often not available to those doing studies on larger temporal and spatial scales. The first is, given the discontinuity of the CZCS data set, they were fortunate to have a series of CZCS images which were coincident with the Saharan dust event. The second is they were able to develop an algorithm for a specific situation where the aerosol types were known. Understandably, it is often simpler to develop an algorithm which is tailored for a specific event. Since Carder *et* al. (1991) do not reference further validation of their *two-component* algorithm, it is not certain that these impressive results (6% error) would hold true over larger temporal and spatial scales.

With regard to the second limitation outlined in Carder *et al.* (1991), they question the effectiveness of the modification Gordon (1983b) implemented in the atmospheric correction algorithm due to the degradation of the calibration lamps. Because there was no rigorous way to quantify the degree of the lamp degradation, the corrections made for the resulting calibration errors can not be scientifically substantiated. For this reason, many CZCS researchers have opted to limit their focus to the first couple years

of the sensor's operation, prior to the deterioration of the calibration lamp (Simpson, 1993). This precautionary step was adopted for this research as well.

Given the calibration drift is a systematic error and this study only involves relative aerosol distributions, it could be argued that the specific study period selected is irrelevent. However, there are two primary reasons the 1979 CZCS data was chosen for this research. Firstly, since the calibration drift increased as the sensor aged and there is doubt as to whether this increase has been effectively quantified, the degree of potential error is statistically reduced by selecting a study period early in the CZCS's lifespan. Secondly, the CZCS was most active during 1979 (Feldman *et al.*, 1989). Because the focus of this research relies heavily on the use of aerosol composites, it is advantageous to select the year with the largest data set.

Related to the CZCS calibration problems, there was a lack of *in situ* measurements which are critical for effective validation of remote sensing instruments. In addition to validating the CZCS algorithm output, the *in situ* measurements are necessary for determining *specific* aerosol concentrations and size distributions. In Chapter II, the necessity of assuming a constant aerosol size distribution in the AVHRR atmospheric correction algorithm was established. Again, when doing large scale analysis, this is clearly not acceptable due to the variability of $n(r)$ which often occurs on small spatial scales (Patterson *et al.*, 1980). This seemingly circular logic is an important point. Simply put, it states that in order to learn something about the aerosol size distribution using CZCS data, a "reasonable" estimate of the average size distribution in the region of question must be known in advance (Gordon and Castaño, 1987). Therefore, due to the lack of *in situ* measurements, the focus of this research is limited to *relative* aerosol distributions.

ANMRC Model Output

The Australian National Meteorological Research Centre (ANMRC) maintains a grid model for forecast purposes. The model generates 12hr and 24hr forecast analyses providing the 11Z and 23Z wind analysis at 8 levels: 1000mb, 850mb, 700mb, 500mb,

300mb, 250mb, 200mb, and 100mb. The actual data in this research consists of a single file of 288 records which span the entire lifetime of the CZCS (November 1978-June 1986). Each record is a 47x47 grid of the monthly averaged horizontal wind components at a given level. A subset of the data was used (a 25x14 grid) which overlaps the region of interest used for the CZCS data set. The u and v wind components are maintained as separate records and have the units of knots. The data was provided by the National Center for Atmospheric Research (NCAR) which archives the ANMRC model output.

In this research, the low level wind field was calculated by an averaging the ANMRC 1000mb and 850mb wind fields. According to Gordon and Castaño (1989), approximately 90% of aerosols are confined to the first *2km* of the atmosphere, meaning the primary transport mechanism would be the low level winds. For a standard atmosphere, the ocean surface can be approximated by the 1000mb level while the 850mb level equates to an altitude of ~*1.5km*.

CHAPTER V

AUSTRALIAN CLIMATE

The Australian continent has a latitudinal span from ~10°S to ~40°S. Its climate can be roughly characterized by two distinct air mass types, tropical air masses which commonly extend north of 25°S and subtropical air masses which commonly extend south of 25°S. In this research, these divisions will be referred to as northern Australia and southern Australia respectively. Naturally, Australia's climate is much more complex and dynamic than this simplified two-tiered system. However, because this research is a synoptic scale study and the smallest temporal scale used for the aerosol analysis is monthly, an overview of the general circulation as well as the seasonal precipitation patterns should suffice.

The climatic discussion which follows was taken from the *World Survey of Climatology, Volume 13: Climates of Australia and New Zealand* (Gentilli *et al.*, 1971).

General Circulation in the Australasian Region

Differential heating, due to the earth-axis tilt and land-water contrasts, causes the jet stream to meander as well as zonally migrate. The radiation budget can differ significantly with latitude due to the earth's tilt as it orbits the sun. In short, in the Austral winter (June-August), the south pole tilts away from the sun which shortens the earth day and minimizes the amount of solar radiation reaching the surface. In contrast, during the Austral summer (December-February), the south pole tilts toward the sun maximizing the solar day. Thereupon, cool air masses migrate equatorward during the winter months and poleward during the summer months. Similarly, the jet stream (located in the region of highest temperature gradient between warm and cool air masses) migrates zonally with the seasons.

There are significant differences between general circulation in the Northern Hemisphere (NH) and the Southern Hemisphere (SH). These differences are primarily

due to the relative lack of land in the SH as compared to the NH. Since surface temperatures tend to be less variable over the ocean than over land, the jet stream migration in the SH is not as dramatic. Unlike the NH, there is almost always a clear distinction between the subtropical and polar jets. Due to the intense temperature gradient at ~50°S resulting from the polar ice cap, the polar jet rarely approaches Australia but instead remains over the southern oceans and Antarctica year round. The tropical easterlies to the north and the subtropical jet to the south are, therefore, the main drivers of weather patterns over Australia.

Northern Australia

As mentioned previously, northern Australia is significantly influenced by the tropics. The prevailing easterlies associated with the lower levels in the tropics are also evident. These winds, often referred to as the trade winds, are more or less southeasterly and very constant. In addition, the incoming solar radiation in the tropics is relatively constant compared to that at the mid-latitudes. As a result, the annual and diurnal temperature extremes in the tropics are moderated significantly. With this is in mind, it follows that tropical regions usually do not experience the four seasons as they occur in the mid-latitudes. More often, there are just two seasons: wet and dry.

In the summer months, northern Australia's easterly flow pattern is disrupted by a low pressure system which dominates the northwest quadrant of the continent (Figure 4). This flow regime marks the onset of the monsoon season, a period during which, at the lowest levels, the prevailing easterlies shift direction and become westerly. Unlike the sporadic tropical cyclones which occasionally result in rainfall over northern Australia, this low pressure system is associated with spells of heavy rain which may persist for several days. These monsoonal rains, which commonly occur between November and March, account for most of the precipitation which falls in the summer months in northern Australia.

During the winter months, the low level wind pattern over northern Australia is dominated by the trade winds (Figure 5). The air masses transported by these easterlies

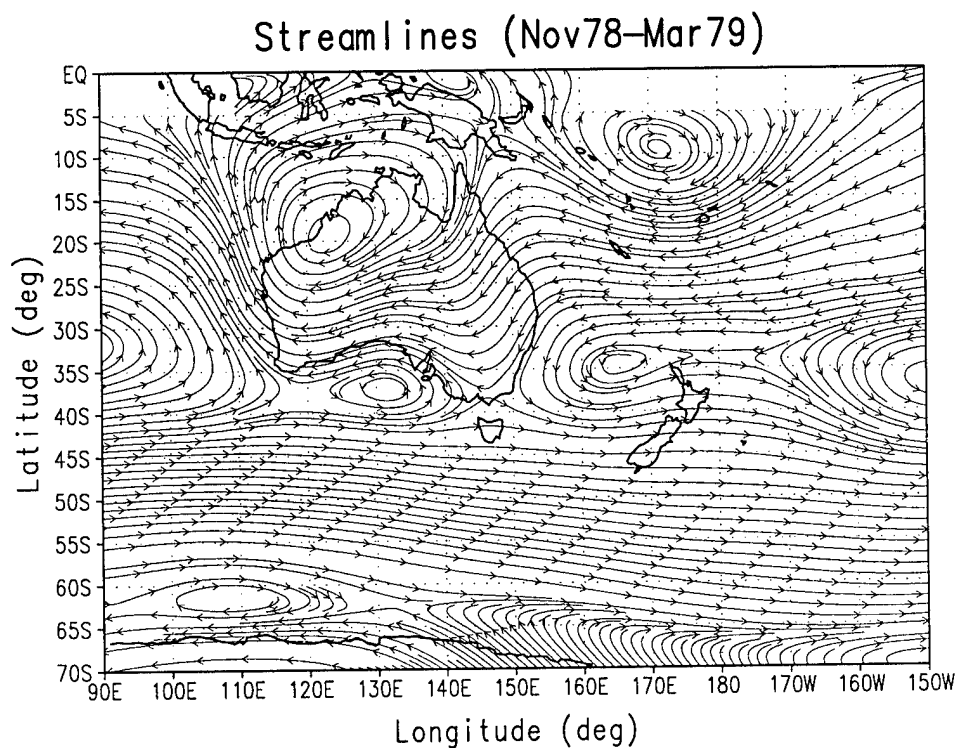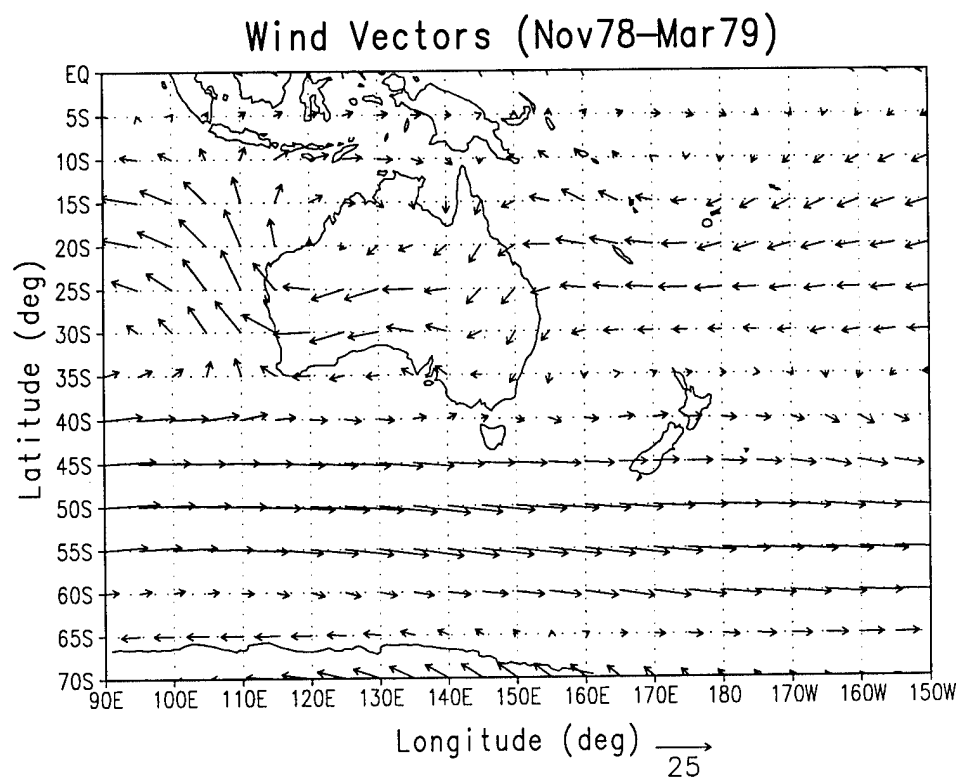## Wind Vectors (Nov78–Mar79)

Streamlines (Nov78–Mar79)

Figure 4. Low level mean wind field for the 1978/79 Austral summer (2 Season). Plots were derived from the ANMRC 1000mb and 850mb grid analysis data for November 1978 – March 1979.

are relatively stable apart from infrequent rains due to tropical cyclones descending from the equator. The northeast coast of Australia also experiences orographic rains induced by the trade winds. Nonetheless, these rain events normally do not produce significant rainfall, and the more stable winter months in northern Australia are relatively dry.

Southern Australia

Although the core of the polar jet stays well south of Australia, significant depressions in the jet can create southerly flow patterns which occasionally carry frontal systems over southern Australia in the winter months. These air masses are unique as they usually originate in the mid-latitudes and travel for thousands of kilometers across the Southern Ocean without continental influences. Being maritime air masses, they are often moisture-rich with relative humidities commonly between 70 and 80%. Although these systems can produce copious amounts of rain, their occurrences are infrequent and only account for a fraction of the rain in southern Australia.

Although its intensity may vary, the subtropical jet is a consistent feature over Australia. Its shape is primarily due to the anticyclones which cyclically cross Australia throughout the year. A belt of high pressure (commonly found between 25°S and 35°S) results from descending air on the poleward side of the Hadley Cell. This belt of high pressure is subdivided by a series of anticyclones which usually form in the tropics of the Indian Ocean (Wallace and Hobbs, 1977). These high pressure systems are clearly depicted in Figures 4 and 5. Although these anticyclones are located further north in the summer months and appear to be more organized, they do occur year round. It is important to remember these figures are annual averages. Therefore, unlike the monsoon low which is a relatively stationary feature in the summer months, the anticyclones are not stationary but instead constantly track eastward across the southern portion of the continent. The relatively consistent and stable northern component of these anticyclones energizes the tropical easterlies. In contrast, the southern component is associated with westerlies which are erratic and often unstable.

Wind Vectors (May79–Sep79)
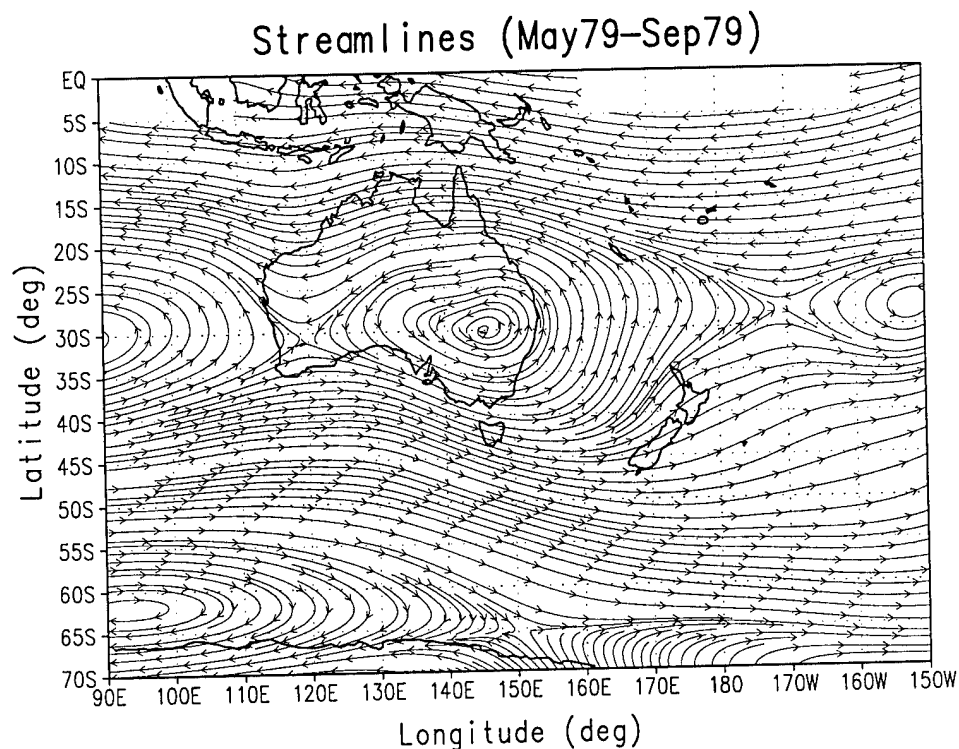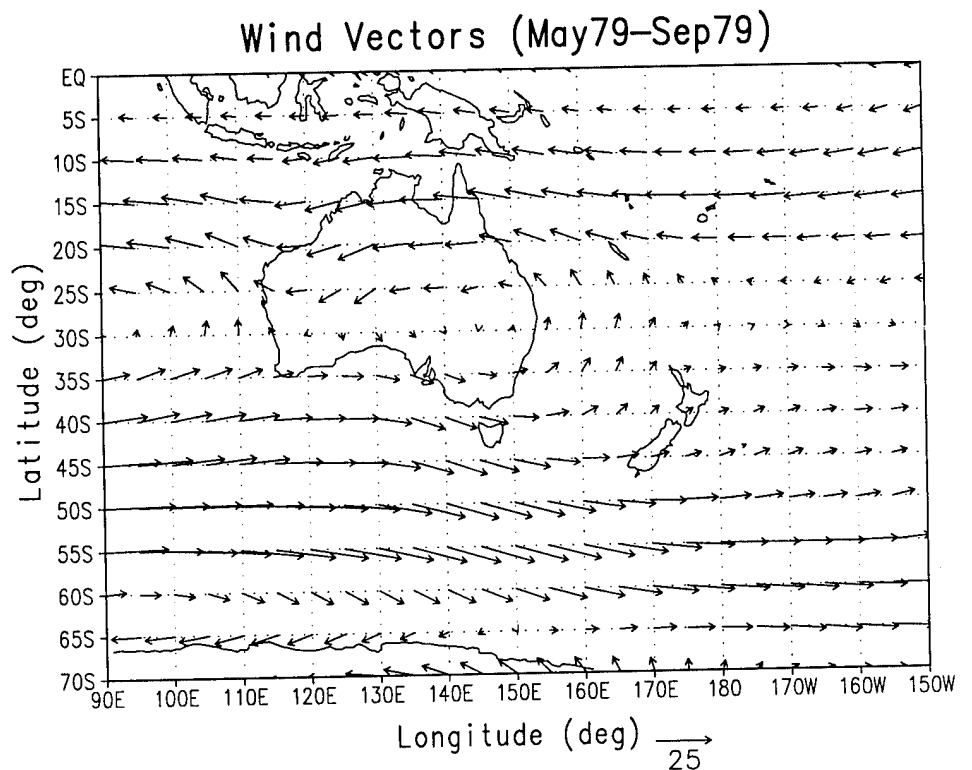

Streamlines (May79–Sep79)

Figure 5. Low level mean wind field for the 1979 Austral winter (2 Season). Plots were derived from the ANMRC 1000mb and 850mb grid analysis data for May 1979 – September 1979.

The subtropical jet often meanders equatorward between these anticyclonic systems. The resulting pressure trough is significantly smaller than the anticyclonic pressure systems by which it is bounded. Yet, it may impact Australian weather in one of two ways. First, in the summer, the trough advects air from the interior of the continent southwards, typically injecting hot dry air into southern Australia. Second, in the winter, the trough often creates an upper air depression which has been coined as an "inter-anticyclonic front". These fronts can bring significant amounts of rain to southern Australia throughout the winter months. Consequently, the summer months in southern Australia tend to be dry while the winter months tend to be wet.

Climatology Synopsis

Unlike the NH where the distinction between the wintertime polar air masses and the summertime subtropical air masses is much clearer, the tropical and subtropical air masses over Australia are often very similar in makeup. Although the distinctions are few, the seasonal differences summarized in Table 1 are significant with regard to the production and transport of aerosols .

Table 1. Australian climatology.

	Winter		Summer	
	Wind	**Precip.**	**Wind**	**Precip.**
North Australia	Easterly	Dry	Westerly/Northeasterly	Wet
South Australia	Westerly	Wet	Westerly	Dry

As mentioned earlier, these climate classifications are generalities which depict a broad overview and do not fully credit Australia's often complex and diverse climate. While the winds are decidedly westerly throughout the year in southern Australia, the northeasterly wind is due to the summertime monsoonal low. In addition, note the wet and dry seasons of northern and southern Australia are completely out of phase. This is

further supported by Figure 6 which depicts the relative monthly rainfall in the 90 districts of mainland Australia. [It does not include Tasmania.]

As Figure 6 suggests, while the precipitation patterns discussed above bring plenty of moisture to the coastal regions of Australia, the amount of precipitation drops off drastically when approaching the interior of the continent. In fact, much of central Australia is desert making it a potential dust source.

For this research, the seasonal classifications used by Gintelli *et al.* (1971) were adopted and are summarized in Table 2.

Table 2. Seasonal classifications.

	4 Season Classification	2 Season Classification
Summer	Dec-Feb	Nov-Mar
Fall	Mar-May	
Winter	Jun-Aug	May-Sep
Spring	Sep-Nov	

The *4 Season Classification* is related to the earth's orbit about the sun where each season represents a separate quadrant. Note, for the 1979 seasonal composites, this classification scheme includes the images from December 1978 and excludes those from December 1979. On the other hand, the traditional twelve month year (January 1979 - December 1979) was preserved for the 1979 annual composite. The *2 Season Classification* is useful for tropical regions which are dominated by two seasons. Note two months, April and October, are not represented because they are thought to be transitional months. Specific to this research, this classification is primarily used to differentiate between the wet and dry seasons for northern and southern Australia.
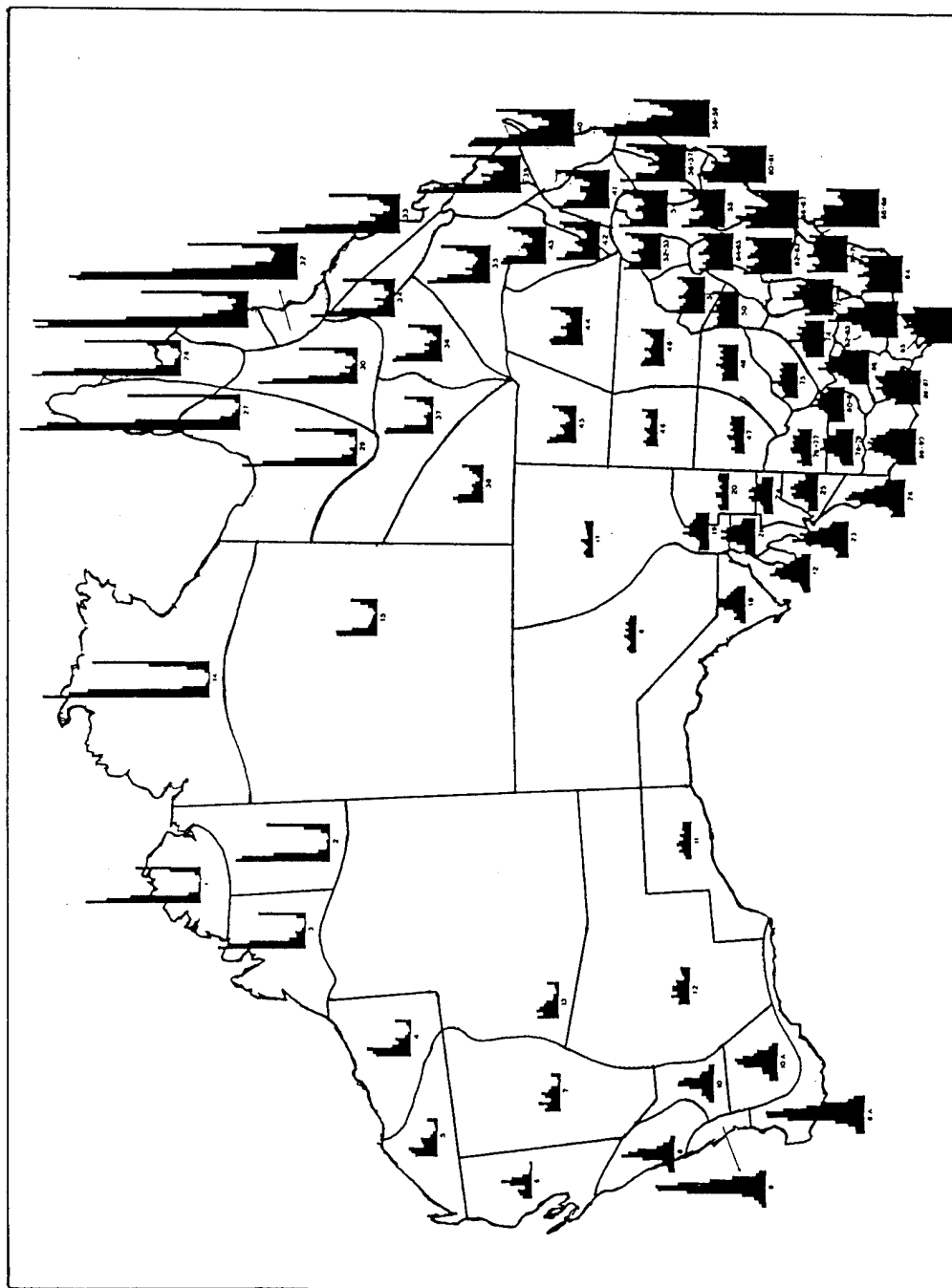
Figure 6. Monthly distribution of rainfall in Australia. Each bar chart shows the relative observed rainfall for its district. Each black collumn represents a month with the first being January and the last being December. (Adapted from the Bureau of Meteorology, 1962.)

CHAPTER VI

RESULTS AND DISCUSSION

Problems with Analysis Due to Low Data Densities

Unfortunately, when viewing the aerosol composites, it is apparent that in many areas of the study region the data coverage is quite sporadic. The 1979 aerosol composite in Figure 7 shows roughly a third of the ocean region was not sampled in 1979. Furthermore, the corresponding 1979 data density in Figure 8, shows that of the locations sampled, the vast majority were sampled less than 25 times during the year. The maximum values over the Gulf of Carpentaria (just east of the Cape York Peninsula) correspond to 69 samples. In this best case scenario, there is ~18.5% coverage of the 365 day calendar year.

Of course, the annual averages represented in Figures 7 and 8 only present part of the picture. These figures depict the spatial coverage for 1979 but say little about the temporal coverage. Figure 9 provides a monthly distribution of the CZCS aerosol images in 1979. It is evident that the number of CZCS images peaked late in the Austral winter (September 1979) while remaining relatively low during the summer months. The issue of temporal coverage can also be addressed by examining the seasonal data density images. These images and their associated aerosol composites are included in Figures 10-17. [Note the *4 Season Classification* is used for these images (Table 2).] Examination of the data density images for each season reveals there is considerably less data coverage during the summer (December 1978 - February 1979) and fall (March 1979 - May 1979). In fact, for the summer months, Figure 11 indicates there are no locations with more than 10 samples. The fall months in Figure 13 reveal slightly improved coverage off the northeast coast of Australia and over the Gulf of Carpentaria where samples sizes exceed 20 in some locations.

The data coverage in the winter (June 1979 -August 1979) and spring (September 1979 - November 1979) is markedly better as is evident in Figures 15 and 17 respectively. In particular, the data coverage over the Tasman Sea is encouraging as it

Aerosol Composite
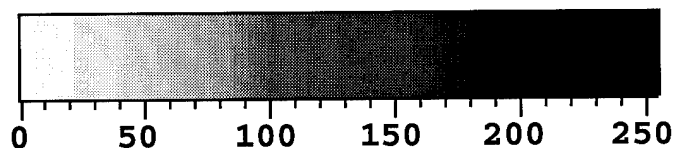## (1979)
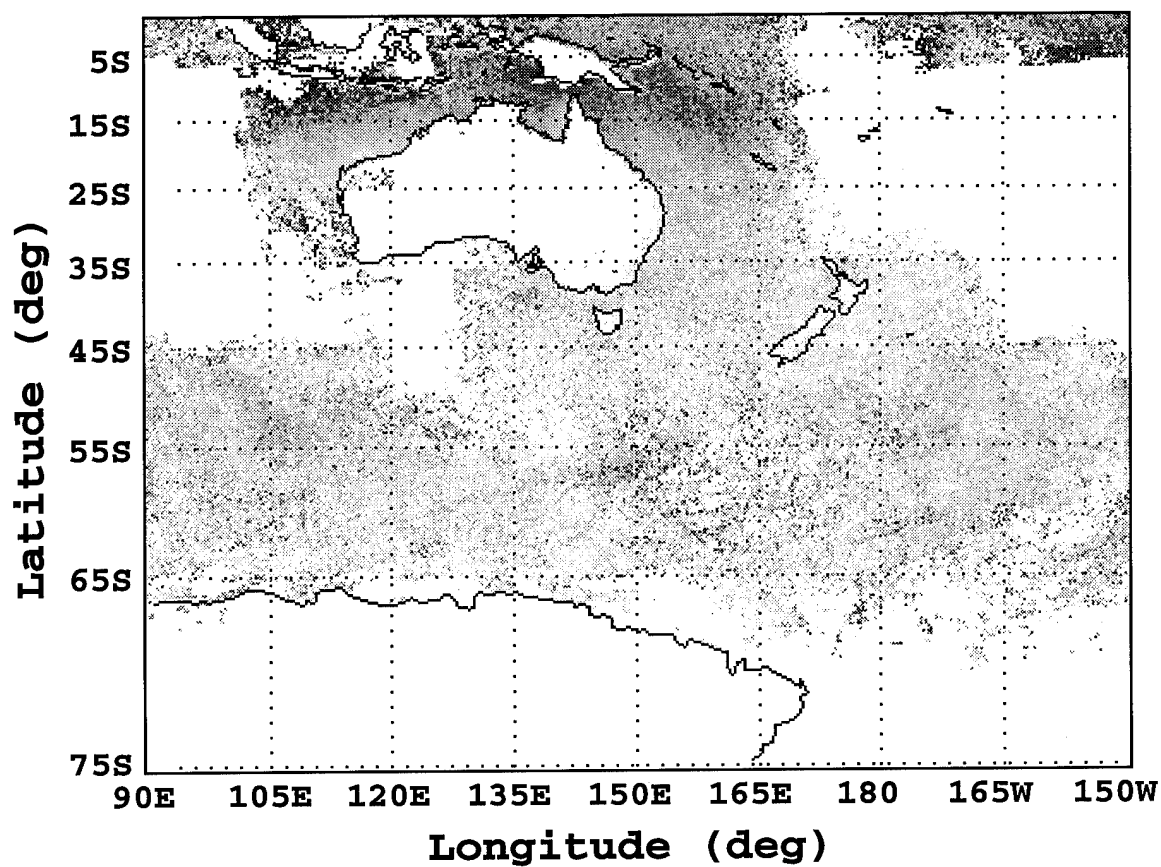
Corrected 670nm Radiance
(unitless)

Figure 7. Aerosol composite for 1979. The values represent the average relative aerosol distribution for the period January 1979 – December 1979.

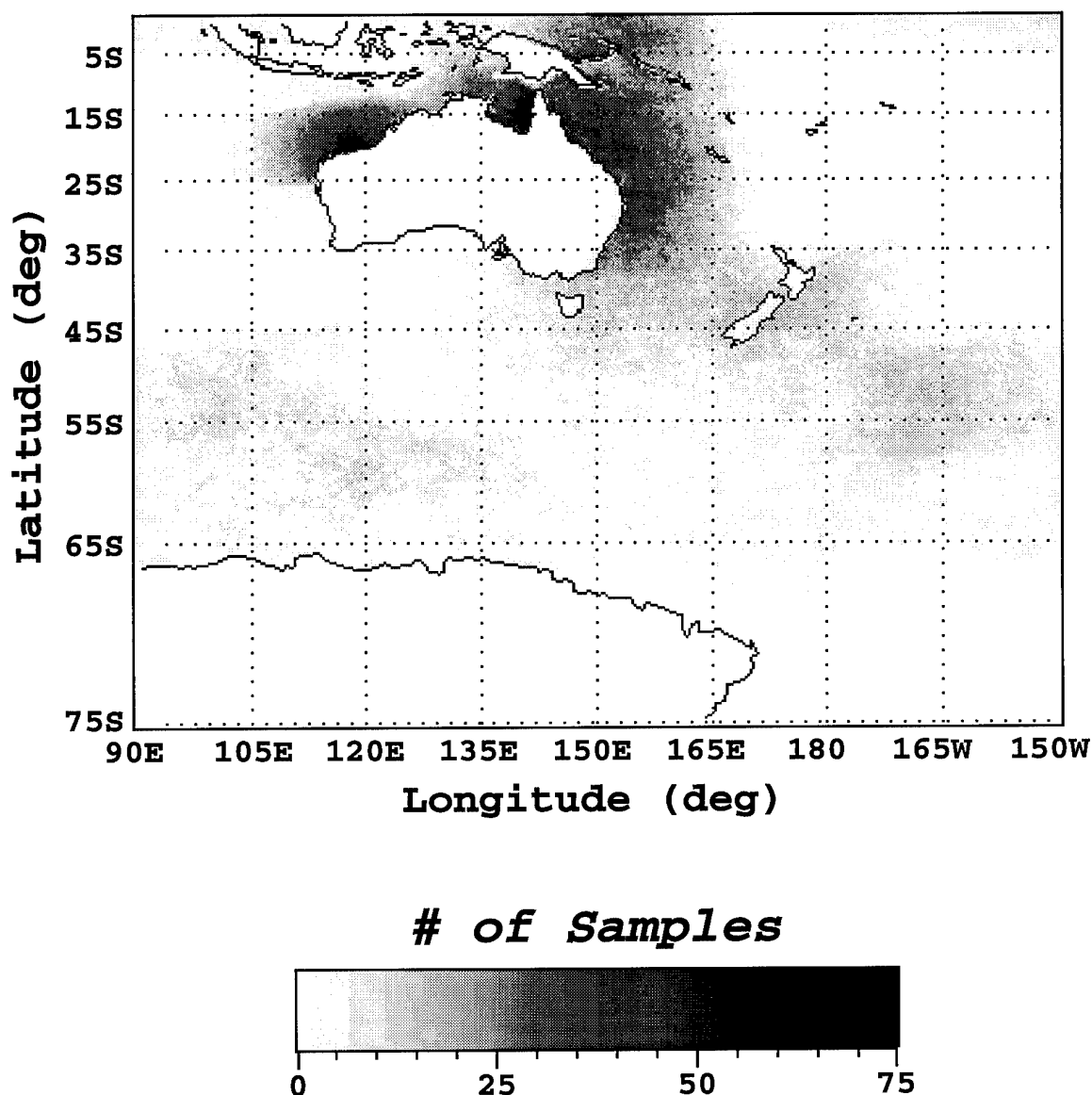# *Data Density*
(1979)

# of Samples

Figure 8. Data density for 1979. The values indicate the number of samples at each pixel used to compute the associated aerosol composite (Figure 7).
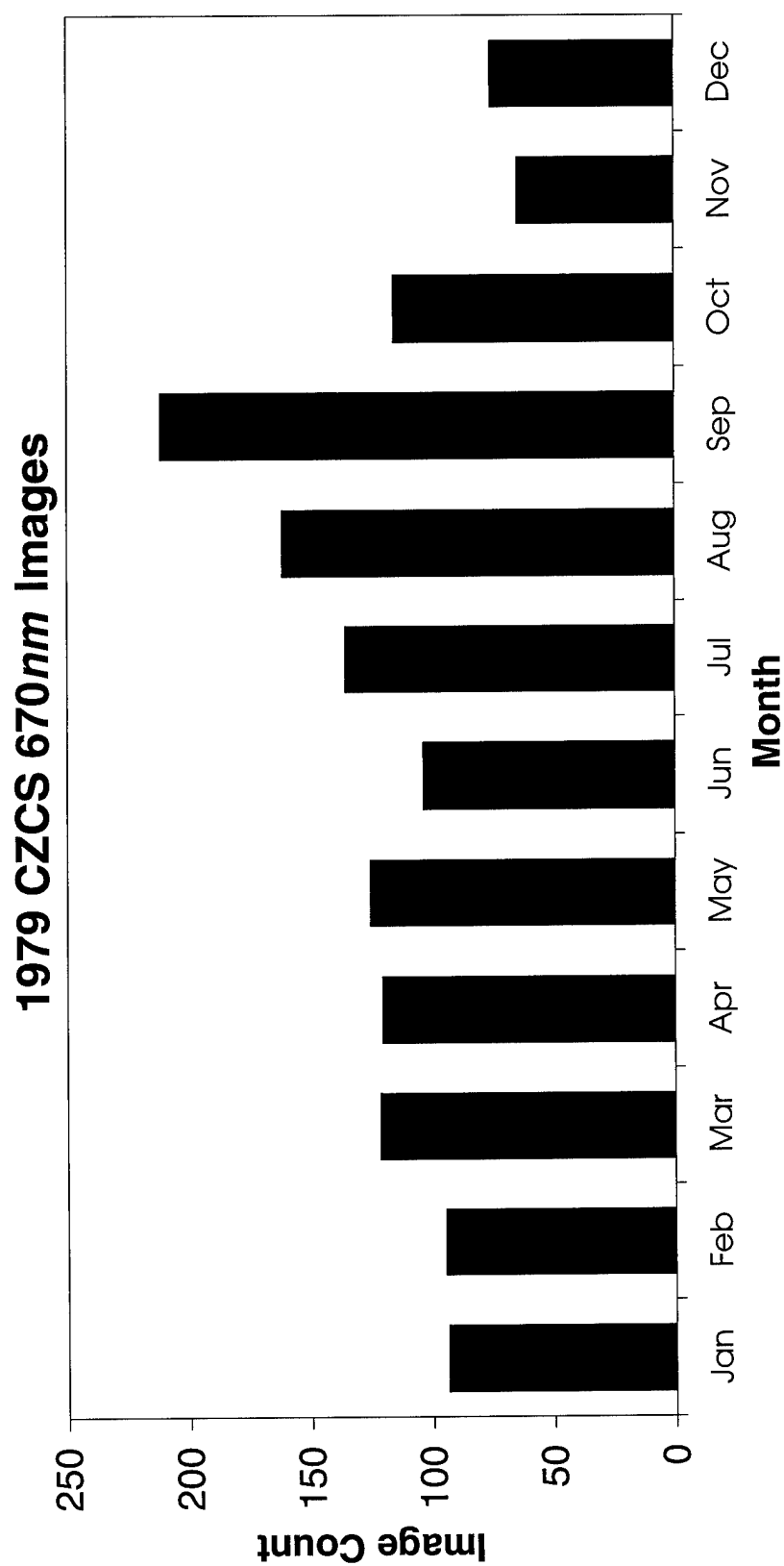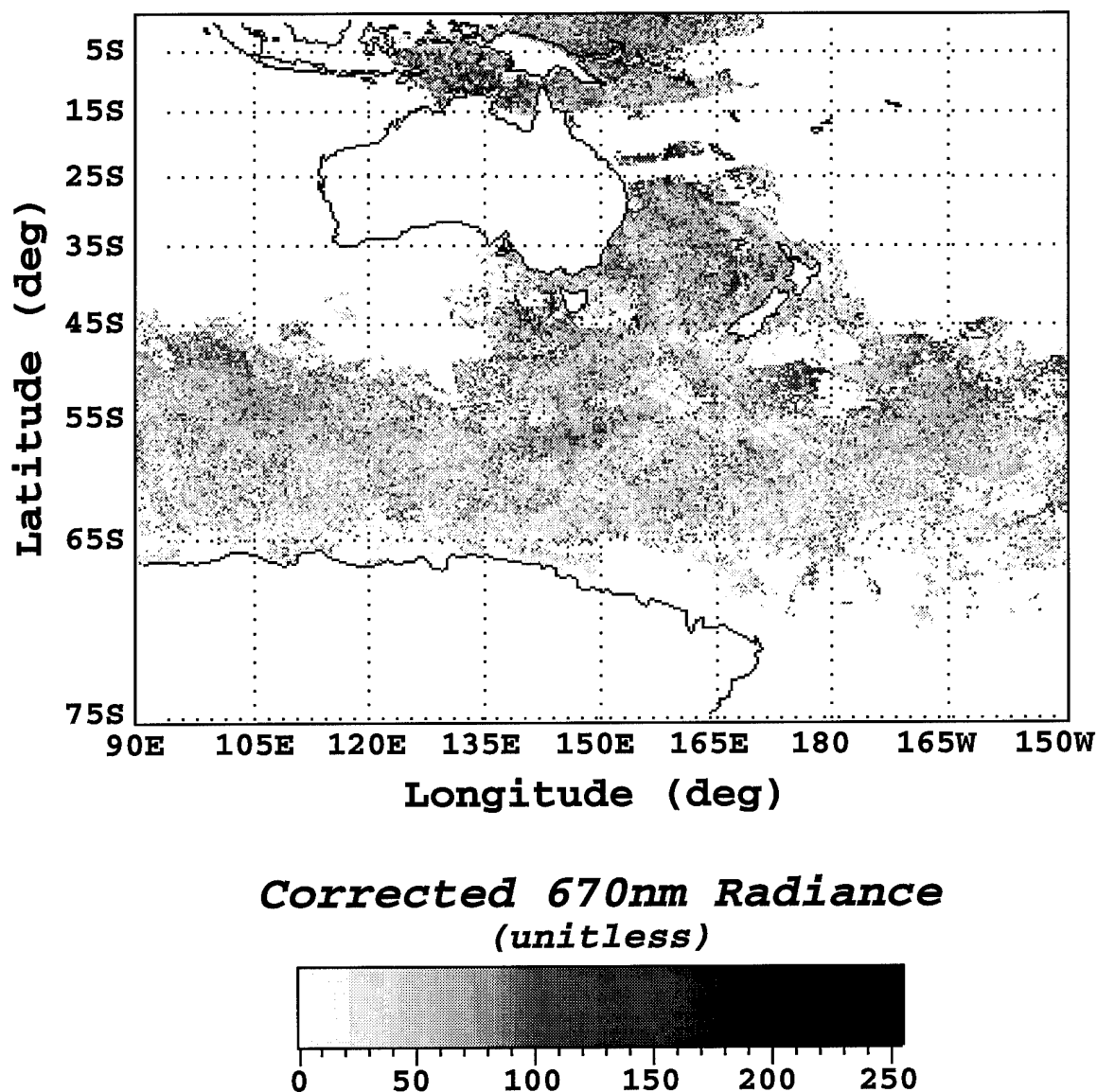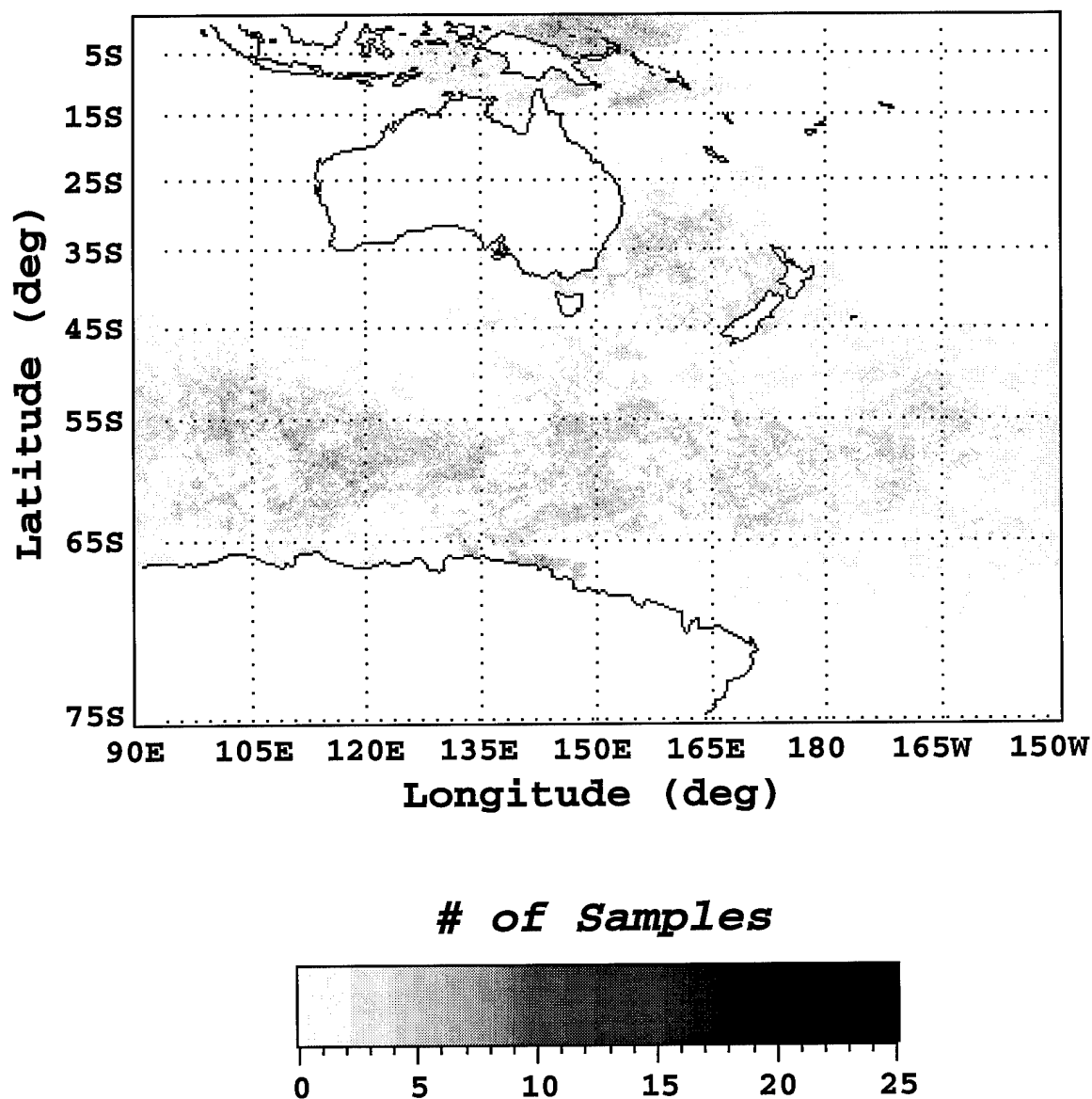
1979 CZCS 670nm Images

Figure 9. Monthly image count for 1979.
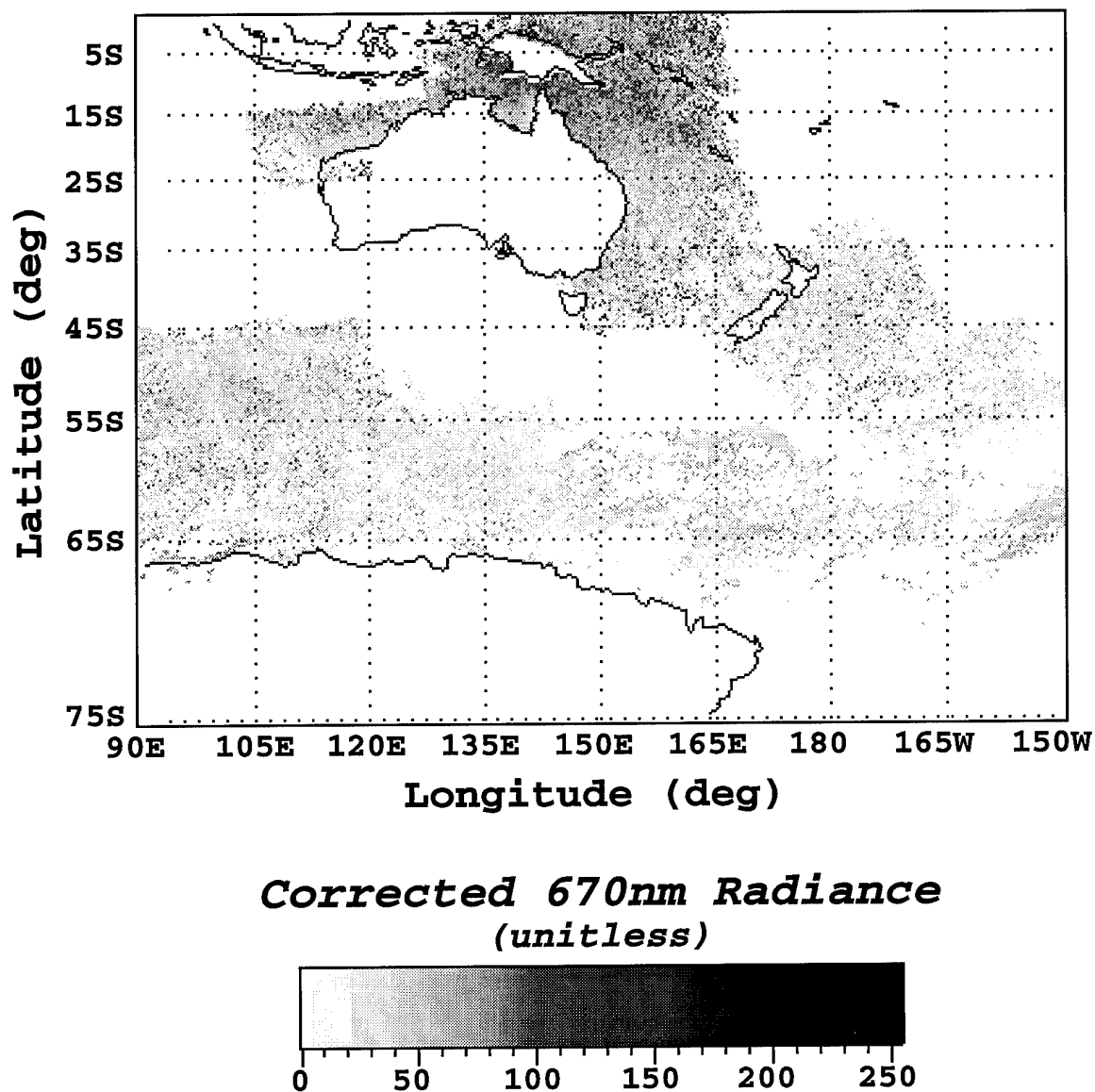
Aerosol Composite
(Dec78-Feb79)

Figure 10. Aerosol composite for the 1978/79 Austral summer (4 Season). The values represent the average relative aerosol distribution for the period December 1978 – February 1979.

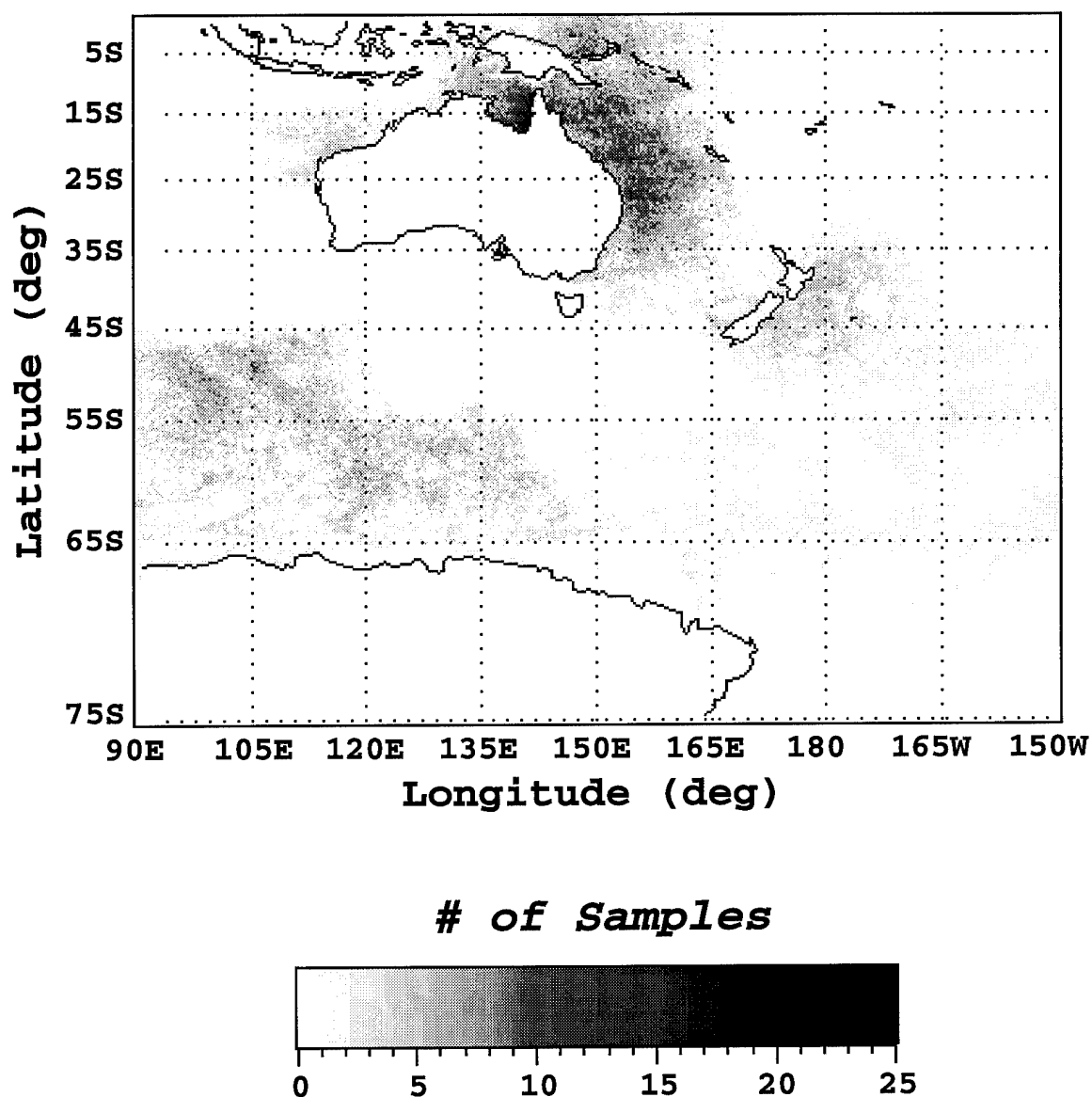# Data Density
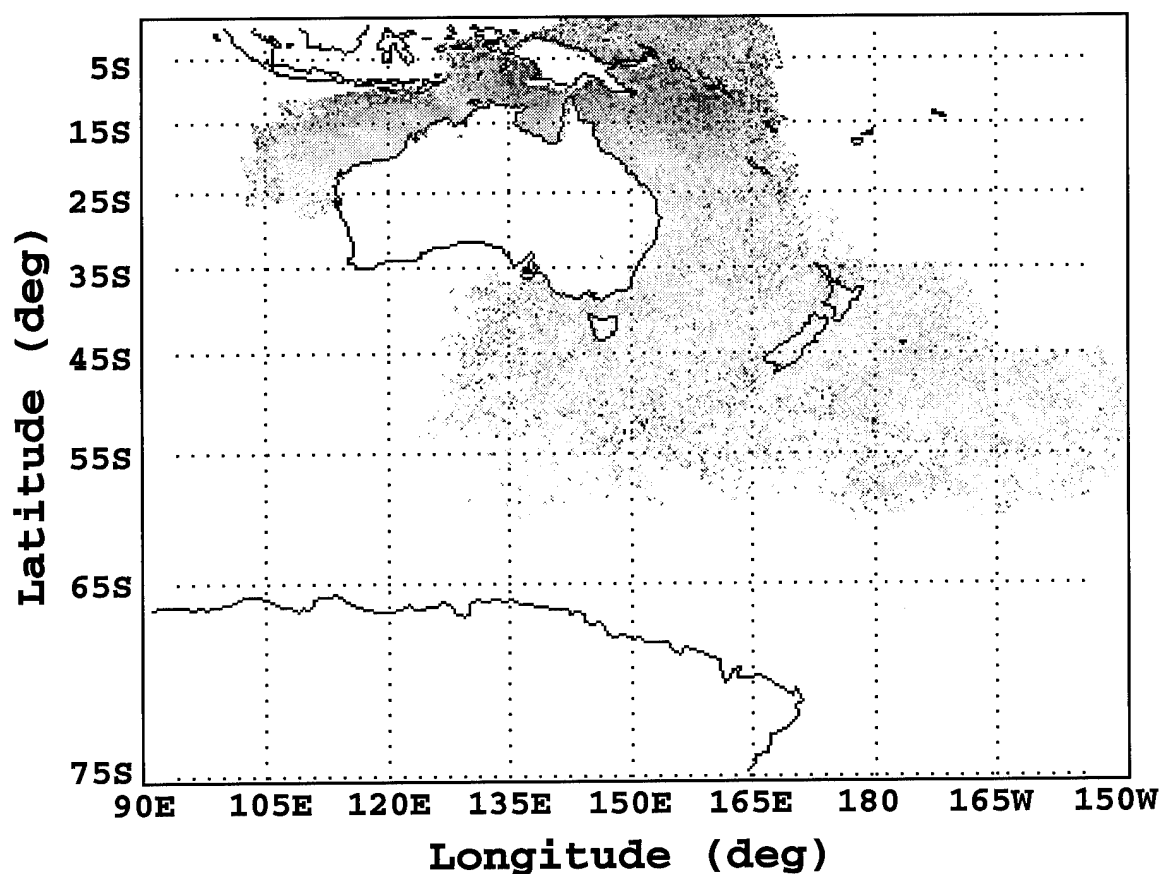## (Dec78-Feb79)

of Samples

Figure 11. Data density for the 1978/79 Austral summer
(4 Season). The values indicate the number of samples at
each pixel used to compute the associated aerosol
composite (Figure 10).

Aerosol Composite
(Mar79-May79)

Corrected 670nm Radiance
(unitless)

Figure 12. Aerosol composite for the 1979 Austral fall (4 Season). The values represent the average relative aerosol distribution for the period March 1979 - May 1979.

Data Density
(Mar79–May79)

# of Samples

Figure 13. Data density for the 1979 Austral fall (4 Season). The values indicate the number of samples at each pixel used to compute the associated aerosol composite (Figure 12).

Aerosol Composite
(Jun79-Aug79)

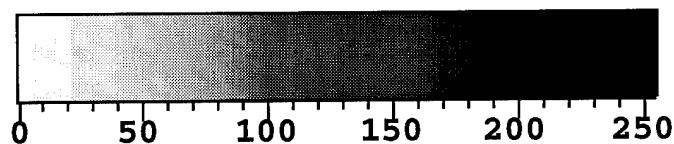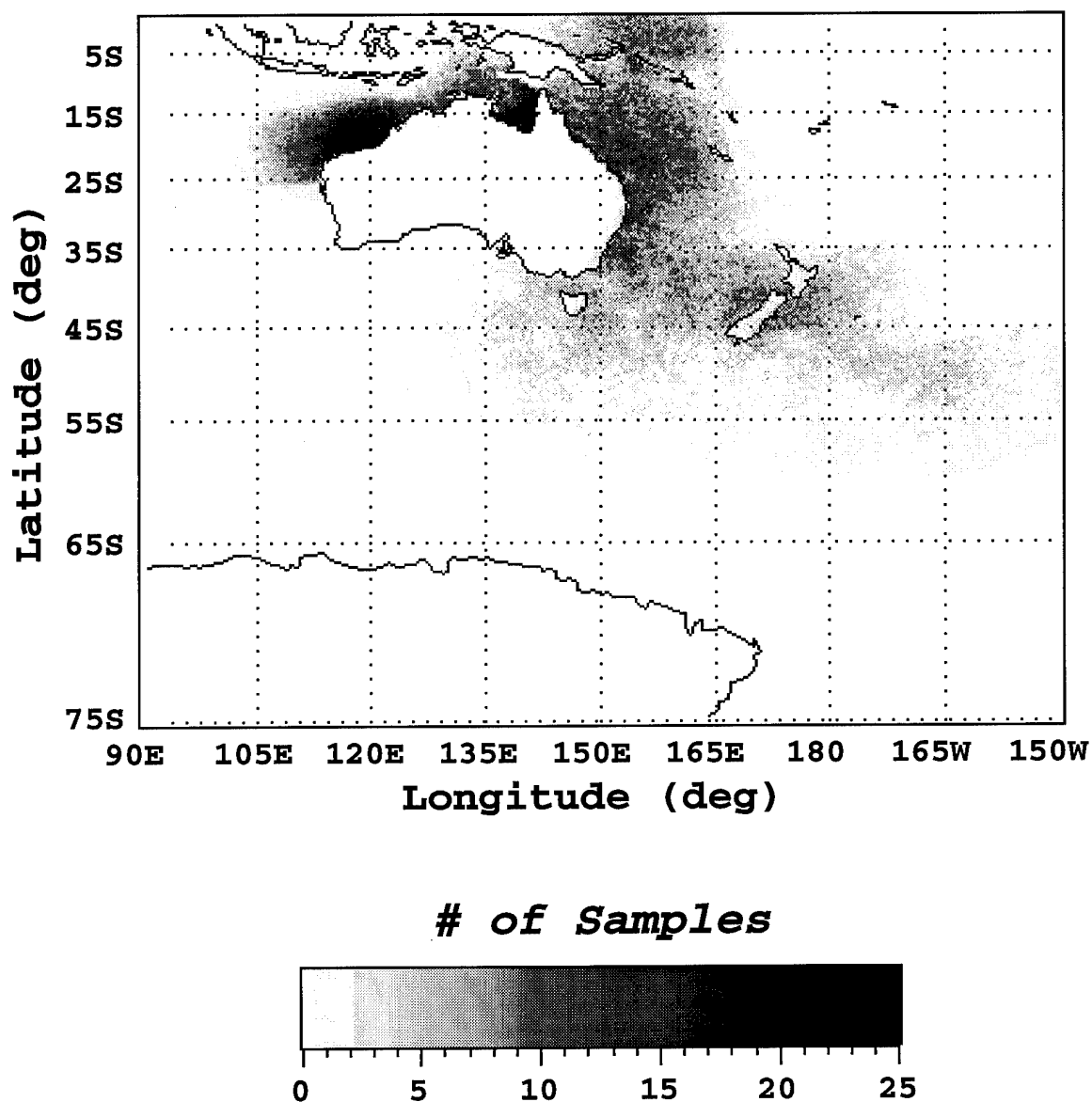**Corrected 670nm Radiance**
(unitless)

Figure 14. Aerosol composite for the 1979 Austral winter (4 Season). The values represent the average relative aerosol distribution for the period June 1979 - August 1979.

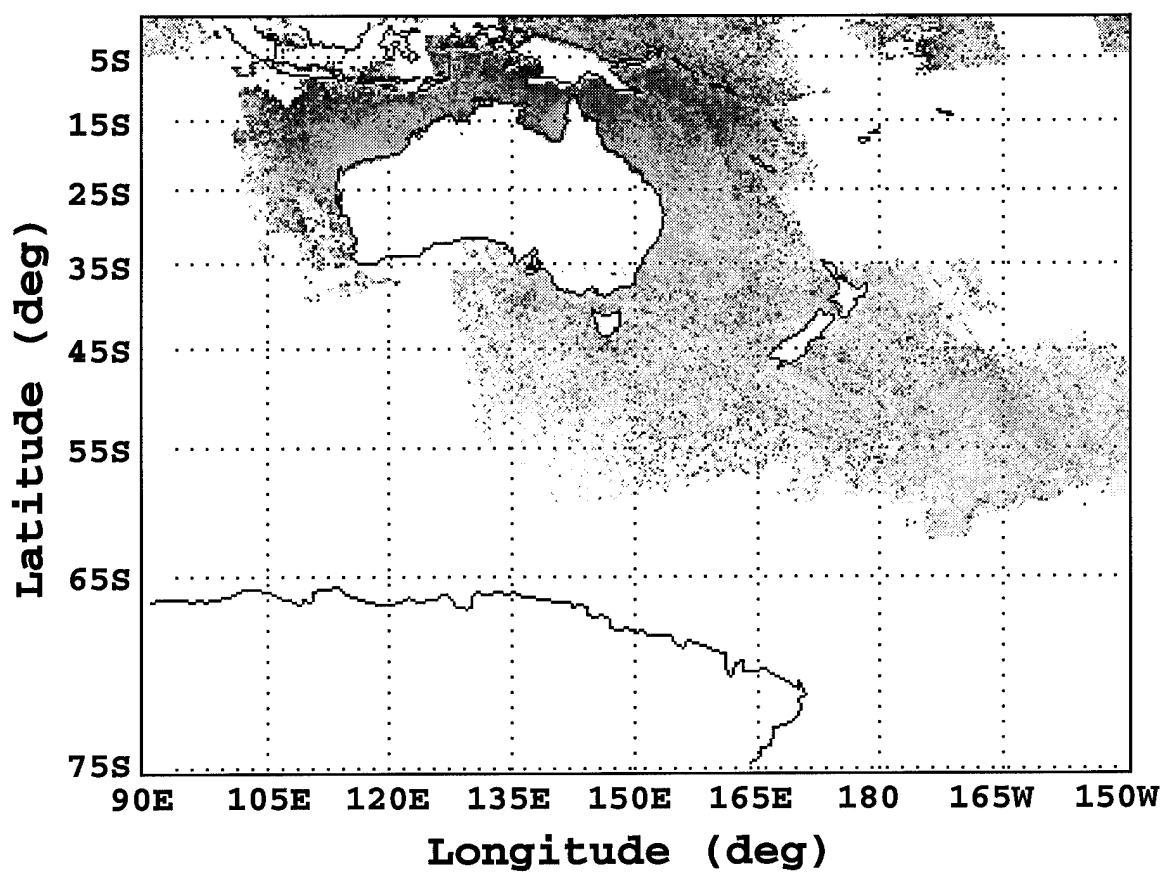# *Data Density*
(Jun79–Aug79)

# of Samples

Figure 15.   Data density for the 1979 Austral winter
(4 Season).   The values indicate the number of samples at
each pixel used to compute the associated aerosol composite
(Figure 14).

Aerosol Composite
(Sep79-Nov79)

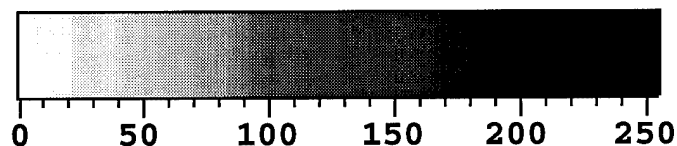**Corrected 670nm Radiance**
(unitless)

Figure 16. Aerosol composite for the 1979 Austral spring (4 Season). The values represent the average relative aerosol distribution for the period September 1979 - November 1979.
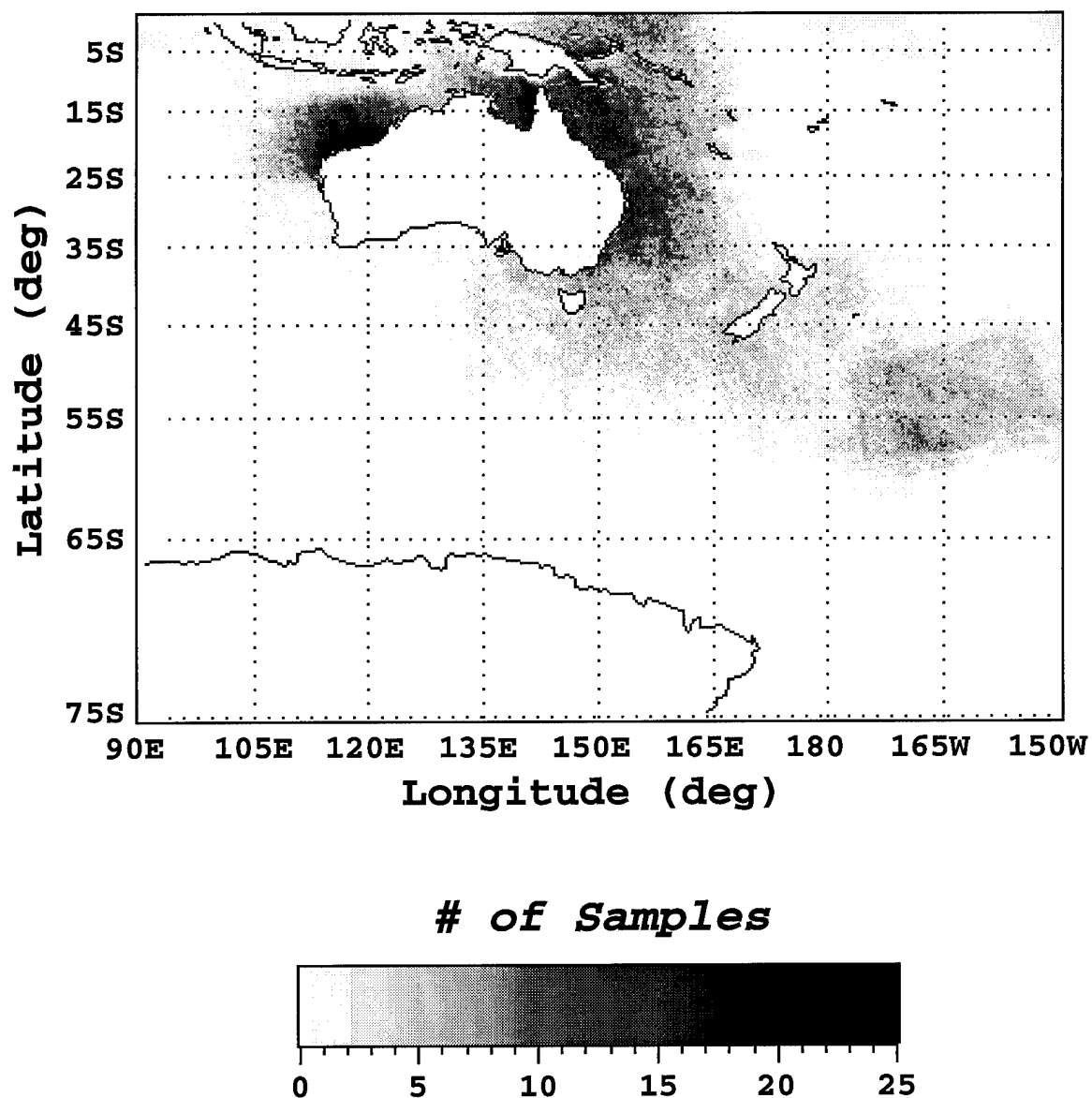
Data Density
(Sep79-Nov79)

Figure 17. Data density for the 1979 Austral spring (4 Season). The values indicate the number of samples at each pixel used to compute the associated aerosol composite (Figure 16).

will allow for analysis of the CZCS data in this region. From Chapter I, it has been suggested that the mineral-rich plume in the sea floor sediments of the Tasman Sea is the result of aeolian dust transport (Healy, 1970; Glasby, 1971; Glasby, 1991). In addition, the well-represented region off the northwest coast of Australia will allow for analysis to determine if there is evidence of elevated aerosol concentrations due to dust storm activity (Pye, 1987).

Overview of the 1979 Aerosol Climatology

In general, Figure 7 suggests much of the SH, especially over the southern oceans, is characterized by relatively low radiance values. This is in agreement with Patterson *et al.* (1980) who suggest the total aerosol concentrations in the SH are relatively low due to a general lack of continental and anthropogenic sources. However, because of the low data densities (< 5 samples for most pixels throughout the Southern Ocean region), there is insufficient evidence to infer the radiances are representative annual averages (Figure 8). On the other hand, there are three areas of particular interest which contain reasonable data coverage and interesting aerosol signatures: (1) the equatorial 'red band', (2) the Indian Ocean region, and (3) the Tasman Sea region.

The Equatorial 'Red Band'

For this research, the equatorial 'red band' has been defined as the area within the study region north of ~15°S. Throughout most of the aerosol composites, this region has consistently high radiance values (e.g. Figure 7). Although the flanks of the 'red band' are the result of only a few scans (≤ 5 samples), the central portion of the signal is relatively well represented (~ 20 to 40 samples) (Figure 8). There are several potential explanations for this signal:

    a) Aerosols generated from biomass burning

    b) Aerosols generated from biogenic hydrocarbon production in the tropics

    c) A false signal resulting from scans over Case 2 water

    d) An artifact of cloud-masking and electronic overshoot

This list is not meant to exhaust all the possible explanations for the 'red band' but instead includes the ones thought to be most viable.

It should be mentioned that aeolian dust is not included in this list because it is thought to be an unlikely source for the signal. Although the desert regions of Australia are potential dust sources, the synoptic wind and rainfall patterns do not support transport to the 'red band' region. While Figure 5 indicates the predominant winds are easterly in the winter months, it could be argued that in the summer months, the wrap-around effect of the monsoon low might serve as a dust transport mechanism (Figure 4). However, the combination of light winds and abundant rainfall associated with the monsoon season suggests this would not be likely.

Aerosols Generated from Biomass Burning

There is evidence that the aerosol byproducts of biomass burning may significantly affect the earth's radiation budget, especially in the tropics (Crutzen and Andreae, 1990; Penner *et al.*, 1992). Because the soot generated in forest and grass fires tends to result in opaque black aerosols, it absorbs and scatters incoming solar radiation. The absorption and scattering result in opposing climate forcing, warming and cooling respectively. In addition, the smoke aerosols may serve as CCN increasing cloud formation and, thereby, indirectly increasing the earth albedo. As a result of these conflicting effects, the overall influence of these aerosols on the atmosphere has not been fully resolved (Charlson *et al.*, 1992).

However, the work of Crutzen and Andreae (1990) and Penner *et al.* (1992) does suggest biomass burning can result in significantly elevated aerosol concentrations. Similarly, Taylor and Zimmerman (1991) used a computer model to show significant contribution of trace gas emissions (CH_4 and O_3) resulting from biomass burning over northern Australia and New Guinea which were in good agreement with observed concentrations. If there are increased gas emissions in this region due to biomass burning, it follows there would also be increased aerosol emissions from the same source. Furthermore, Dignon and Penner (1991) state there are considerably more

burns in the northern Australia than in the south due to markedly increased vegetation growth during the monsoon season. Because much of the 'red band' is located between Australia and New Guinea, one might contend the signal in this region is a result of biomass burning.

On the other hand, there is evidence which suggests biomass burning does not fully explain the existence of the 'red band'. If biomass burning were the predominant aerosol source, one would expect to see a well-defined seasonal aerosol signal since the degree of burning and its byproducts are directly related to vegetation growth. Figures 18-21 are the aerosol composites and the associated data density images for the Austral summer (November 1978 - March 1979) and winter (May 1979 - September 1979) using the *2 Season Classification* (Table 2). From Chapter V, the summer months in the tropics of the study region are particularly wet due to the monsoon season. Since there is considerable growth during this period, the number of burns, both natural and deliberate, increases sharply in the dry winter months which follow (Andreae, 1991; Watson *et al.*, 1991). From Figures 18 and 20, it is apparent that the 'red band' exists throughout 1979, in both the wet and dry season. In fact, the CZCS data suggests the signal intensifies during the summer months which does not support the findings of Andreae (1991) and Watson *et al.* (1991).

In addition, the meridional extent of the 'red band' suggests biomass burning is not likely to be the only aerosol source. In Figure 7, the signal is evident in varying degrees across the entire study region north of ~15°S. In particular, the segment of the 'red band' east of 180° longitude was only evident in the CZCS data during November 1979 and December 1979. These monthly aerosol composites and the associated data density images are included as Figures 22-25. Because of the predominantly easterly flow pattern during these months (Figures 26 and 27), aerosols resulting from biomass burning would not be expected to be found east of New Guinea. On the other hand, because these signals are the result of only a few scans (Figures 21 and 23), one could argue the winds may have briefly shifted during the period of these scans and are, therefore, not apparent in the monthly wind averages. Andreae (1991) has shown
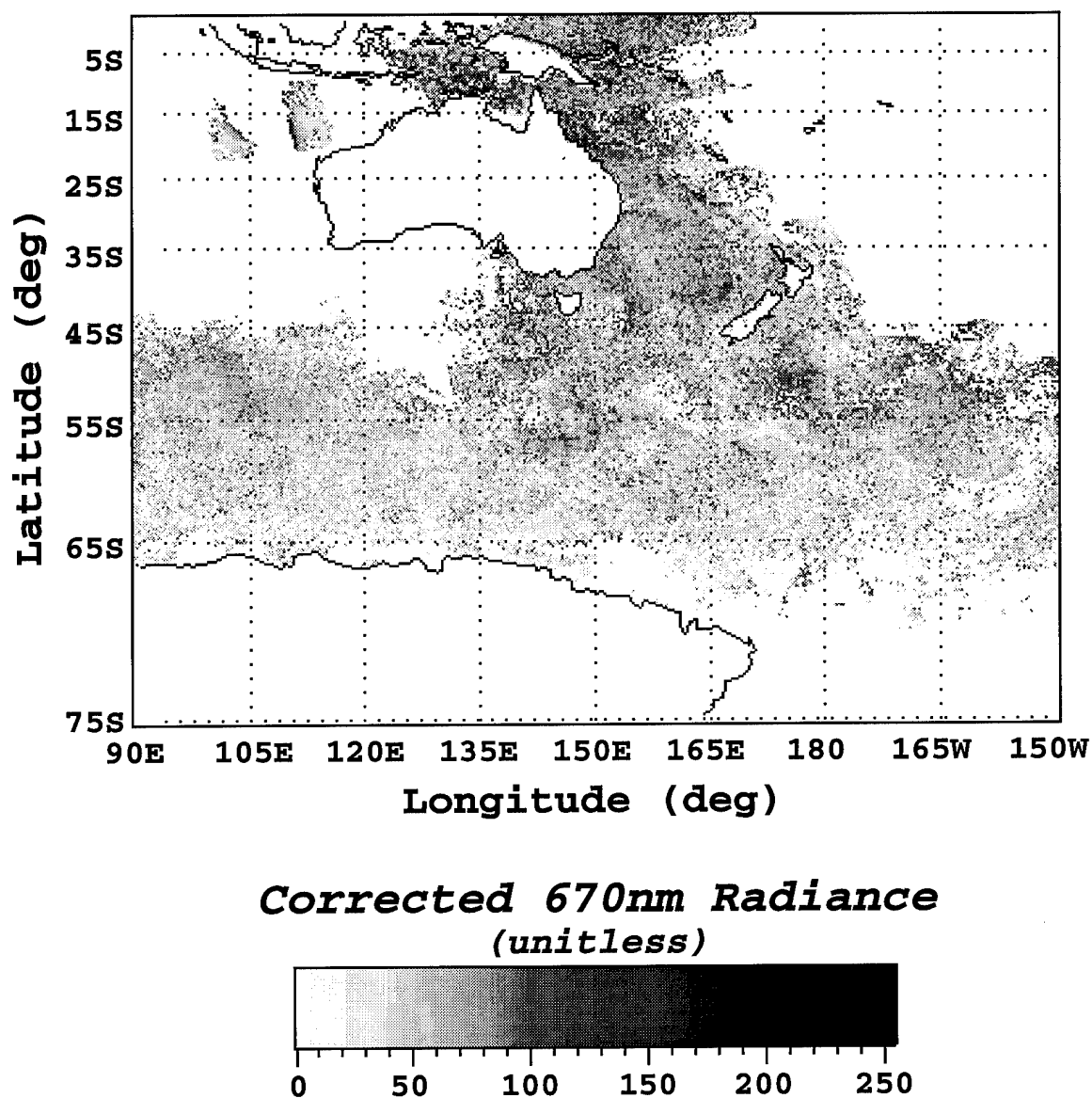
Aerosol Composite
(Nov78-Mar79)

Figure 18. Aerosol composite for the 1978/79 Austral summer (2 Season). The values represent the relative aerosol distribution for the period November 1978 – March 1979.

Data Density
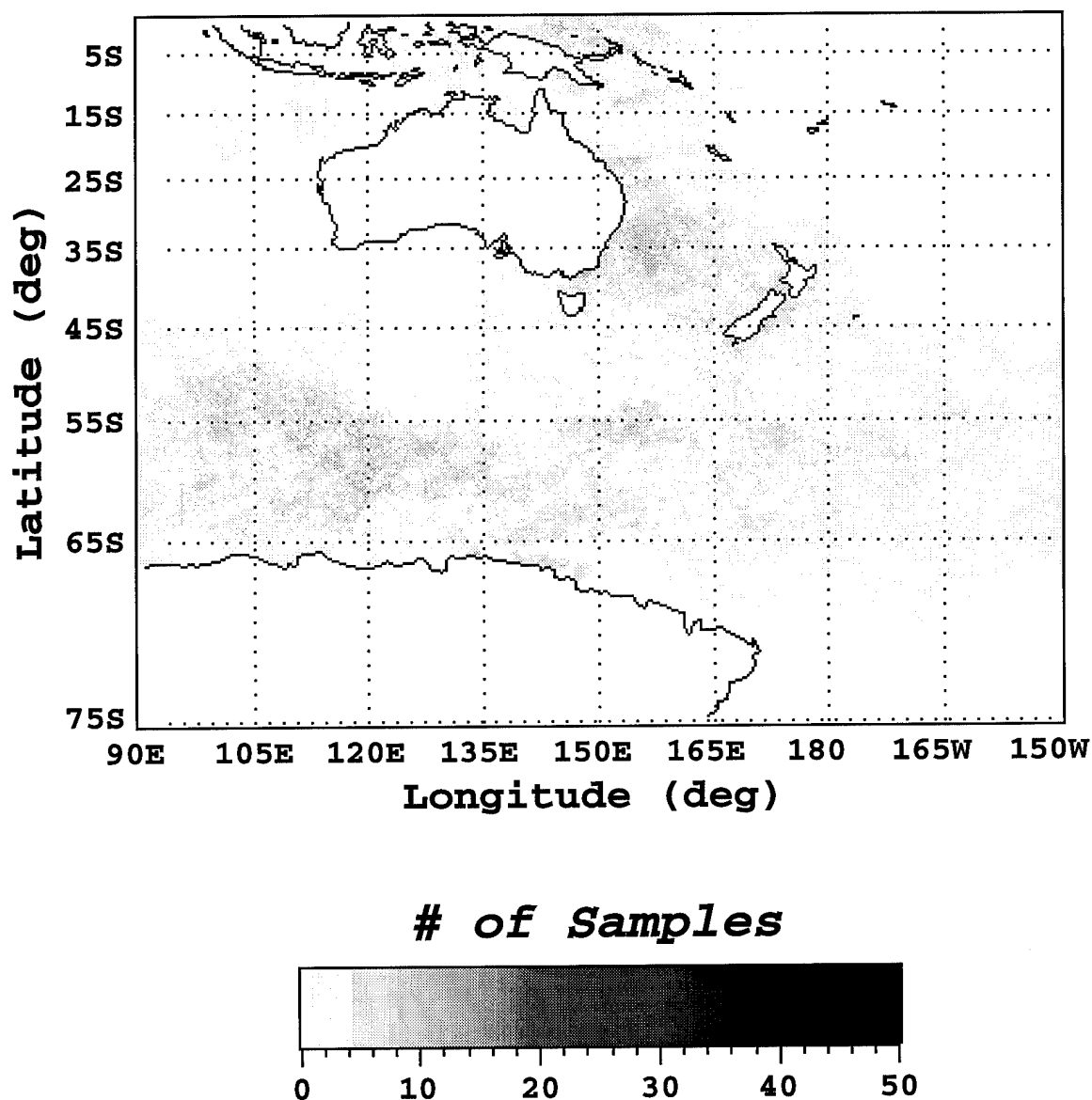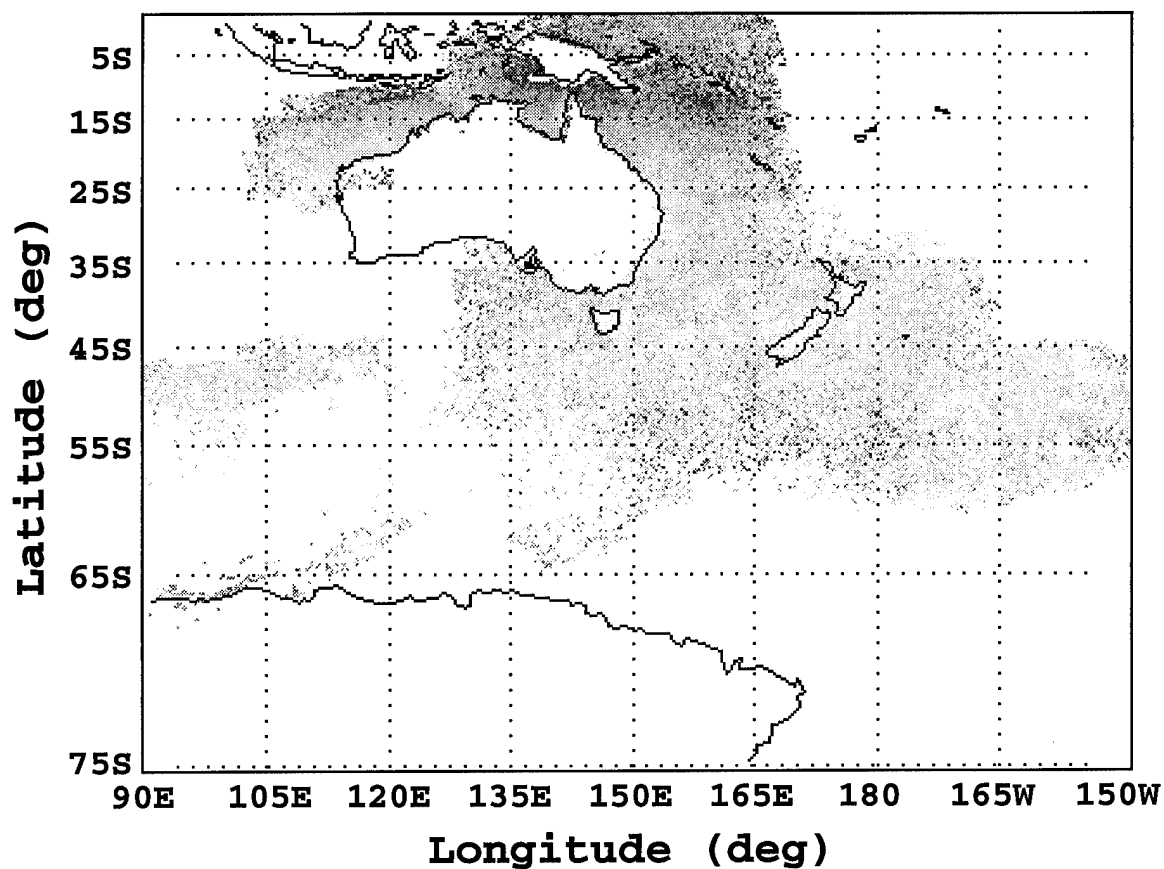## (Nov78-Mar79)

of Samples

Figure 19. Data density for the 1978/79 Austral summer (2 Season). The values indicate the number of samples at each pixel used to compute the associated aerosol composite (Figure 18).

Aerosol Composite
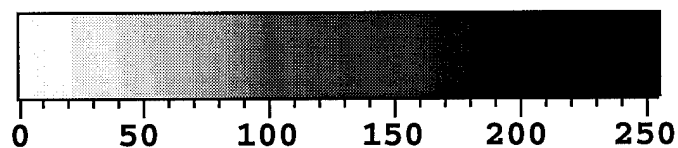## (May79-Sep79)

Corrected 670nm Radiance
(unitless)

Figure 20. Aerosol composite for the 1979 Austral
winter (2 Season). The values represent the relative
aerosol distribution for the period May 1979 –
September 1979.

Data Density
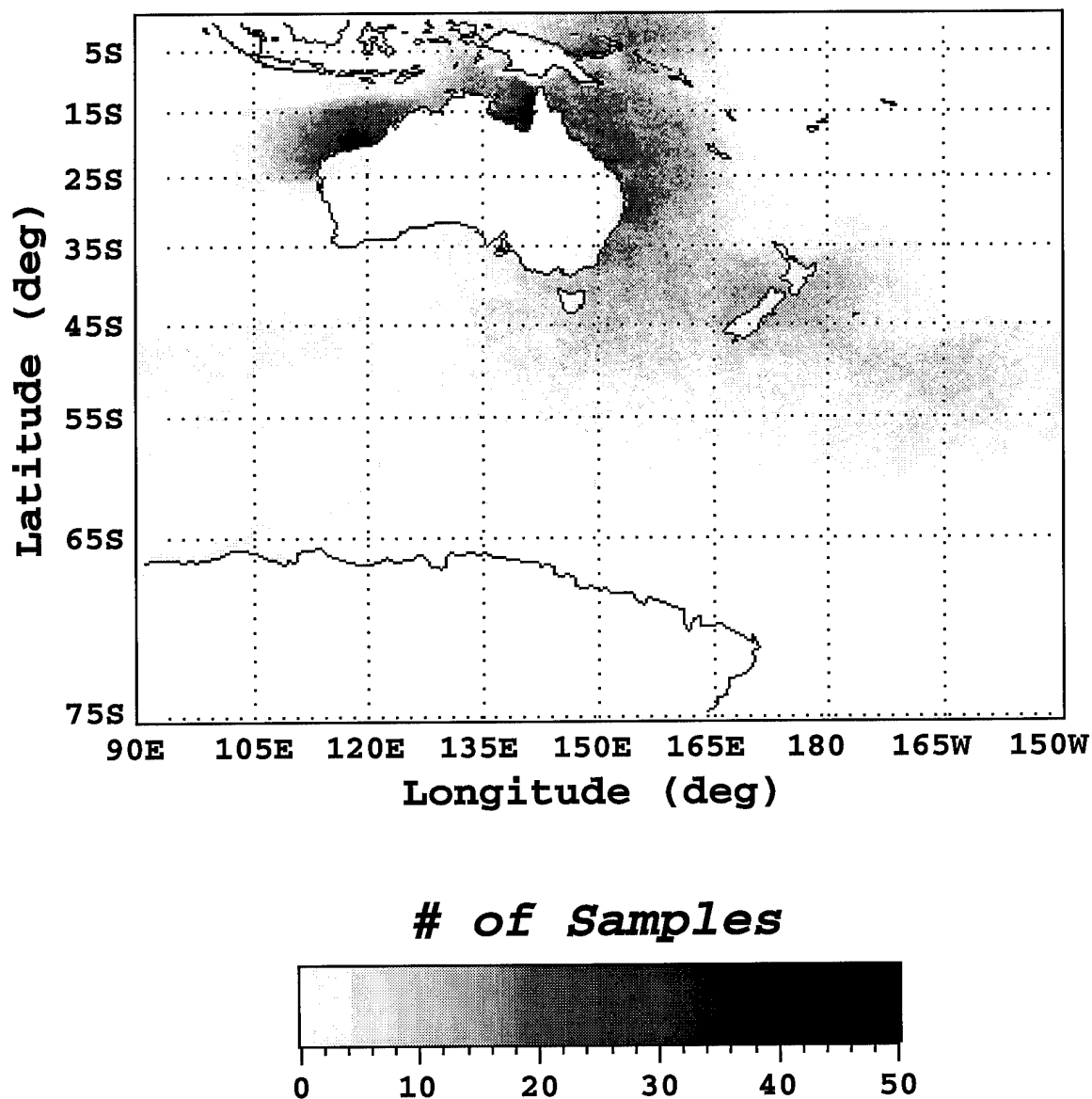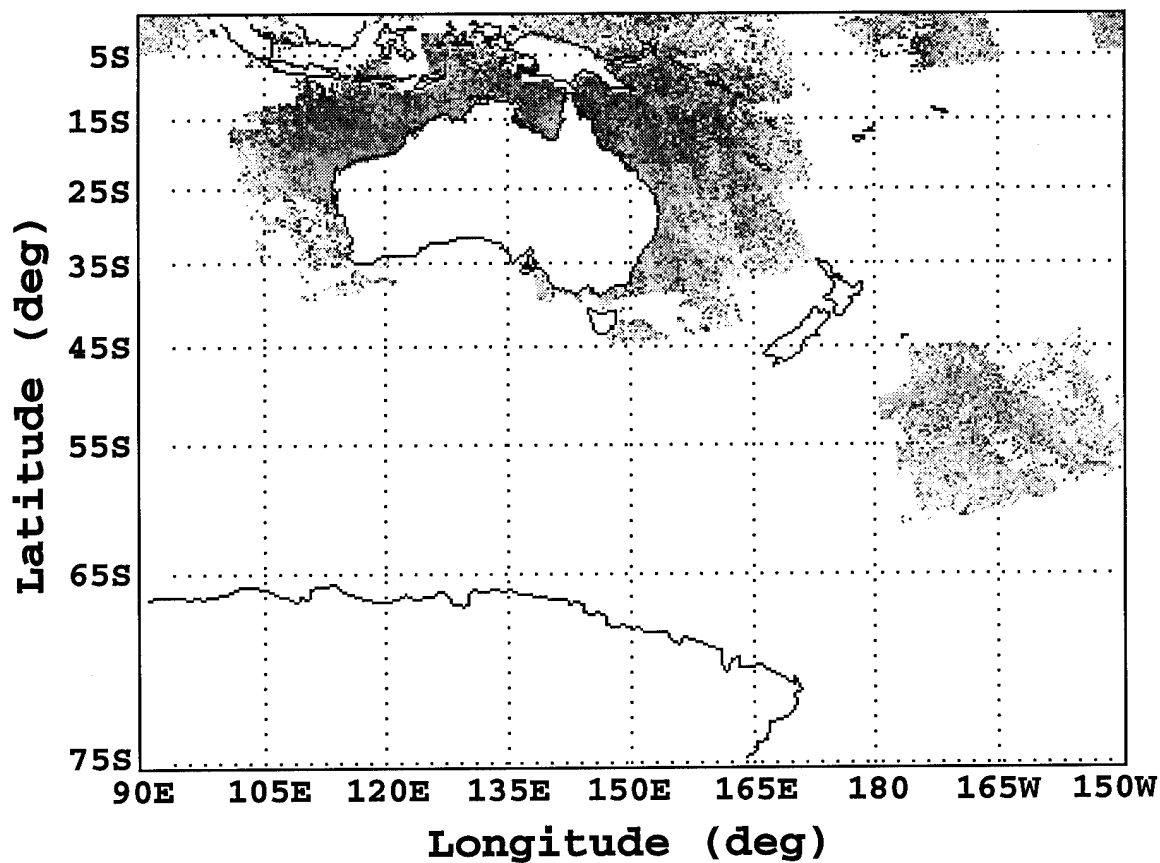## (May79-Sep79)

of Samples

Figure 21. Data density for the 1979 Austral winter (2 Season). The values indicate the number of samples at each pixel used to compute the associated aerosol composite (Figure 20).

Aerosol Composite
(Nov79)

Corrected 670nm Radiance
(unitless)

Figure 22. Aerosol composite for November 1979. The values represent the average relative aerosol distribution.

Data Density
(Nov79)

# of Samples

Figure 23. Data density for November 1979. The values
indicate the number of samples at each pixel used to
compute the associated aerosol composite (Figure 22).

Aerosol Composite
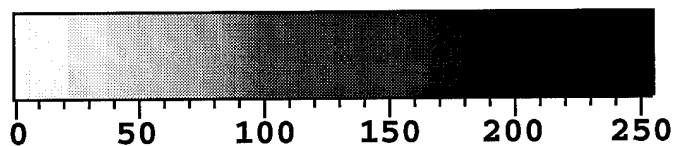## (Dec79)

Corrected 670nm Radiance
(unitless)

Figure 24.   Aerosol composite for December 1979.   The
values represent the average relative aerosol distribution.

Data Density
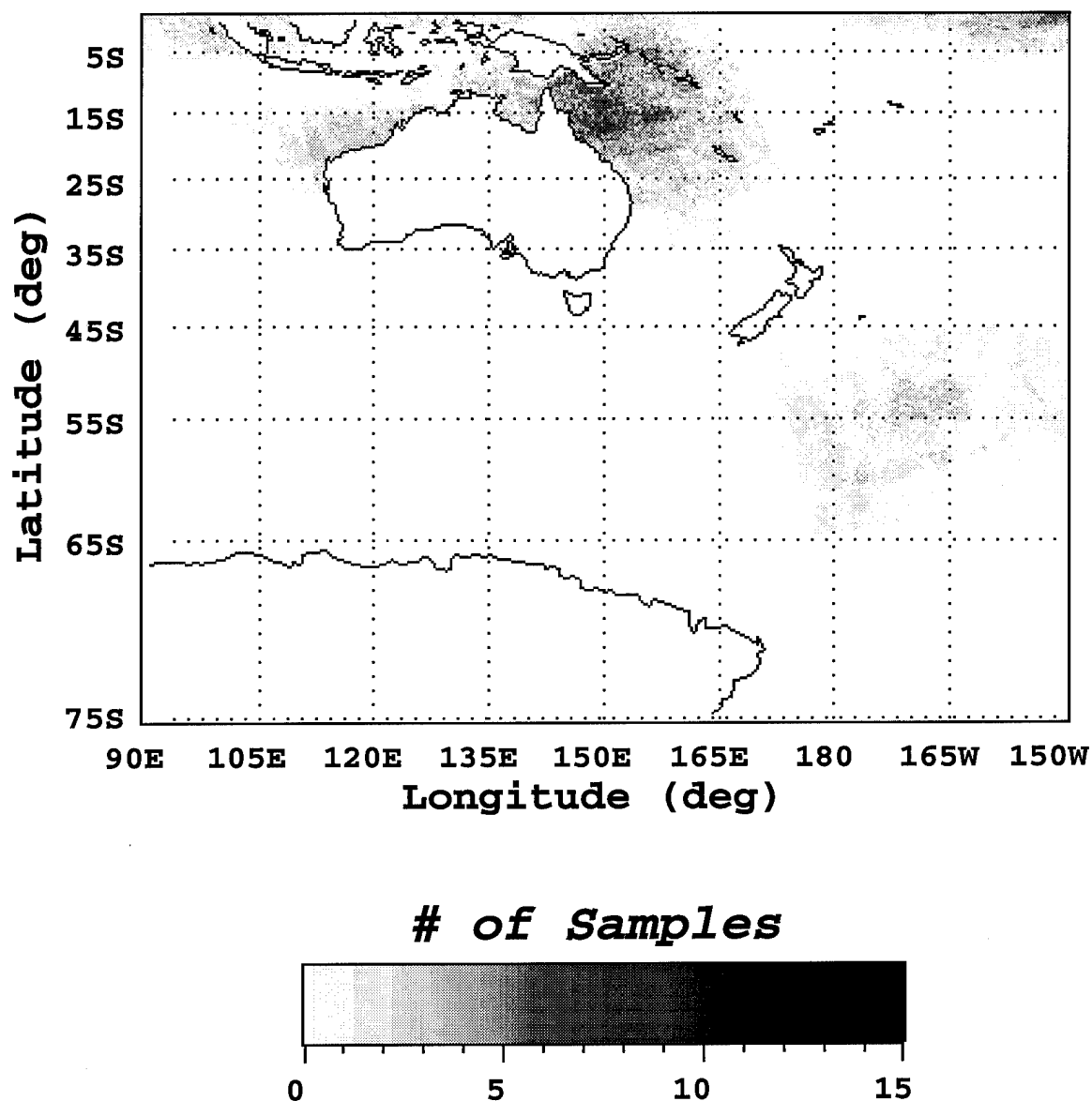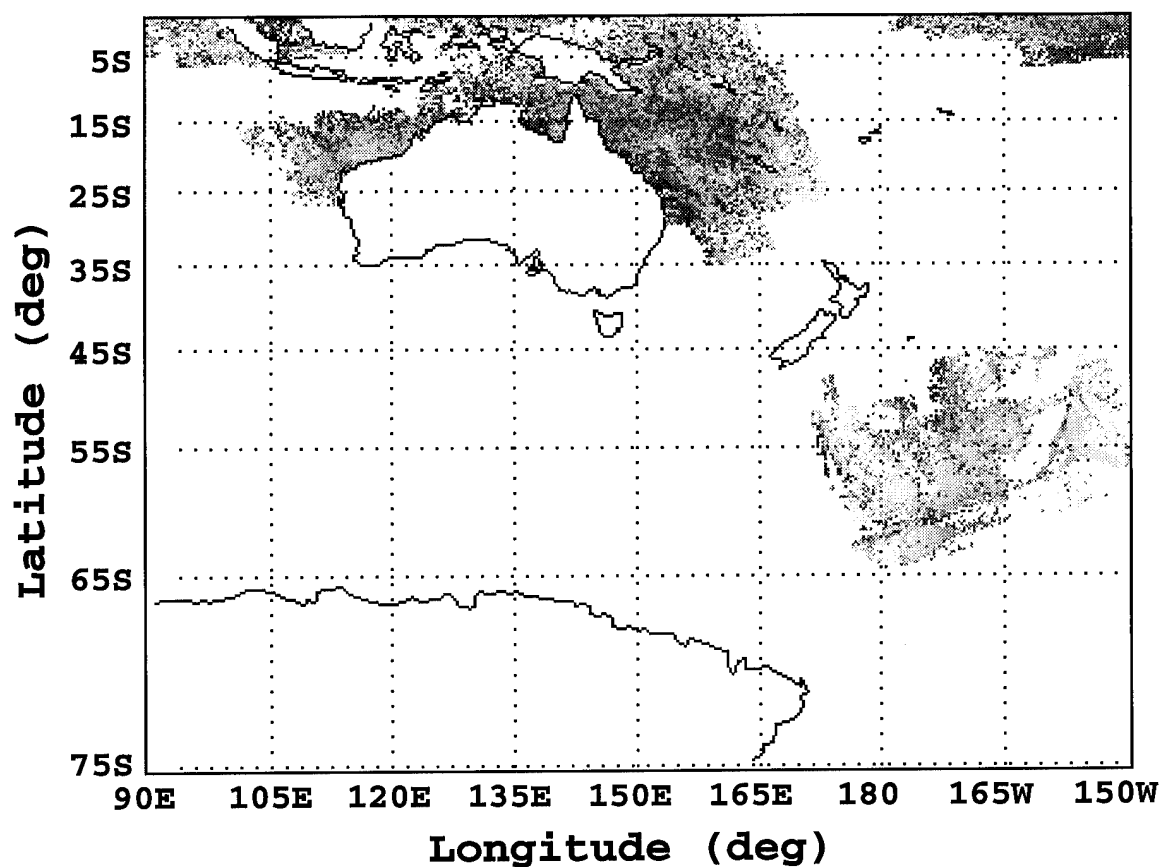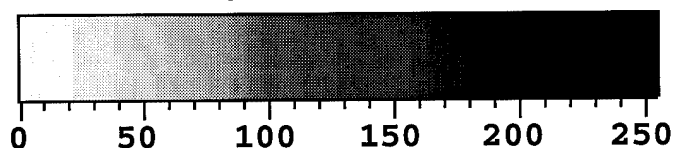## (Dec79)

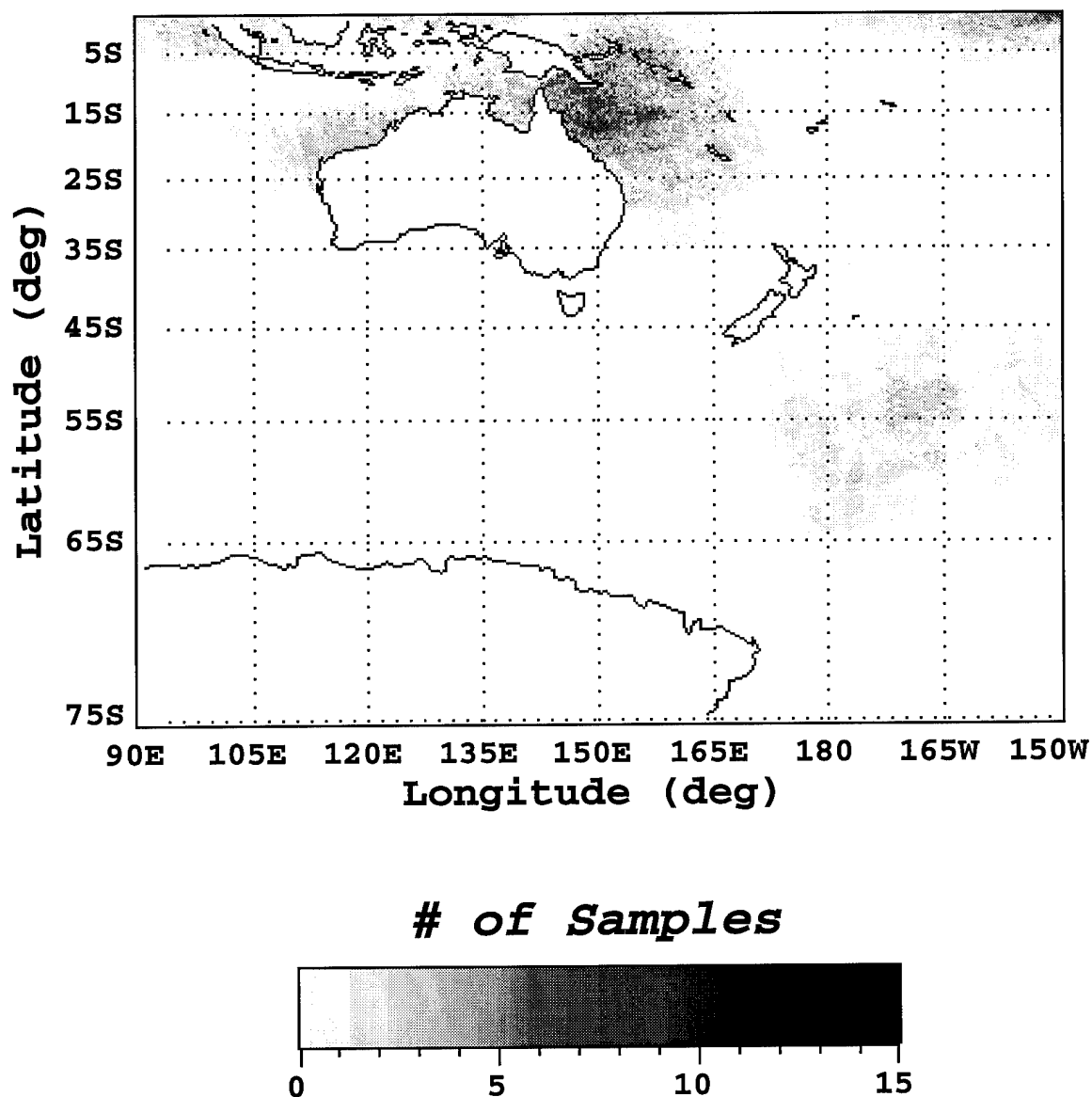# # of Samples

Figure 25. Data density for December 1979. The values
indicate the number of samples at each pixel used to
compute the associated aerosol composite (Figure 24).

Wind Vectors (Nov79)

Longitude (deg) $\longrightarrow$ 25

Streamlines (Nov79)

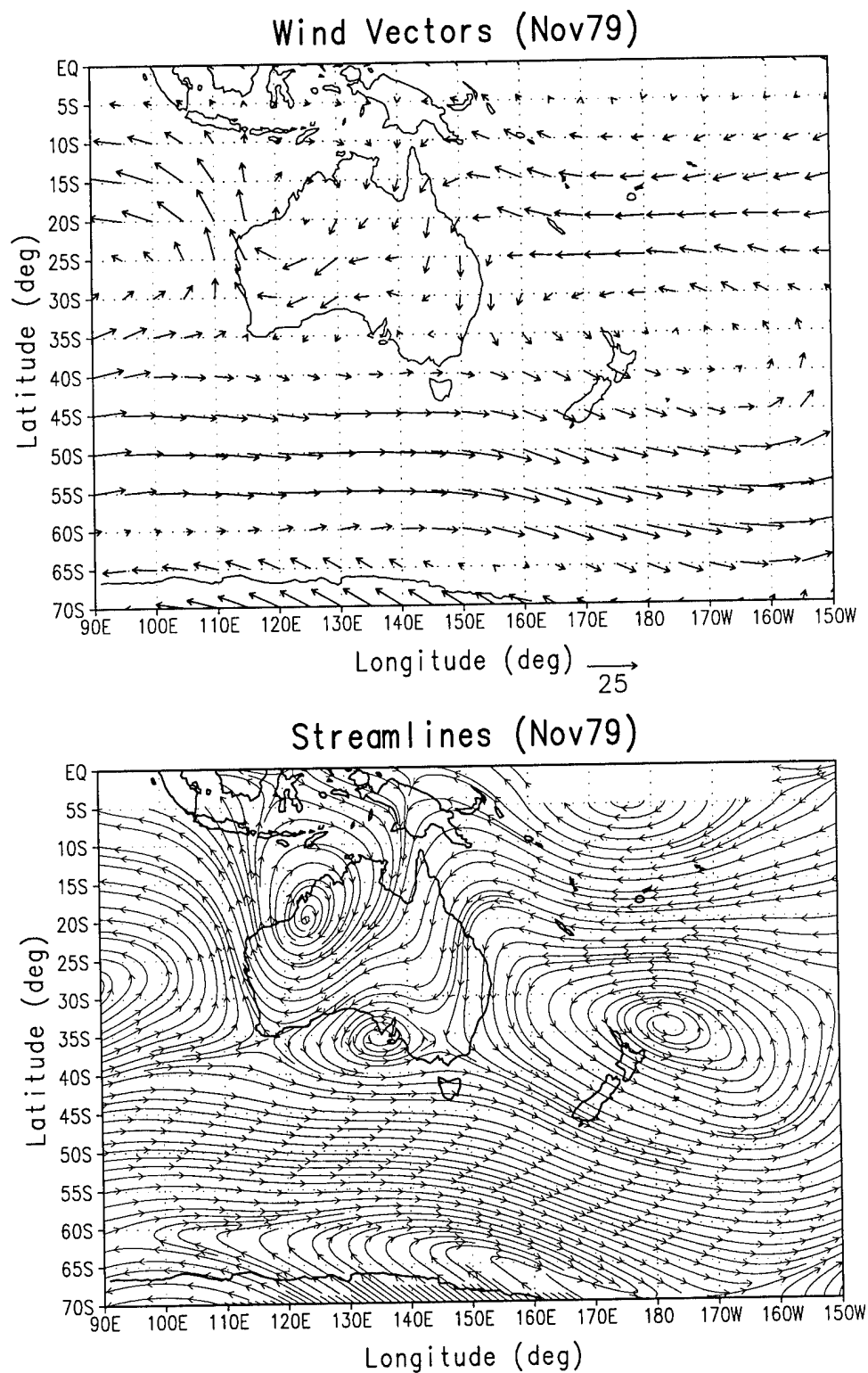

Figure 26. Low level mean wind field for November 1979. Plots were derived from the ANMRC 1000mb and 850mb grid analysis data.

Wind Vectors (Dec79)
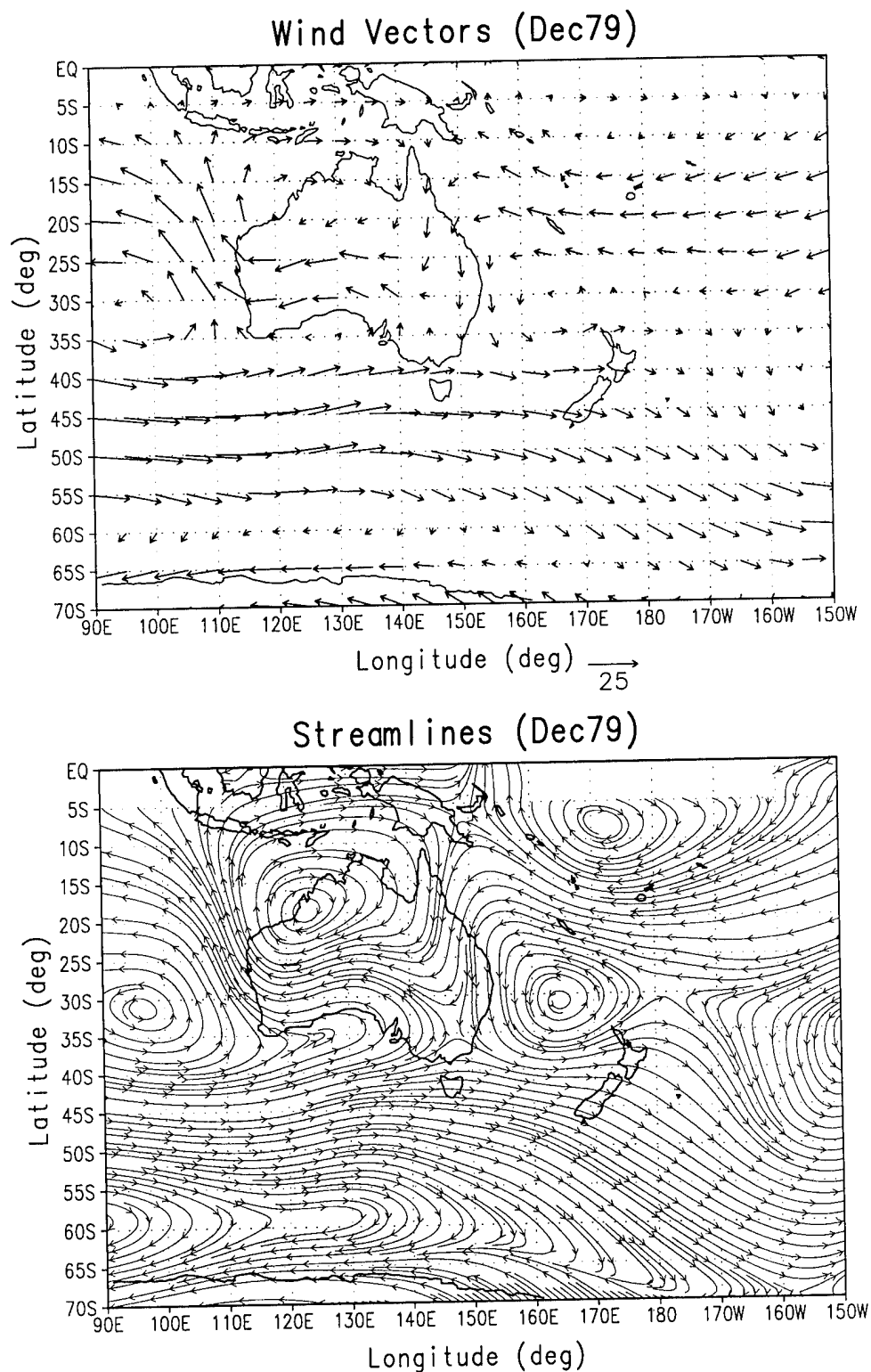

Streamlines (Dec79)

Figure 27. Low level mean wind field for December 1979.
Plots were derived from the ANMRC 1000mb and 850mb grid
analysis data.

smoke resulting from biomass burning in the tropics can be transported for thousands of kilometers. However, he also points out, due to dispersion, settling, and removal by precipitation, the concentration of smoke particulates is significantly reduced as the smoke cloud is transported further from its source. The distance from the eastern tip of New Guinea to the extreme northeast component of the study region is approximately 6,000 *km*. If it were accepted that a mechanism for westerly transport existed during the period of the five scans in December 1979 (Figure 25), the probability that the winds were light is great. When an average westerly wind speed of 20 *kph* is assumed (a rather generous assumption), the smoke cloud would have to travel for nearly three weeks before it would reach the location in question. The wind data in Figure 27 suggests this would be highly unlikely.

As a result, although it is thought that biomass burning contributes to the aerosol signature between Australia and New Guinea, particularly in the winter months, the CZCS data suggests it is not the only source of the 'red band' signal.

Aerosols Generated from Biogenic Hydrocarbon Production in the Tropics

According to Heicklen (1976), there are two primary sources of organic hydrocarbons in the atmosphere: CH_4 emissions from natural sources (>86%) and terpene emissions from vegetation (~9%). [The remaining atmospheric hydrocarbons are thought to be of anthropogenic origin.] Of particular interest in this research, the terpene vapors released by vegetation may undergo gas-to-particle photochemical reactions producing organic aerosols.

Due to the complexity of the primary and secondary processes which form these aerosols, little is known about the extent of their contributions to total aerosol concentrations (National Research Council, 1993). However, it has been hypothesized that over dense forest regions, the aerosol contributions resulting from terpene emissions may be significant. In particular, Pandis *et al.* (1991) have shown this seems to be the case during stagnant conditions in North American national forests where the emissions of reactive organic hydrocarbons are often appreciable. Furthermore, the

National Research Council (1993) feels there is reason to believe these organic aerosols may significantly affect visibility in the national forests due to their light scattering properties.

Therefore, due to the dense tropical forests in northern Australia and New Guinea, it seems reasonable to conclude organic aerosols could potentially contribute to the 'red band' signal evidenced in this region. However, the same arguments mentioned in the previous section with regard to the average wind field would most likely preclude it from being a source for the eastern portion of the signal.

A False Signal Resulting from Scans Over Case 2 Water

In general, the optical properties of ocean water have been categorized into two classes: Case 1 and Case 2 water. Case 1 water is dominated by the biological constituents of the ocean, i.e. phytoplankton and their immediate degradation products. It typically ranges from blue to green in color, becoming more green with increased biological activity. In addition to all the elements in Case 1 water, Case 2 water also contains "terrigenous material associated with coastal runoff, suspended material, and yellow substance." The yellow substance is "dissolved organic matter of terrestrial origin in some stage of decay" (Simpson, 1993). Case 2 water is generally located in coastal regions where the terrestrial sources are plentiful.

According to Simpson (1993), although Case 2 waters make up a relatively small percentage of the total ocean surface, they are often "scientifically, environmentally, and economically extremely important because they often coincide with the locations of major oceanic fisheries and human recreational zones." Due to the specular properties of the suspended terrestrial material in Case 2 water, the water-leaving radiance for the aerosol channel (670*nm*) will not necessarily be near zero. [From Chapter II, this is a fundamental assumption in the atmospheric correction algorithm.] As a result, there is reason to doubt the reliability of the CZCS imagery over Case 2 water as the aerosol radiances measured may be erroneously high (Simpson, 1993).

Because the ocean floor between Australia and New Guinea is a continental shelf, Case 2 water could be a factor in this region. Shallow depths (less than $50m$ in some locations of the region in question) are often associated with relatively large amounts of suspended material due to the turbidity of the water (Simpson, 1993). In addition, due to the mountainous topography of New Guinea, it would be expected that there may be considerable runoff in the summer months when precipitation is plentiful. Milliman and Meade (1983) have suggested that the rivers in New Guinea and the islands north of Australia carry significant amounts of sediment into the surrounding oceans. Naturally, in the ocean regions immediately surrounding the islands, the terrestrial material in this runoff would contribute to the potential errors associated with Case 2 water. In theory, it is also conceivable that the westerly equatorial undercurrent would transport these sediments east of the islands, thereby, providing a possible explanation for the eastern portion of the 'red band' signal.

Although the conclusion is speculative in nature, the region of the 'red band' immediately surrounding New Guinea might be attributed, at least in part, to the ocean color. While the turbidity of the waters in the continental shelf might help explain the enhanced signal throughout the year, the increased runoff during the summer months would support the apparent intensification of the signal during the same period (compare Figures 18 and 20).

An artifact of Cloud-masking and Electronic Overshoot

There are two residual problems in the CZCS data which may account for erroneously high radiance measurements (Simpson, 1993). The first results from limitations in the CZCS cloud-masking algorithm and the second is a result of electronic overshoot of the sensor.

The CZCS masking algorithm is broken up into two segments: land-masking and cloud-masking. Using the Channel 5 data ($700-800nm$), the algorithm assumes a predetermined minimum radiance count from which those pixels exceeding this threshold are considered to be contaminated by land or clouds. Once a pixel has been

flagged, the radiance is converted into an albedo percentage to further distinguish between clouds and land.

Because the 'red band' is located in the tropics, the issue of cloud-masking becomes particularly important. Due to the moisture-rich airmasses and the convective heating in and around the ITCZ (Intertropical Convergence Zone), tropical regions are commonly associated with persistent cloud cover (Wallace and Hobbs, 1977). Evidence of this can be found in Figure 28. While cloudiness over the region of the 'red band' typically increases in the Austral summer, relatively extensive cloud coverage exists throughout the year.

Related to the cloud-masking portion of the algorithm, the first residual problem results from undetected clouds which can "produce significant errors in the derived water-leaving radiances" (Simpson, 1993). In short, in regions where the clouds are sufficiently thin, the measured radiance may not meet the predetermined threshold. Naturally, this results in cloud pixels which are not effectively masked and therefore, erroneously contribute to the aerosol radiance (L_a). These 'thin cloud' conditions typically occur in high wispy cirrus clouds and at the edge of clouds. Cirrus clouds are often partially transparent due to relatively low concentrations of cloud droplets which may then be mistakenly represented as aerosols. However, cloud formations at lower levels (i.e. cumulus and stratus) tend to be relatively dense within the cloud's interior (Wallace and Hobbs, 1977). Nonetheless, these clouds can contribute to elevated aerosol radiances as well. In this case, the 'thin cloud' conditions apply to the cloud edges, where continuous formation and dissipation of cloud droplets often occurs.

Hooker *et al.* (1993) points out an additional problem with the CZCS cloud-masking algorithm which is primarily confounded to the equatorial region. Because the ascending node of the Nimbus-7 occurred near local noon, the images near the equator were taken when the sun was positioned behind the sensor which would result in significant sun glint directly below the sensor. While tilting the sensor $\pm20°$ north or south may reduce this problem, due to the solar-sensor geometry, there was no effective way to satisfactorily correct for it altogether. The cloud-masking algorithm would
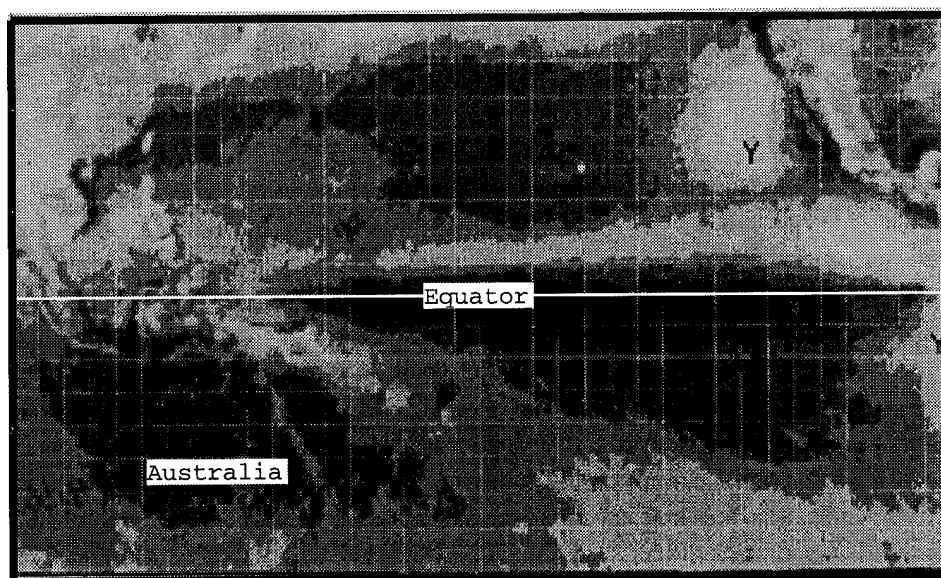
January 1967–1970
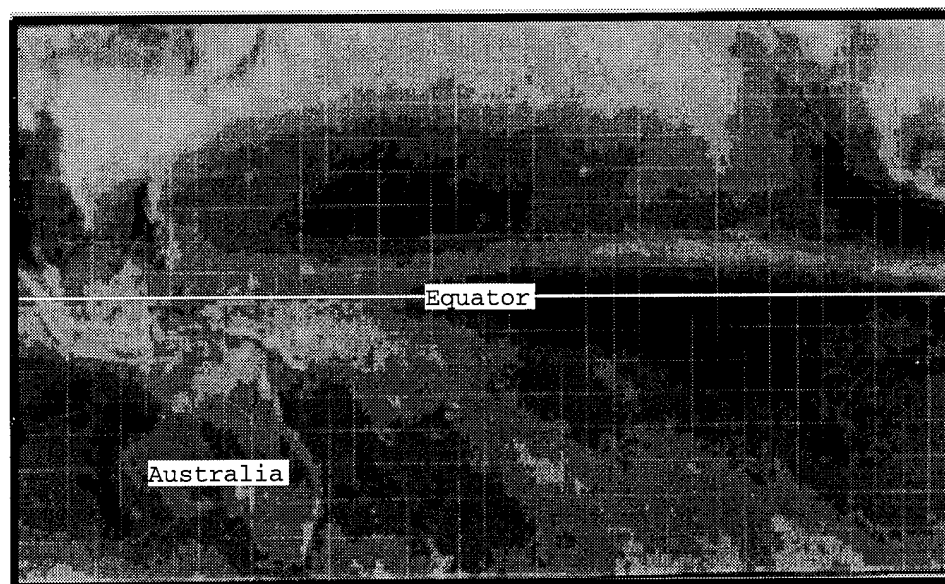
July 1967–1970

Figure 28. Persistent cloud formations. Reflectivity as determined from satellite observations. The brightest areas are characterized by persistent cloudiness. (Adapted from U.S. Air Force and U.S. Department of Commerce, 1971.)

typically mask the center of these images where the radiance values exceeded the threshold. However, the reflection off the ocean surface did not have a sharp boundary but instead gradually decreased in intensity with distance from nadir. This meant the radiance gradient would eventually drop below the threshold for cloud-masking, resulting in a ring of elevated radiances around the edges of the masked region. [This is analogous to the 'thin cloud' conditions mentioned above.] As a result, it was discovered that, in some cases, the center of CZCS images in the equatorial region may have been contaminated by specular radiances from the ocean surface.

The second residual problem results from electronic overshoot of the CZCS (Simpson, 1993). Due to the slow response time of the analogue amplifiers in Channels 1-4, it has been shown that unrealistically high radiance counts can be recorded in pixels east of a cloud. Because cloud radiances often saturate the sensor at these lower wavelengths, the sensor experiences a lag as it scans east of the cloud and temporarily registers elevated radiance values. [Recall from Chapter II, the CZCS scans from west to east.] According to Mueller (1988), this lag may extend over considerable distances (up to 100 pixels or ~80km in extreme cases). The CZCS algorithm attempts to correct for this by extending the cloud mask east of an apparent cloud, but the effectiveness of this correction has not been quantitatively determined.

Since the 'red band' is located in a particularly cloudy region, it is possible that the residual problems addressed above are potential sources for the elevated signal.

Evidence of Elevated Aerosol Concentrations over the Indian Ocean and Tasman Sea

As was mentioned in Chapter II, dust events are most frequent in arid regions with little vegetation. A global distribution of the major dust sources and the predominant dust trajectories from these regions is included in Figure 29. The extensive arid and semi-arid regions in much of central Australia suggest it is a potential dust source. In addition, due to the transport trajectories, the figure indicates the regions off the coast
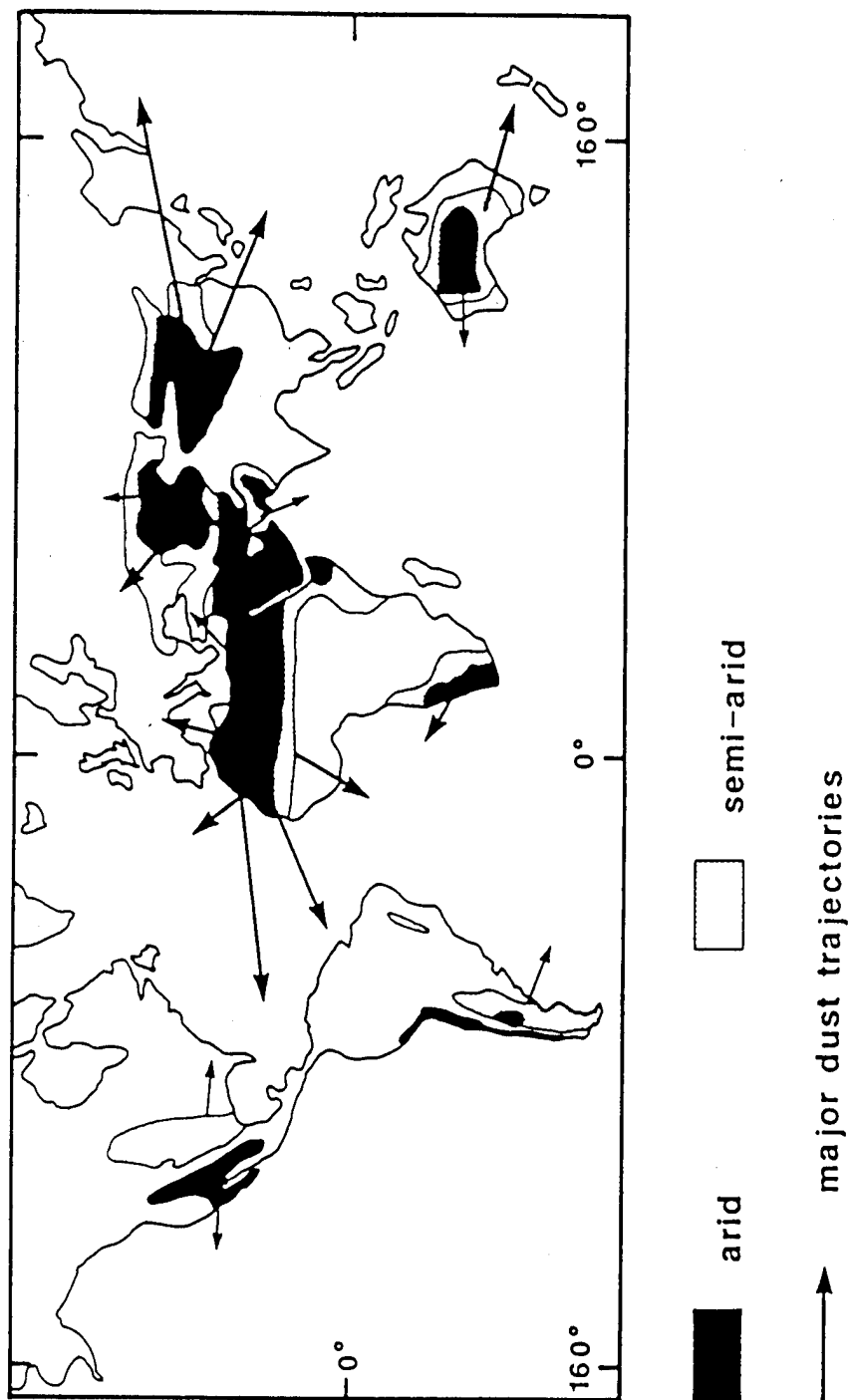
Figure 29. Distribution of areas with high dust-storm activity and major dust trajectories. (From Pye, 1987.)

of Australia over the Tasman Sea and Indian Ocean might contain elevated aerosol concentrations (Pye, 1987).

Indian Ocean Region

There is little empirical evidence of elevated dust concentrations off the northwest coast of Australia over the Indian Ocean (Pye, 1987). [In the following discussion, this region will be referred to as the Indian Ocean Region or IOR (Figure 1).] Because an Australian dust source and transport mechanism many exist, one might theorize suspended dust would contribute to increased aerosol concentrations over the IOR (Figure 29). For 1979, the average low level wind field is in agreement with this theory indicating there was relatively strong easterly and southeasterly flow off the northwest coast of Australia (Figure 30).

When comparing the seasonal aerosol composites in Figures 10, 12, 14, and 16, it is apparent there are elevated $670nm$ radiances over the IOR in the 1979 Austral spring (Figure 16). The corresponding data density image reveals relatively good data coverage for the same region (Figure 17). In addition, Figure 31 reveals that the average flow pattern over northwest Australia was dominated by a trough. Keeping in mind that this is an average flow pattern, the prevalent effect was to advect airmasses northeasterly over the interior of the continent. Due to the arid conditions, these airmasses are expected to have been hot and dry (Figure 29). At the base of the trough, the flow became southeasterly which would eject the airmass from the northwest coast of Australia over the Indian Ocean. The wind speed indicates a core of relatively high winds existed over this route as well. Finally, the spring season (September - November) is typically a relatively dry period in northern Australia (Figure 6). These observations suggest that the potential for dust storm activity may have been significant.

Unfortunately, there is additional information in the aerosol composites which may seem ambiguous. First, note the IOR includes coverage north of 15°S which has been identified as the 'red band'. Thus, the potential sources and uncertainties of the elevated radiances mentioned in the previous section apply. In addition, the intensity
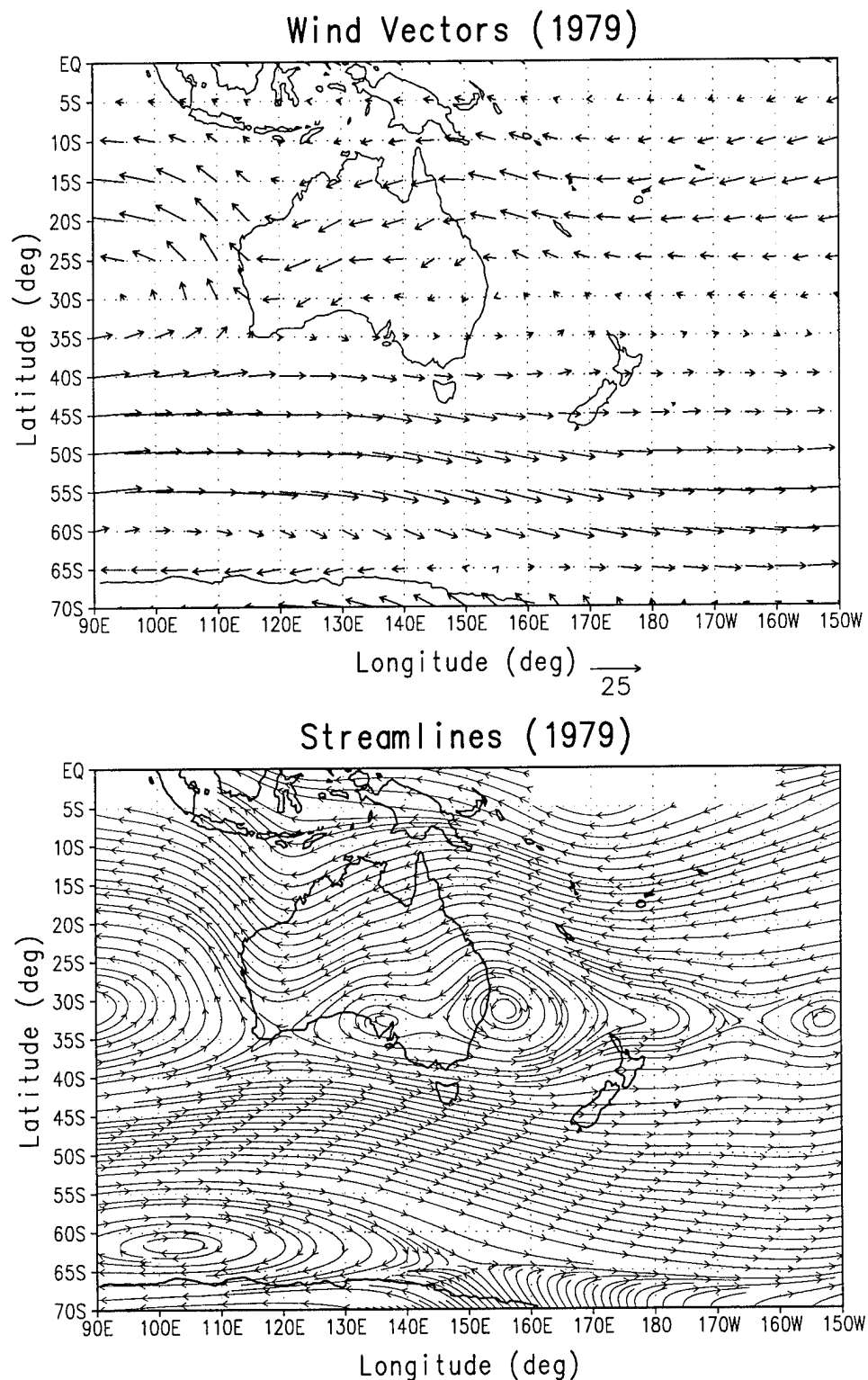
Wind Vectors (1979)

Longitude (deg) $\xrightarrow{25}$

Streamlines (1979)

Longitude (deg)

Figure 30.   Low level mean wind field for 1979.   Plots were derived from the ANMRC 1000mb and 850mb grid analysis data for January 1979 — December 1979.

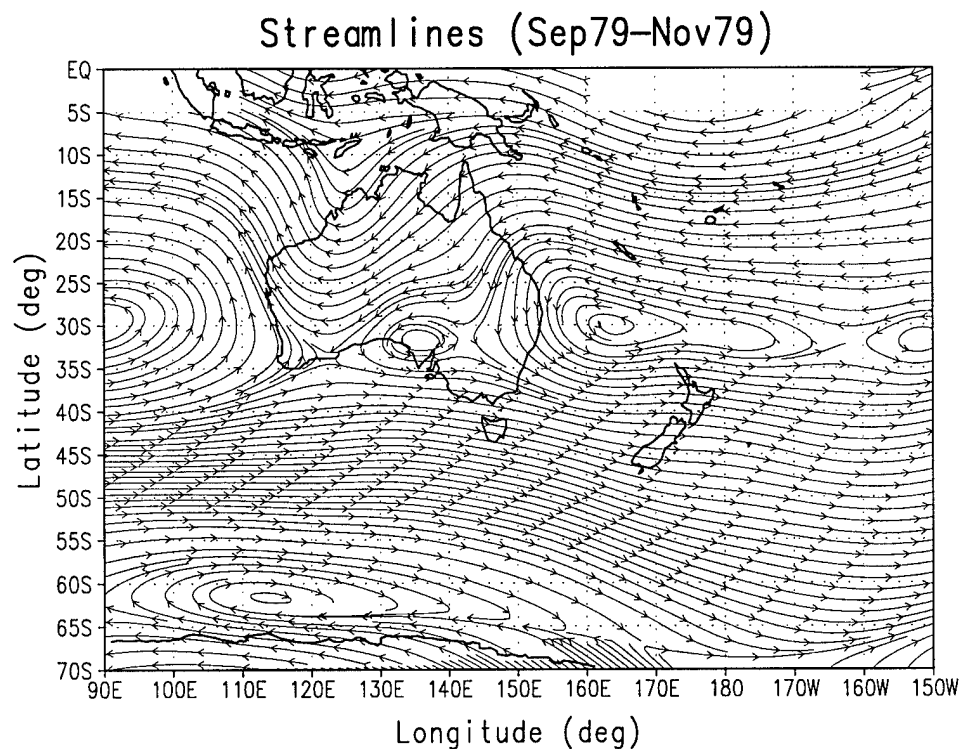## Wind Vectors (Sep79–Nov79)

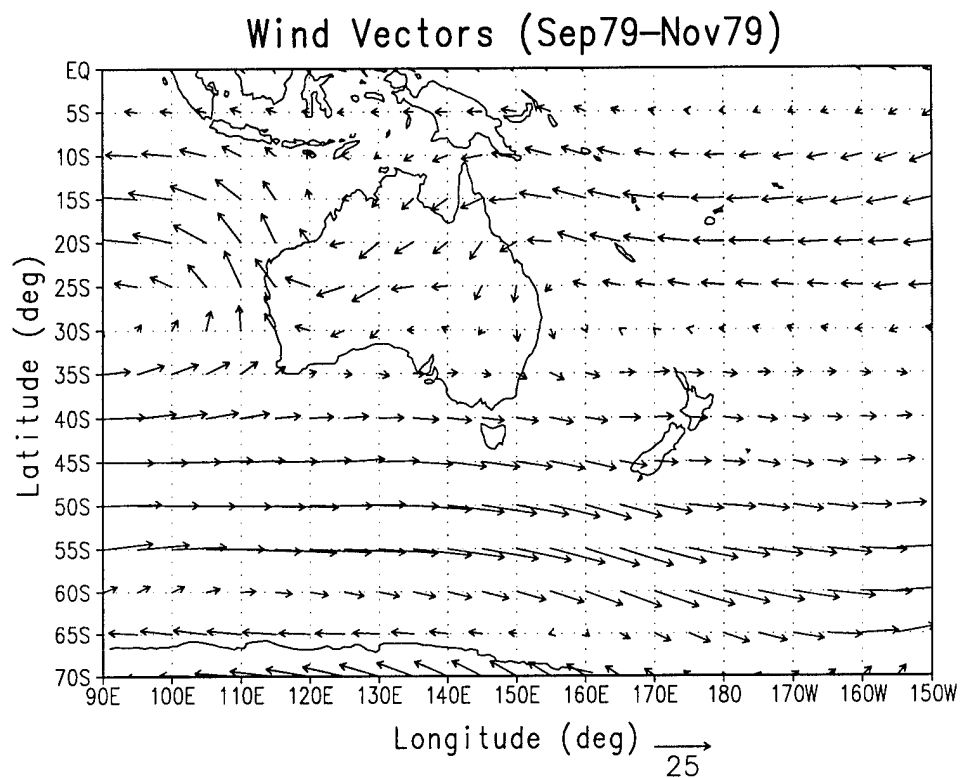

Streamlines (Sep79–Nov79)

Figure 31. Low level mean wind field for the 1979 Austral spring (4 Season). Plots were derived from the ANMRC 1000mb and 850mb grid analysis data for September 1979 – November 1979.

pattern deserves further comment. Firstly, since aerosol concentrations tend to decrease downwind from the source, one would expect the radiance signal to be highest immediately off the coast of Australia. In fact, Figure 16 indicates the opposite case is true as the radiance values are lowest at the coast and increase with distance from it. Secondly, a comparison of the IOR in Figures 16 and 17 reveals the radiance value at each pixel and the associated data density seem to be inversely related. In other words, the aerosol pattern seems to be similar to the data density pattern but opposite in intensity, meaning pixels with high data densities are typically associated with relatively low radiance values. [This pattern is also evident over the east coast of the Gulf of Carpentaria.] This suggests that the higher radiance values are not necessarily representative of higher aerosol concentrations.

Further explanation requires a look at the individual monthly aerosol composites which make up the spring season (September 1979 - November 1979). These composites and their data densities are included in Figures 22, 23, and 32-35. It is apparent that the high radiance values over the IOR were most extensive during November 1979 (Figure 22).

While the November 1979 aerosol composite (Figure 22) indicates the elevated radiances also occurred near the Australian coast, there still is a pattern of increasing radiances with distance from the coast which contradicts the expected settling effect mentioned above. However, there are at least two physical scenarios which could explain the pattern in the $670nm$ signal over the IOR. The first is that a dust event originated in the desert regions of northwestern Australia (Figures 26 and 29). The resulting cloud was then advected over the IOR and eventually became isolated from the coastal region. The second scenario is identical to the first in that a dust cloud is generated and then advected over the IOR. This time, however, a light rainfall near coastal regions of the IOR removes a portion of the suspended dust from the tail end of the cloud. From Chapter V, the onset of the monsoon season typically occurs in November while dramatic increases in rainfall do not occur until December (Figure 6) which adds credibility to this scenario.

Aerosol Composite
(Sep79)
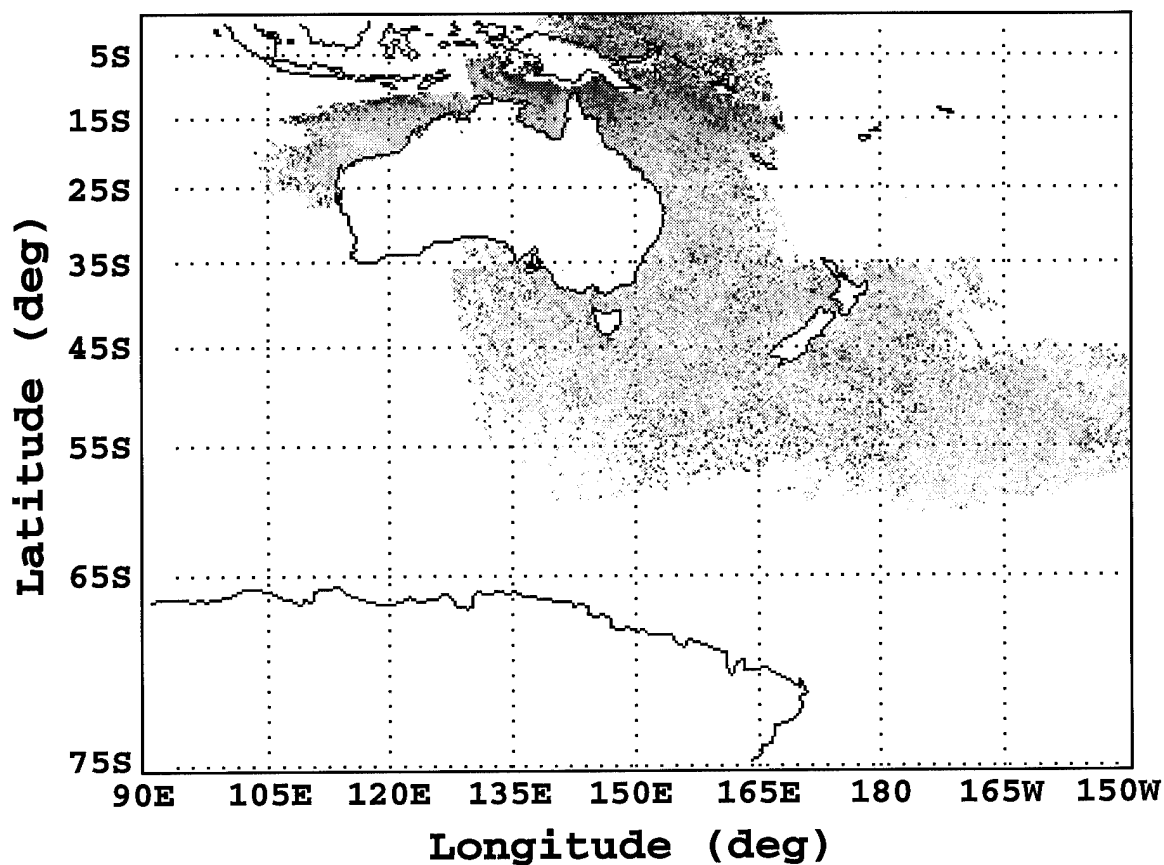
Corrected 670nm Radiance
(unitless)

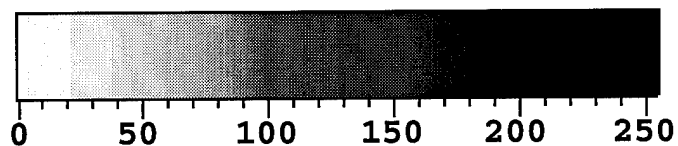Figure 32. Aerosol composite for September 1979. The values represent the average relative aerosol distribution.

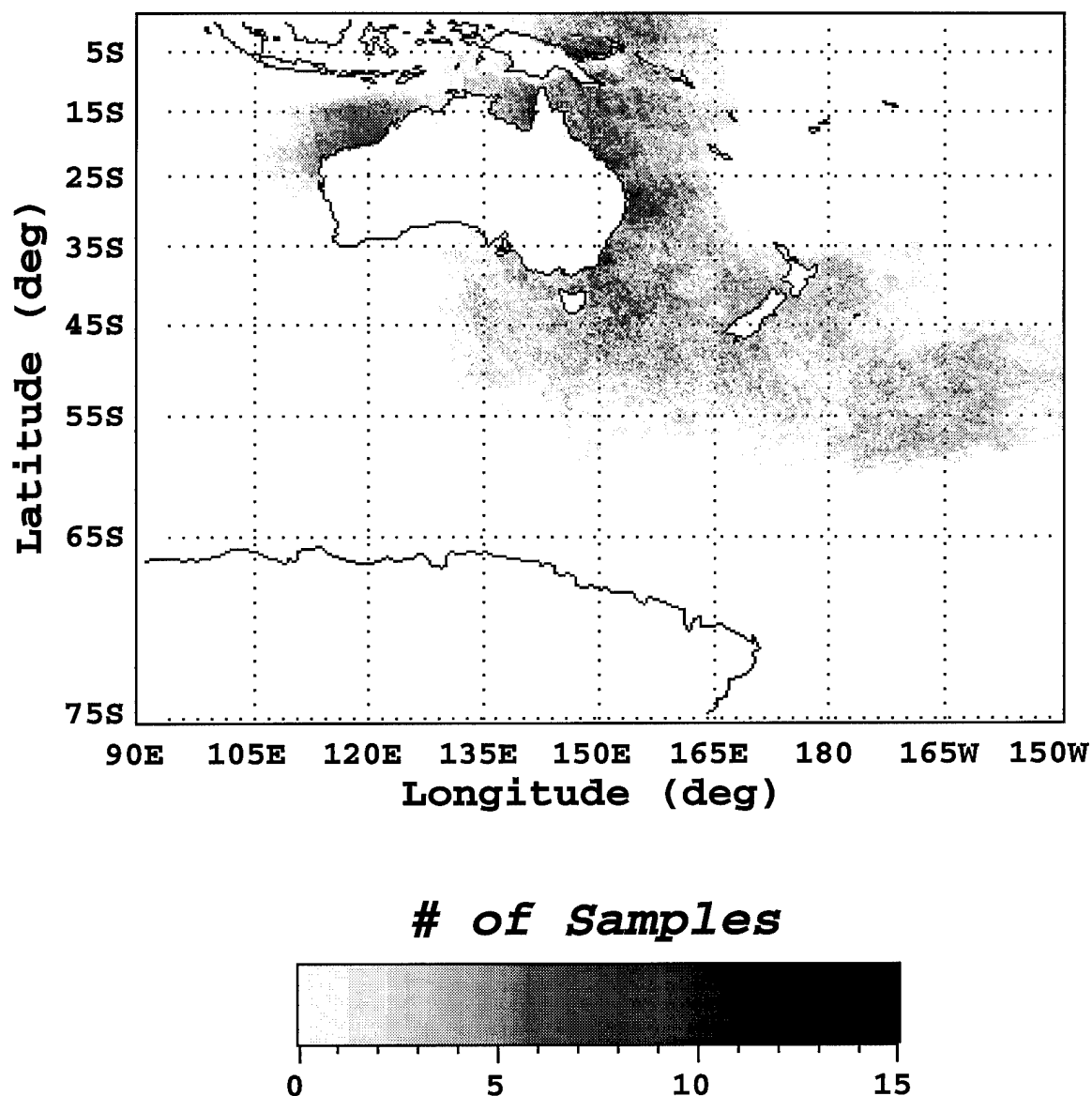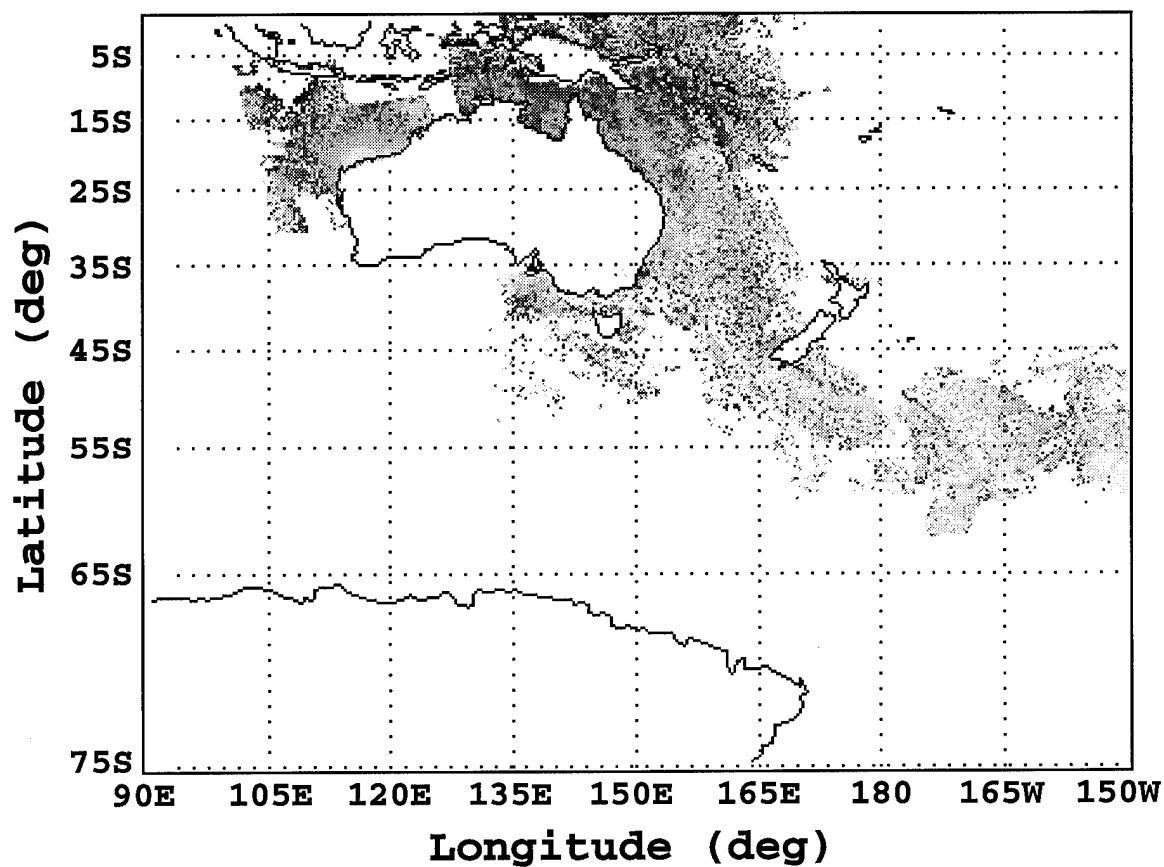# Data Density
(Sep79)

# of Samples

Figure 33. Data density for September 1979. The values indicate the number of samples at each pixel used to compute the associated aerosol composite (Figure 32).

Aerosol Composite
(Oct79)

Corrected 670nm Radiance
(unitless)
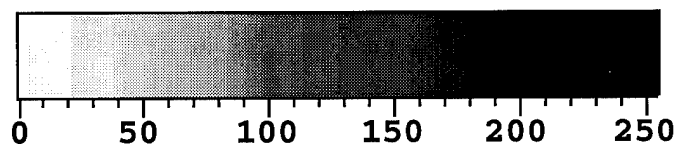
Figure 34. Aerosol composite for October 1979. The
values represent the average relative aerosol distribution.

Data Density
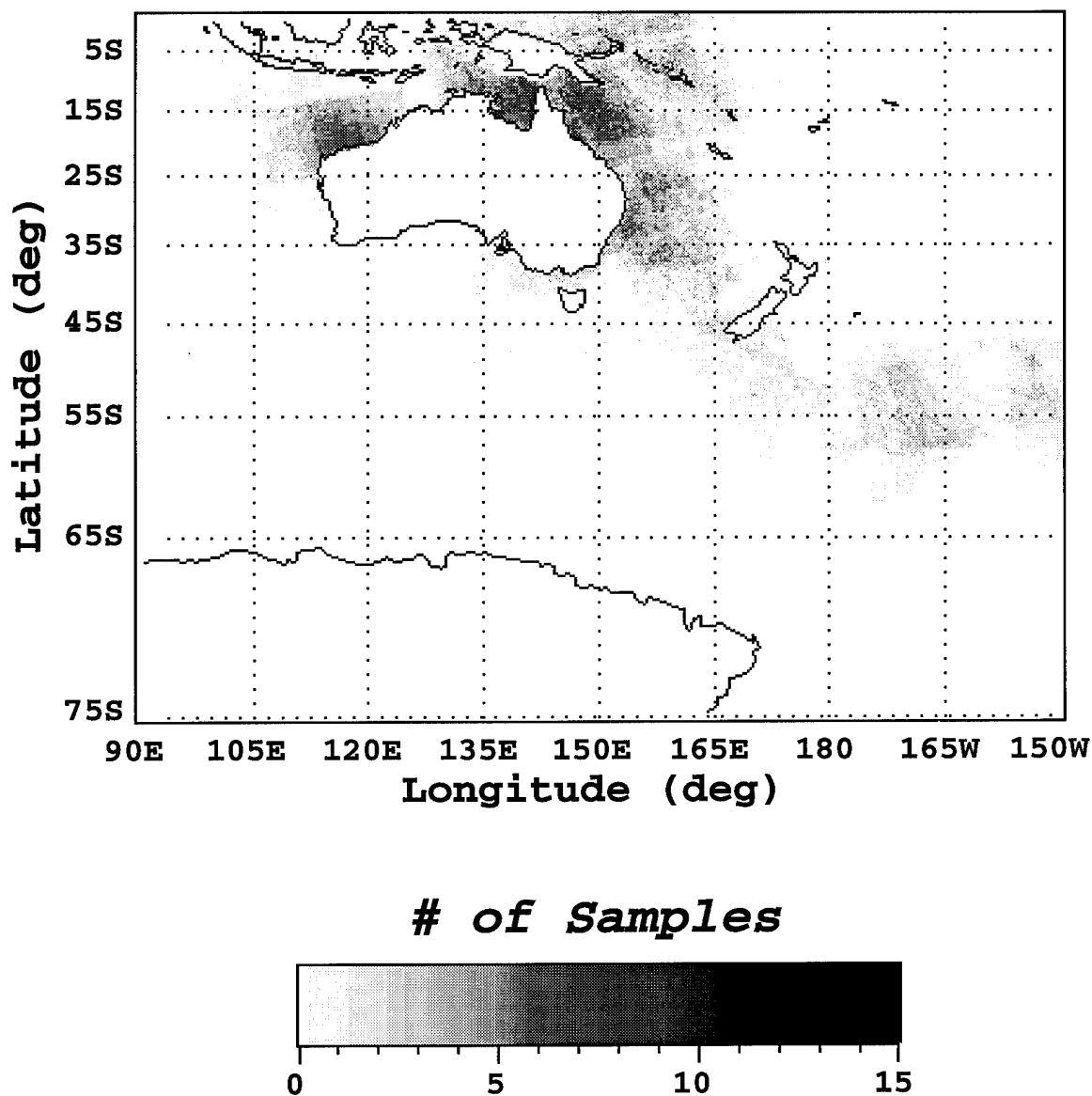## (Oct79)

of Samples

0   5   10   15

Figure 35. Data density for October 1979. The values
indicate the number of samples at each pixel used to
compute the associated aerosol composite (Figure 34).

Due to the low data densities in the offshore region of elevated radiances over the IOR, it could be argued that the high radiances were the result of one or two dust storms. If this were the case, it should be apparent when looking at the daily images. A summary of these daily images is included in Figure 36. To create this figure, two subsets of data were extracted from each daily image. [Each subset was an 18x11 grid.] The first subset was selected in a coastal region within the IOR while the second was approximately 500km offshore. On the days when data existed in both subsets, the average radiance for each subset was plotted. In other words, each point in Figure 36 represents a specific spring day where a comparison can be made between the offshore and coastal aerosol radiances. [This occurred on fourteen separate days spanning a seventy-seven day period.] In general, like the seasonal composite (Figure 16), it is evident that the daily average radiances are lower at the coast than offshore. As a result, it can be concluded that the shape of the radiance signal over the IOR in Figure 16 is a reality and not just an artifact of random scan times.

Finally, the daily images in November 1979 provide evidence which suggests the 670nm radiance signal over the IOR is not solely due to dust aerosols (Figures 37-45). [Note that averaging was not necessary in these composites since each pixel is the result of a single sample.] The highest radiance values seem to be consistently located around the perimeters of regions that have been masked which frequently occur in the center of the images (e.g. Figure 42). In addition, examination of the associated cloud images (Channel 5) reveals clouds were only significant in four of the nine daily composites for November 1979. Therefore, although 'thin cloud' conditions and electronic overshoot are most likely a factor, the data suggests sun glint is probably a significant contributor to the elevated radiances over the IOR in the 1979 spring composite (Figure 16).

Tasman Sea Region

Unlike the Indian Ocean Region, there have been a number of references to elevated mineral aerosol concentrations over the Tasman Sea due to dust storm activity within Australia. [This region will be referred to as the Tasman Sea Region or TSR in the discussion which follows (Figure 1).] In 1929, Marshall and Kidson (reviewed by
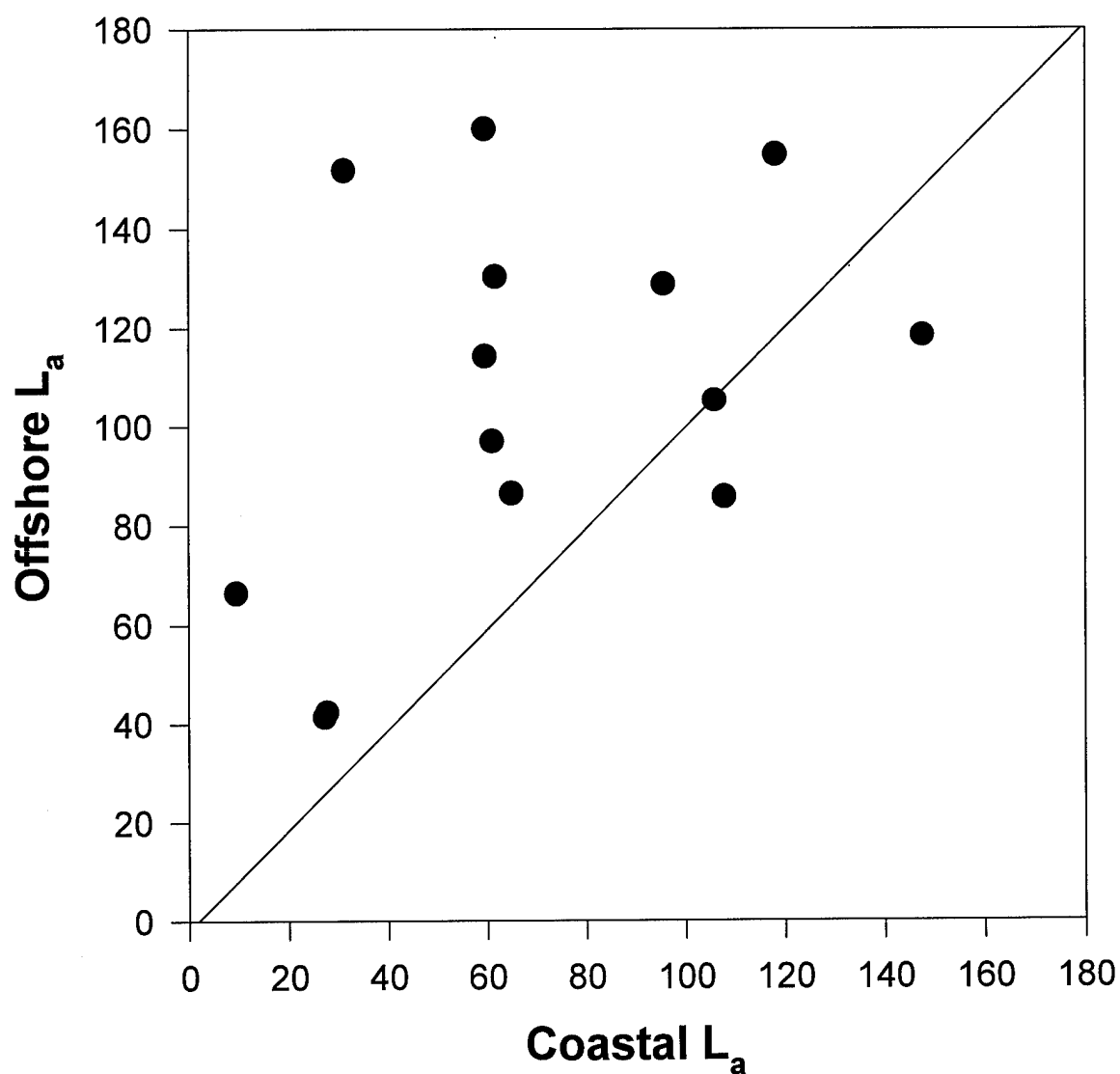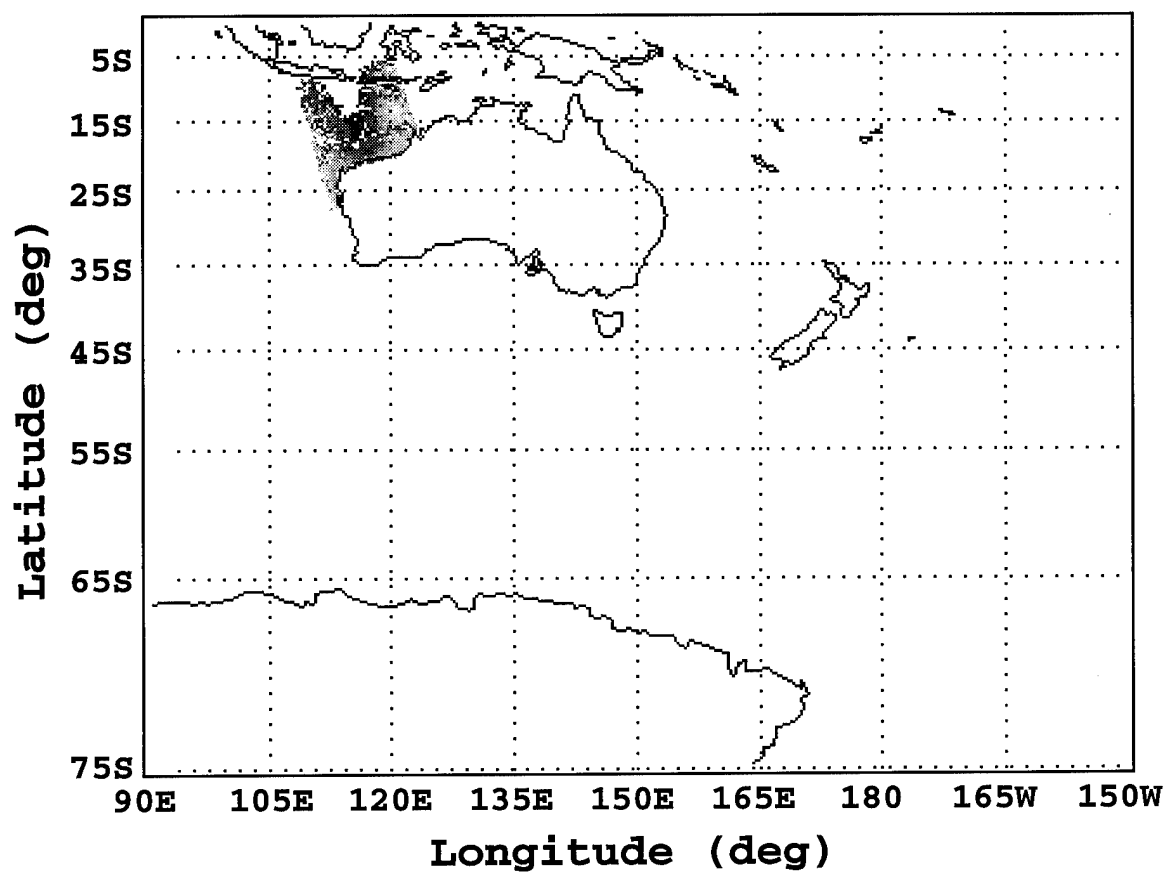
Average Daily L_a (Sep79-Nov79)

Figure 36. Average daily aerosol radiance. The points represent spring days for which an average aerosol radiance was computed at an offshore and a coastal region within the IOR.

Aerosol Composite
(1Nov79)

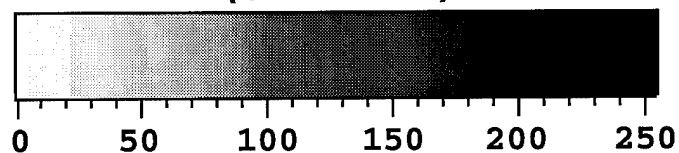**Corrected 670nm Radiance**
(unitless)

Figure 37. Aerosol composite for November 1, 1979. The composite is a sum of three scans at 04:12, 04:14, and 04:16 GMT. The values represent the relative aerosol distribution.

Aerosol Composite
(2Nov79)

Corrected 670nm Radiance
(unitless)

Figure 38. Aerosol composite for November 2, 1979. The composite is a sum of two scans at 04:33 and 04:35 GMT. The values represent the relative aerosol distribution.

Aerosol Composite
(3Nov79)

Corrected 670nm Radiance
(unitless)

Longitude (deg)
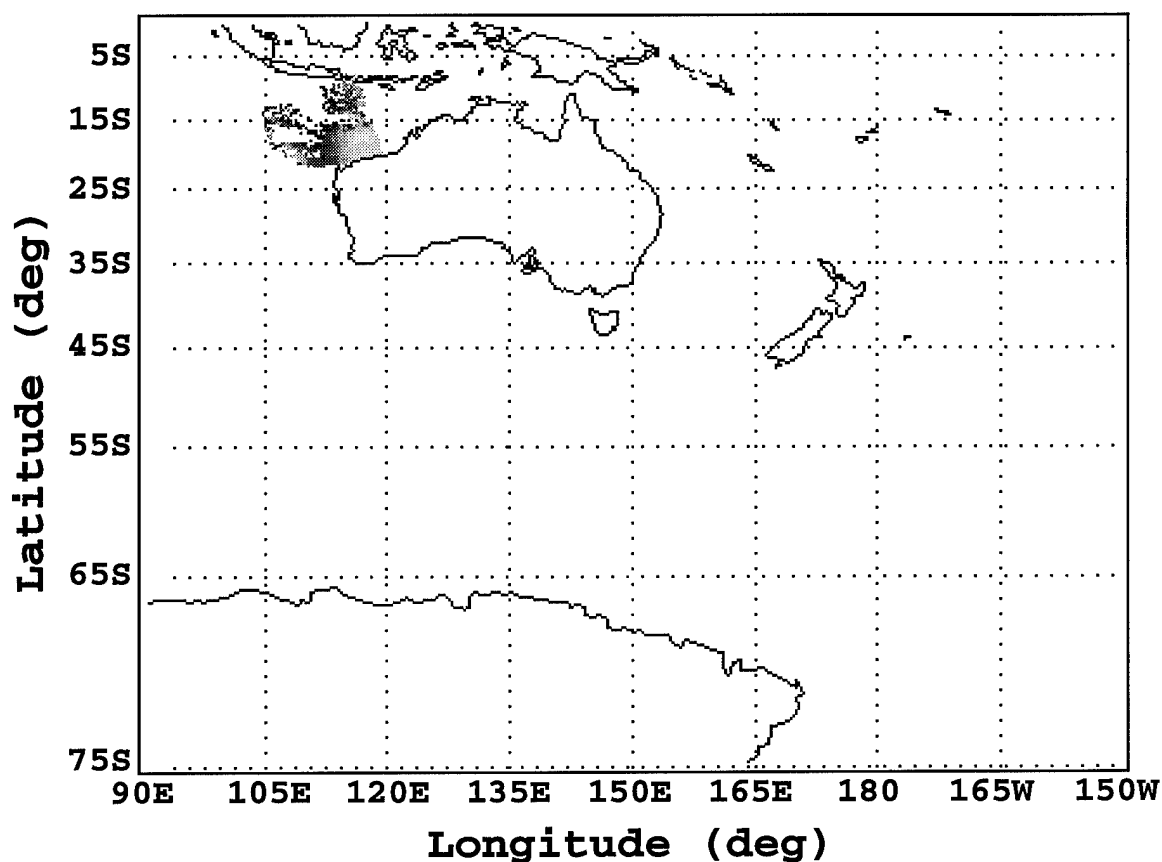
Figure 39. Aerosol composite for November 3, 1979. The composite is a sum of two scans at 04:50 and 04:52 GMT. The values represent the relative aerosol distribution.

Aerosol Composite
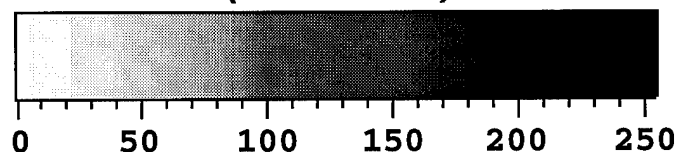## (5Nov79)

Corrected 670nm Radiance
(unitless)

Figure 40. Aerosol composite for November 5, 1979. The composite is a sum of two scans at 03:44 and 03:45 GMT. The values represent the relative aerosol distribution.

Aerosol Composite
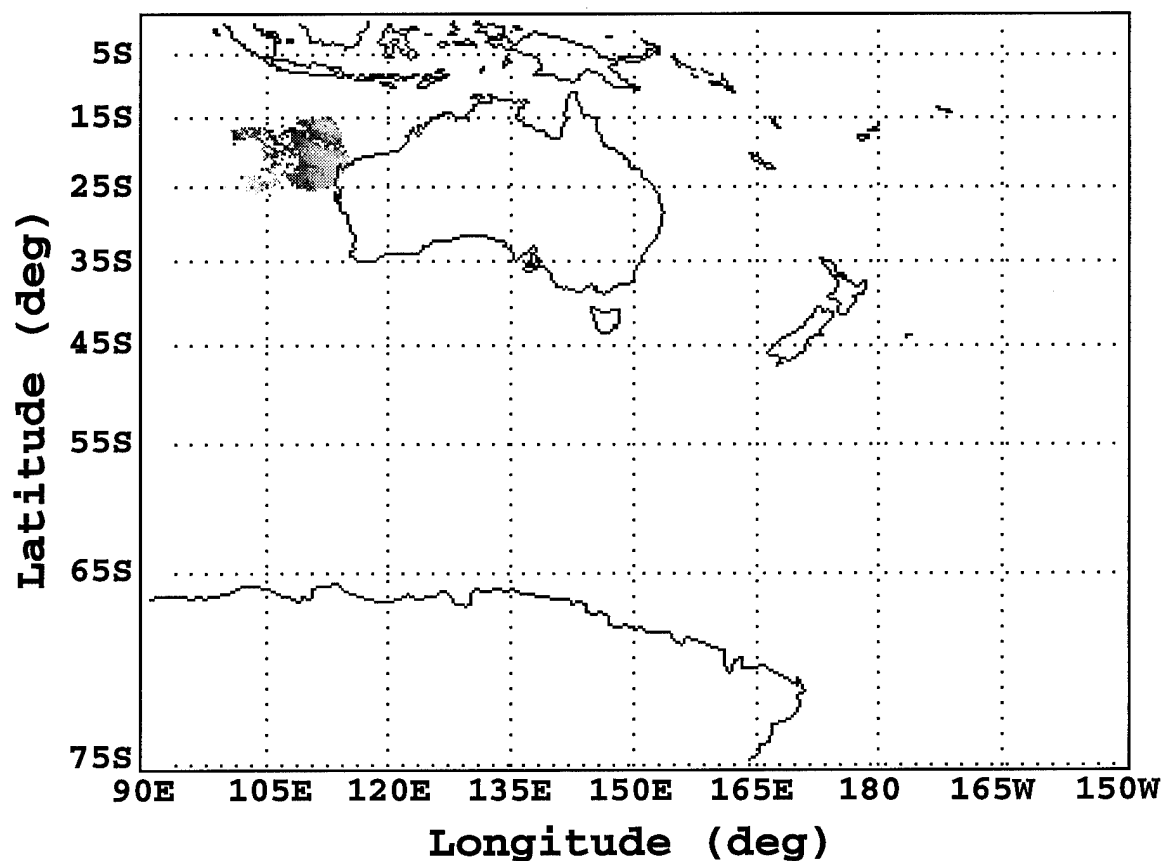## (11Nov79)

Corrected 670nm Radiance
(unitless)

Figure 41. Aerosol composite for November 11, 1979.
The composite is a sum of two scans at 03:52 and
03:54 GMT. The values represent the relative aerosol
distribution.

Aerosol Composite
(13Nov79)

Corrected 670nm Radiance
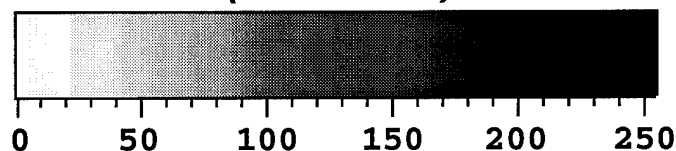### (unitless)

Figure 42.   Aerosol composite for November 13, 1979.
The composite is a sum of two scans at 04:30 and
04:32 GMT.   The values represent the relative aerosol
distribution.

Aerosol Composite
(17Nov79)

Corrected 670nm Radiance
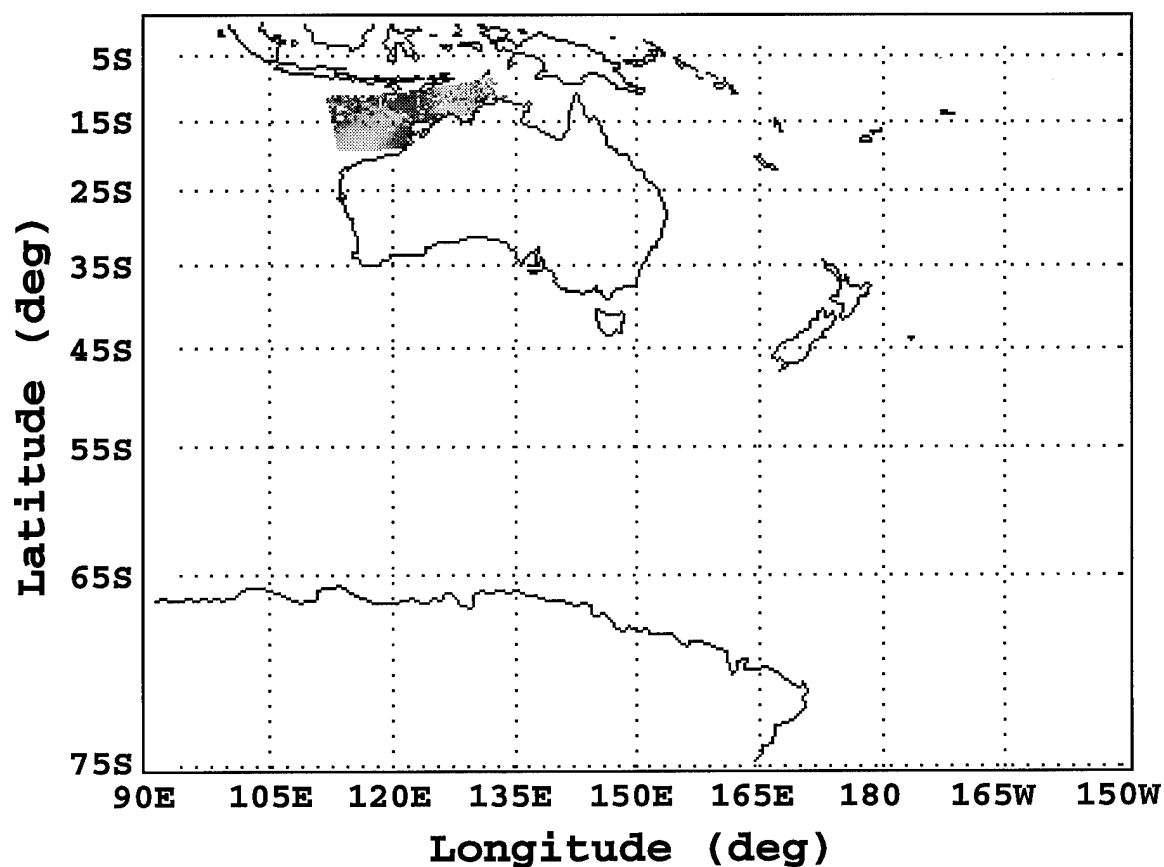*(unitless)*

Figure 43. Aerosol composite for November 17, 1979.
The composite is a sum of two scans at 04:01 and
04:03 GMT. The values represent the relative aerosol
distribution.

Aerosol Composite
(18Nov79)

Corrected 670nm Radiance
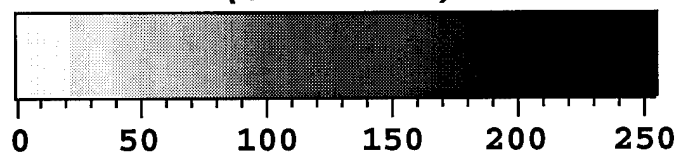### (unitless)

Figure 44. Aerosol composite for November 18, 1979.
The composite is a sum of two scans at 04:22 and
04:24 GMT. The values represent the relative aerosol
distribution.

Aerosol Composite
(23Nov79)

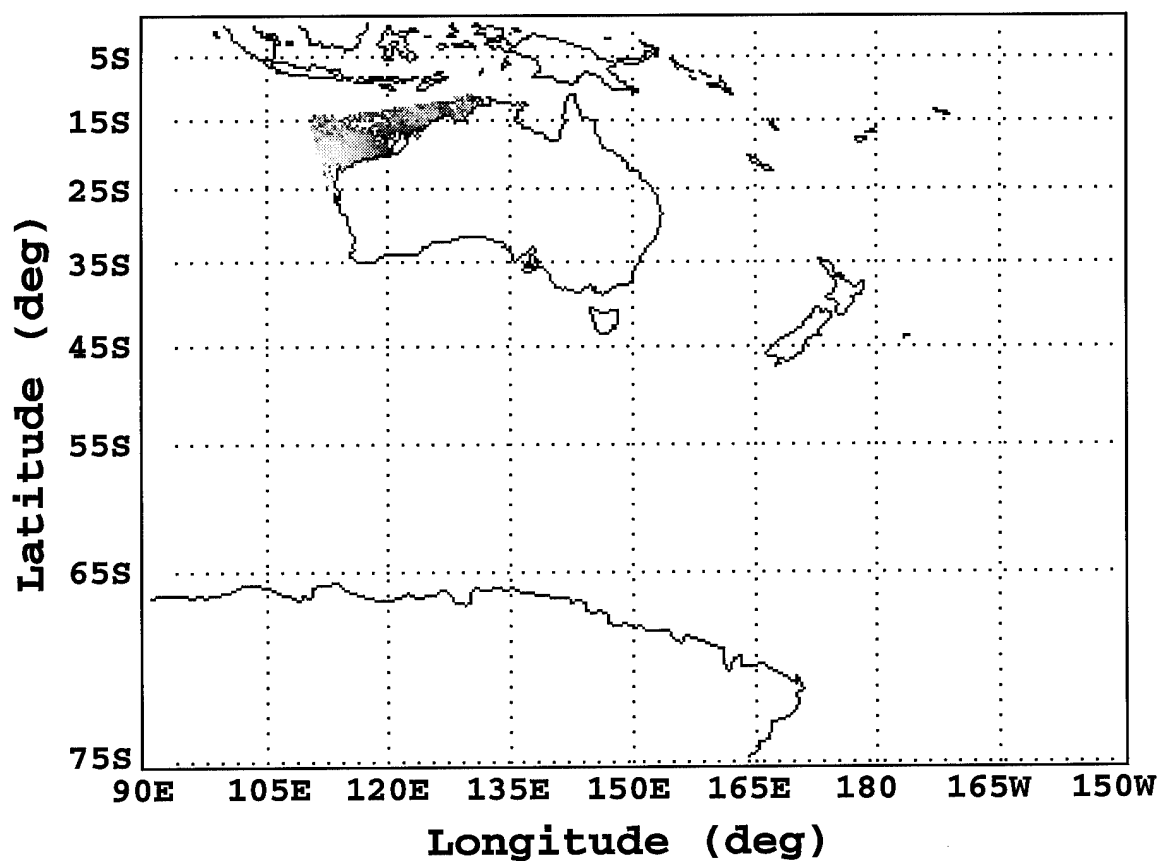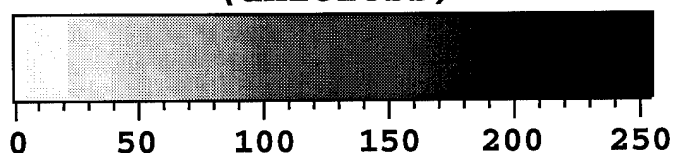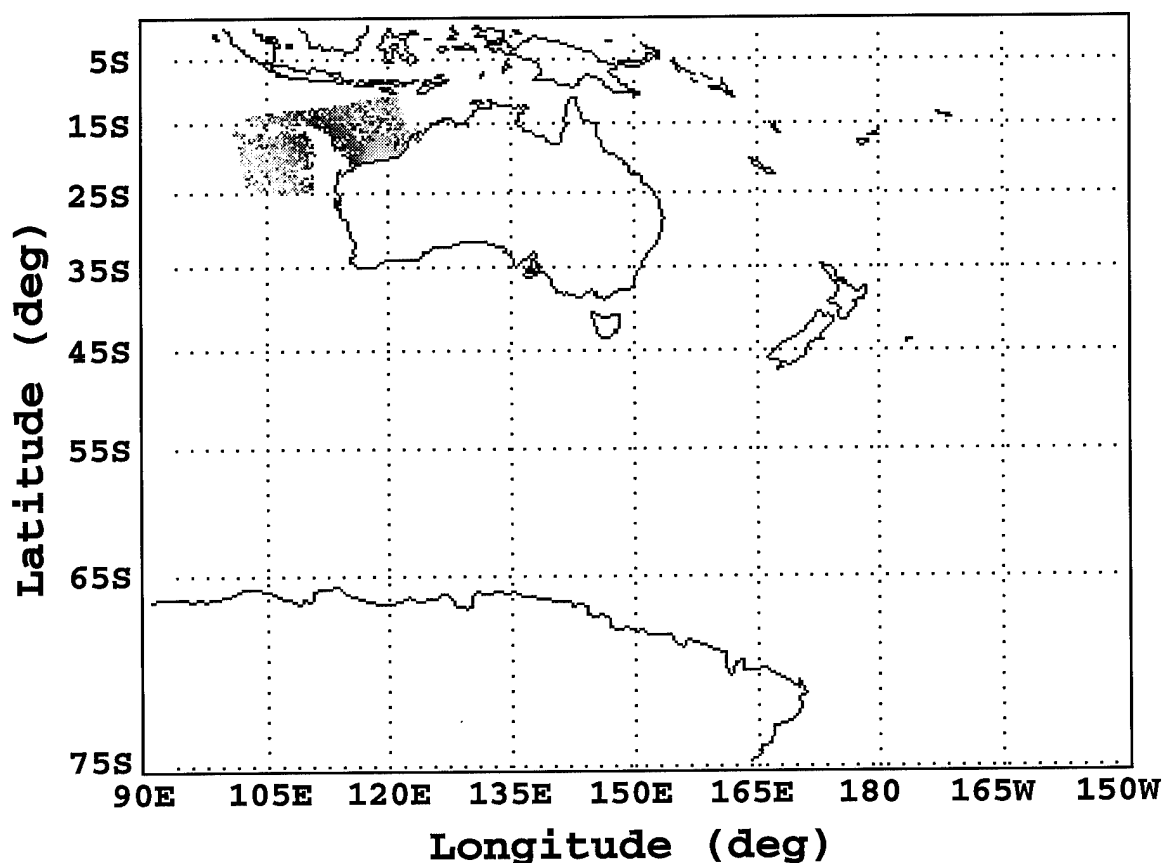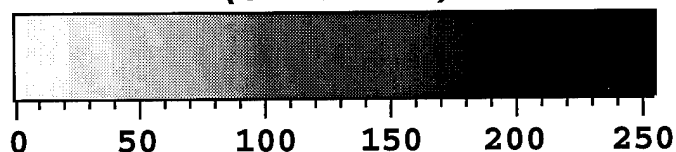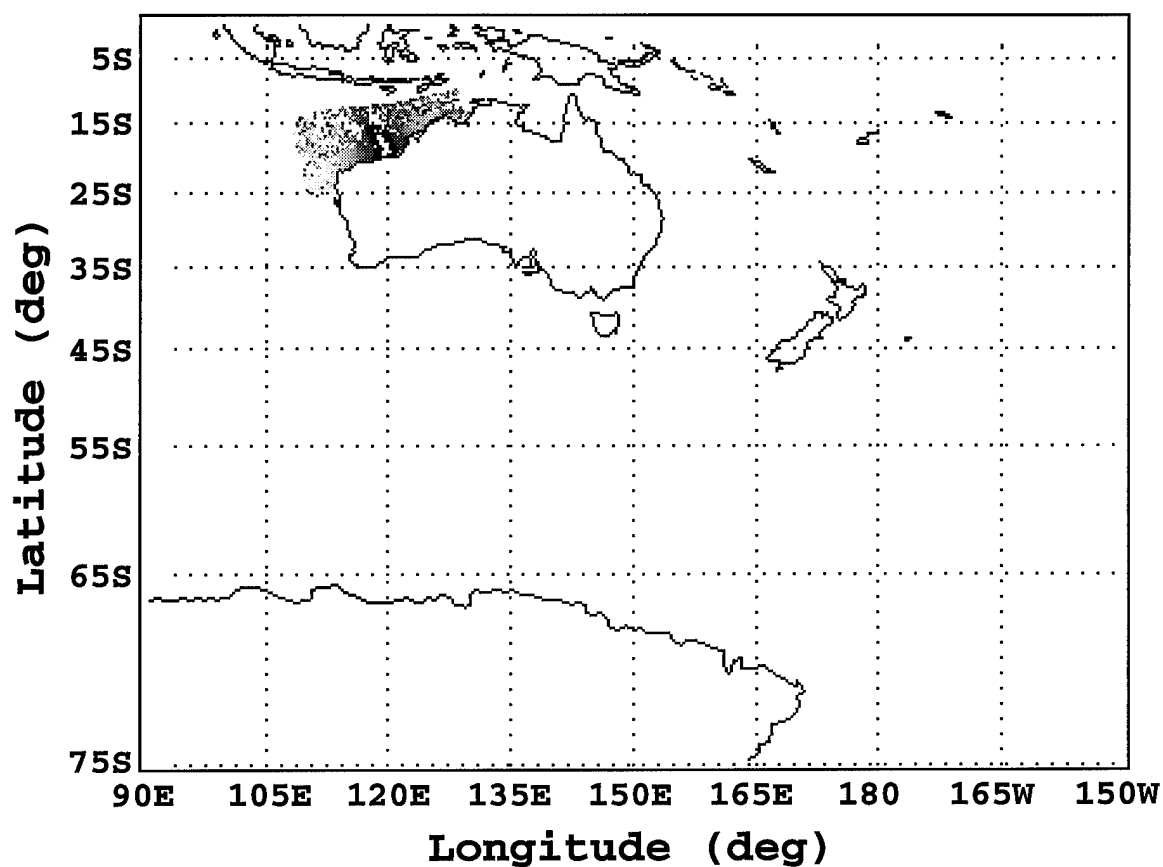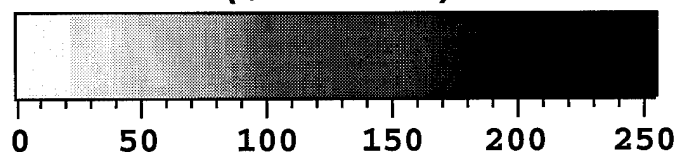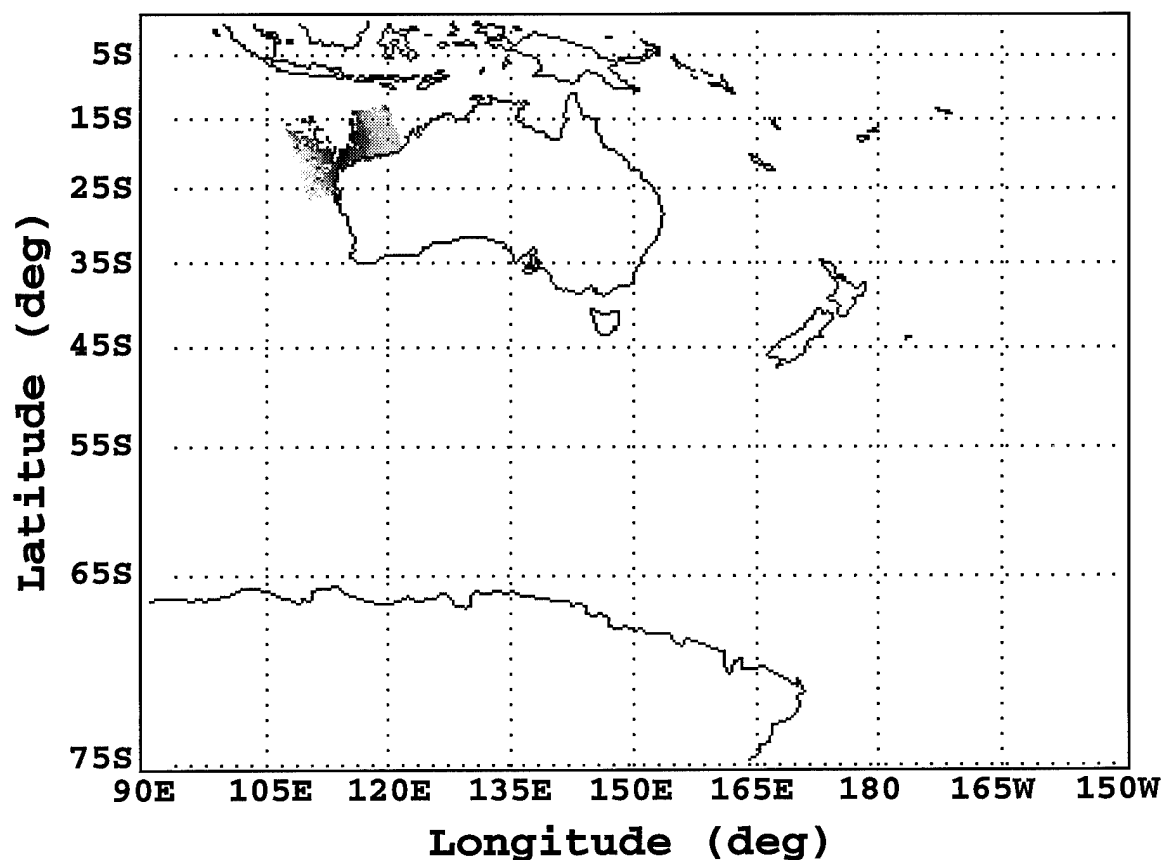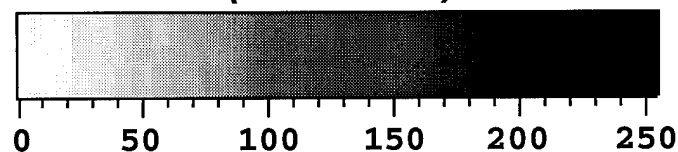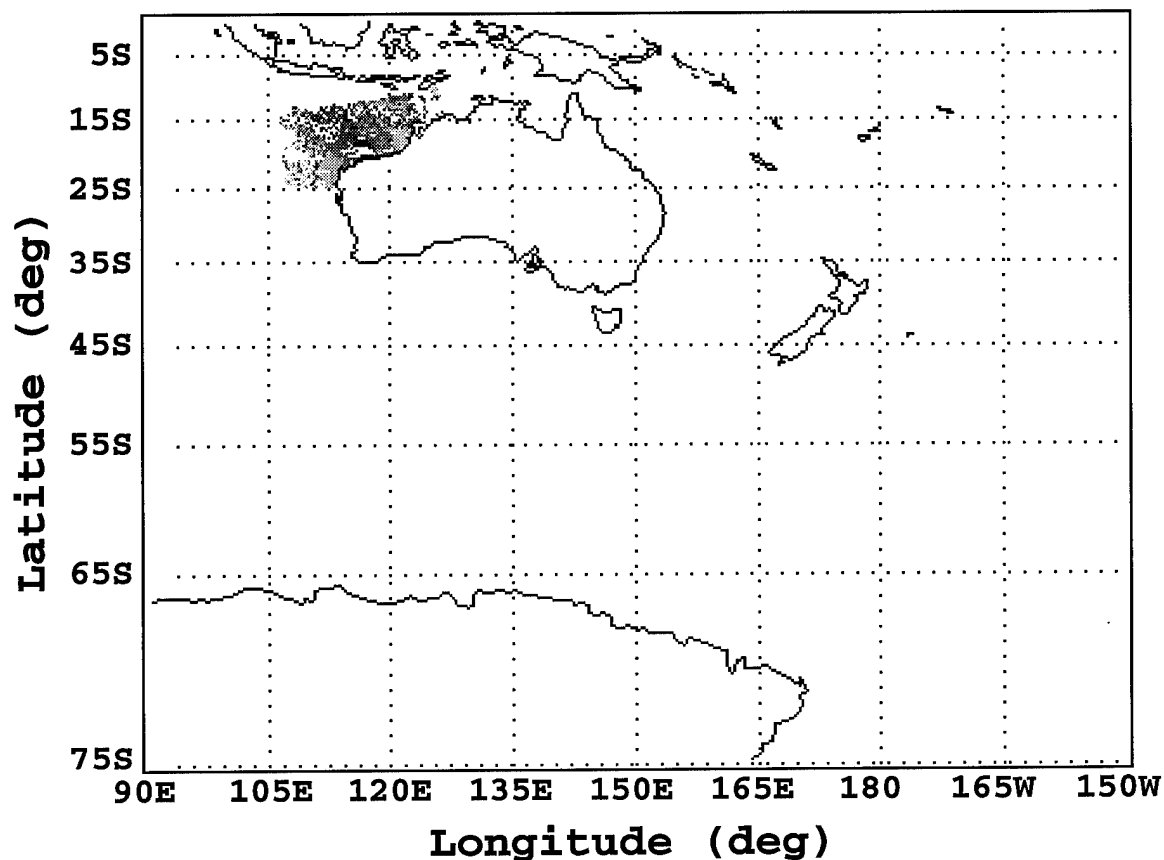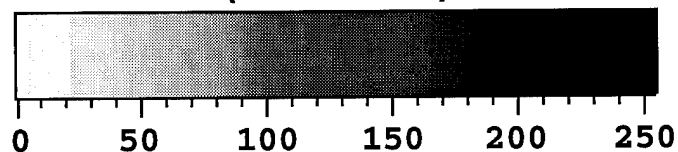## *Corrected 670nm Radiance*
(unitless)

Figure 45.   Aerosol composite for November 23, 1979.
The composite is a sum of two scans at 04:11 and
04:13 GMT.   The values represent the relative aerosol
distribution.

Healy (1971)) reported on the fallout of dust over New Zealand between 6-9 October, 1928. Because the composition of the dust was unlike anything indigenous to New Zealand, it was suggested that the dust originated in Australia and was transported across the Tasman Sea. Additional evidence for this is the mineral-rich marine sediments in the Tasman Sea (Glasby, 1971; Glasby, 1991). It was hypothesized that these sediments were the result of aeolian dust transport resulting from episodic dust storms in Australia.

According to Pye (1987), a significant number of dust storms in Australia occur in the central-eastern regions of the continent (Figure 46). From Chapter II, while much of the dust originates from the desert regions within the interior of the continent (e.g. Alice Springs), the regions in southeastern Australia which are cultivated and used for grazing are also potential dust sources. In addition, while the migrating anticyclones track across central and southern Australia year round, the summer months in southern Australia are relatively dry (Table 1). Depending on the proximity of these anticyclones with respect to the continent, they may transport warm dry air from the center of the continent to the coasts. For example, when an anticyclone sets up over the east coast of Australia, the counterclockwise circulation in the northwest quadrant of the system advects air across the continent's interior before it is carried east of Australia, over the Tasman Sea. Because the southern regions of these anticyclones are commonly associated with gusty winds, the conditions would be conducive to the onset of a dust event.

Although Figure 8 shows reasonable data coverage over the northwest quadrant of the TSR, the 1979 aerosol composite (Figure 7) does not show significantly elevated average radiance over the same region. On the other hand, there is evidence of such a signal over the TSR in the 1979 summer season (Figure 10) when climatic conditions support the occurrence of dust events. Furthermore, because the belt of anticyclones is located further south in the summer months, fewer inter-anticyclonic fronts reach the TSR. As a result, the cloud coverage would be expected to decrease during the summer season (Figure 28). This is significant in that it suggests the potential for errors
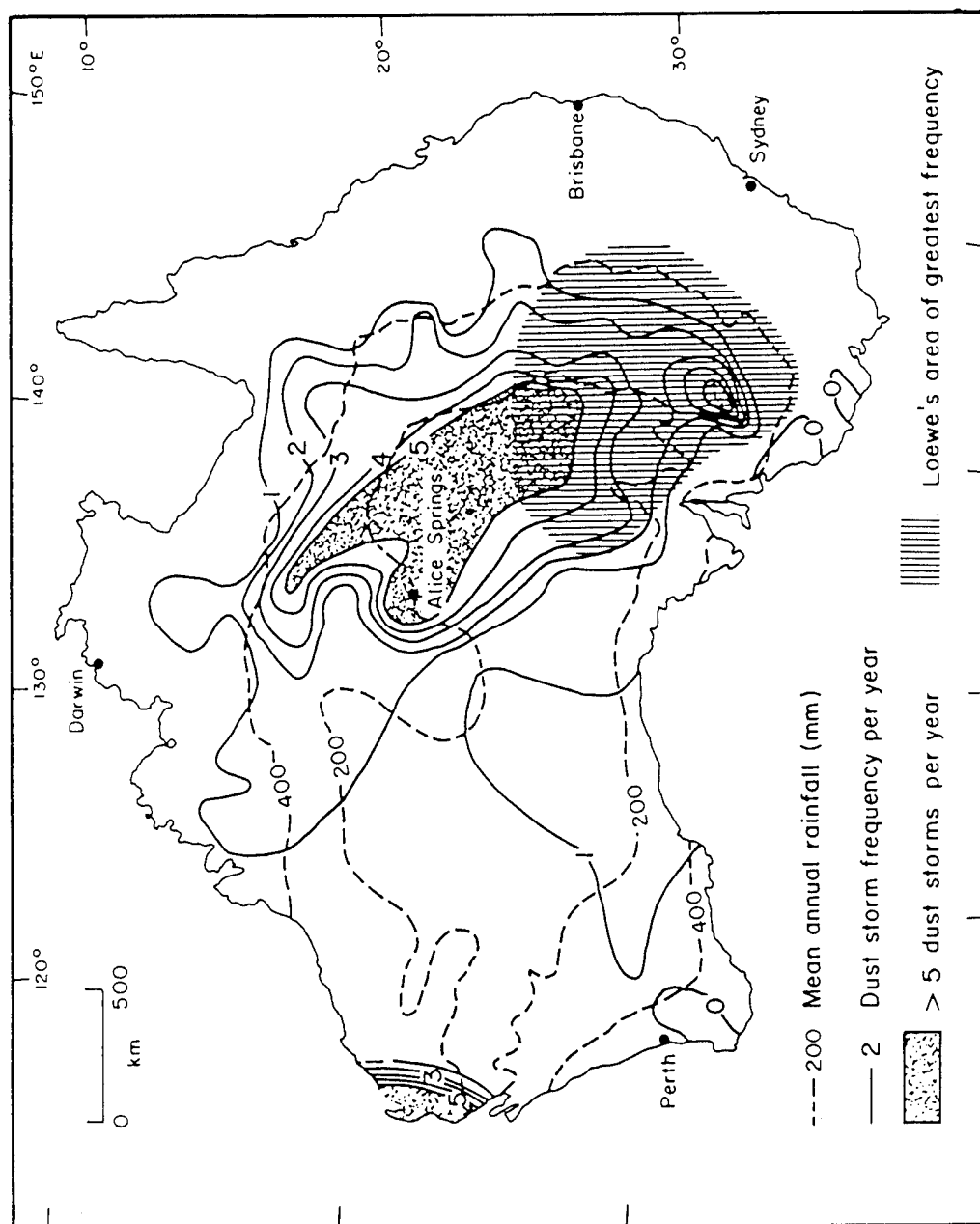
Figure 46. Average numbers of dust-storm days per year in Australia, 1957-1982, also showing the high area of incidence according to Loewe (1943), and 200 mm and 400 mm annual isohyets. (From Pye, 1987.)

in the CZCS algorithm over cloudy regions would be reduced. Unfortunately, Figure 11 indicates the data coverage was less than ideal for the same period ($\leq$ 5 samples per pixel). While the radiance signal over the TSR does not verify the existence of increased dust aerosol, it is consistent with the existing empirical evidence and the seasonal atmospheric transport pattern.

CHAPTER VIII

SUMMARY AND CONCLUSION

The Coastal Zone Color Scanner (CZCS) was a multichannel spectrometer which was operational from November 1978 to June 1986 (Feldman *et al.*, 1989). Experimental in nature, the mission of the CZCS was to test the feasibility of mapping the phytoplankton productivity of the world's oceans with a space-borne ocean color sensor. In theory, the CZCS passively measured radiances which were assumed to be a combination of the water-leaving radiance and the backscattered radiance from aerosols and air molecules. Because the success of the CZCS algorithm was largely dependent on its ability to determine accurate water-leaving radiances, atmospheric correction was an important step (Gordon, 1993). The atmospheric correction algorithm used the Channel 4 data (660-680nm) to account for the effects of aerosol and Rayleigh scattering. The underlying assumption in this algorithm was that the water-leaving radiance for Channel 4 was approximately zero. Gordon *et al.* (1983a) have shown that the atmospheric correction for the CZCS data set was 90% accurate over the Middle Atlantic Bight. Furthermore, because the effects of Rayleigh scattering can be determined *a priori*, the Channel 4 data is considered to be an effective tool for large scale aerosol analysis (Gordon and Castaño, 1989).

The primary goal of this research was to use the CZCS data base to study aerosol distributions in the Australasian region. This was achieved by compositing monthly, seasonal, and annual images of the Channel 4 data. Of the seven and a half year data set, only the first fourteen months (November 1978 - December 1979) were analyzed. There were essentially two reasons for this. First, data coverage was most extensive in the first year of the CZCS's operation. Second, due to a systematic drift error in the sensor, the statistical certainty of the calibration of the instrument decreased as the sensor aged (Simpson, 1993).

Due to a relative lack of continental and anthropogenic sources, the average aerosol concentrations in the SH are thought to be significantly less than those in the NH.

However, because much of central Australia is desert, it is thought to be the primary source of continental aerosols within the study region. In addition, due to the location of the source regions and the dominant wind patterns over the continent, it has been suggested there are two major transport pathways for dust aerosols generated by Australian dust storm activity: (1) off the northwest coast over the Indian Ocean and (2) off the east coast over the Tasman Sea (Healy, 1970; Glasby, 1971; Pye, 1987; Glasby, 1991). Because dust events are governed by climatic factors, chiefly wind conditions and precipitation patterns, the aerosol signatures which result would be expected to have seasonal fluctuations.

The 1979 670nm composite shows the Channel 4 radiance values in the study region were relatively low with the exception of the equatorial region (Figure 7). Unfortunately, largely due to its experimental nature, the CZCS data set did not provide continuous global coverage. In fact, as the 1979 data density shows, the coverage within the study region was spatially incomplete and temporally inconsistent (Figure 8). Thus, the utility of the 1979 aerosol climatology for large scale analysis is significantly diminished. On the other hand, Figure 8 also indicates there were areas, specifically off the coasts of Australia, with relatively good coverage.

The most striking feature in the 1979 670nm composite is the 'red band' of enhanced radiances in the equatorial region. There are two potential aerosol sources in the 'red band' region. Evidence indicates that increased aerosol concentrations may occur in dense forest regions due to biogenic hydrocarbon production (Heicklen, 1976; Pandis et al., 1991; National Research Council, 1993). Because many of the land masses in the equatorial 'red band' are covered with tropical forests, it seems reasonable to conclude hydrocarbon aerosols may contribute to the elevated radiances. In addition, there is a widespread practice of biomass burning in Australia and New Guinea. Crutzen and Andrea (1990) and Dignon and Penner (1991) state the material byproducts of these burns can significantly increase regional aerosol concentrations. From this, it also seems reasonable to conclude the elevated radiances in the center of the 'red band' may be, in part, attributed to biomass burning.

In contrast, it has been suggested that radiance values in the 670nm channel are not necessarily the result of increased aerosol concentrations but are instead, the artifact of a faulty algorithm (Gordon, 1993; Simpson, 1993). Within the 'red band', there are two potential sources for such error. There is evidence that CZCS images over Case 2 water may exhibit erroneously high radiance values due to a violation of the near-zero water-leaving radiance assumption (Gordon, 1993; Simpson, 1993). Because the ocean floor between Australia and New Guinea is a continental shelf with rather shallow depths and the island river systems produce significant amounts of suspended material, this region would most likely be categorized as Case 2 water. Simpson (1993) also discussed the difficulties encountered by the CZCS over cloudy regions. Elevated radiances often occur around the perimeters of masked clouds. This effect is thought to be due to undetected cloud pixels and/or electronic overshoot of the sensor. Because the equatorial region often has persistent cloud coverage, there is concern that the elevated radiances in the 'red band' are due to clouds and not aerosols. In addition, there is evidence that sun glint may contribute to elevated radiances near the center of CZCS images over equatorial regions (Hooker *et al.*, 1993).

A second area of interest was identified over the Indian Ocean Region (IOR). Pye (1987) states that a dust source and transport mechanism exists in northwest Australia which would support the occurrence of dust events within the IOR. Furthermore, the climatology for northwest Australia indicates dust storm activity may be prevalent in the spring months. Elevated radiances are evident in this region in the 1979 spring composite (Figure 16).

However, because the signal increases with distance from the Australian coast, it would seem that this contradicts the expectation that the intensity of a dust cloud fades with increased distance from its source. There are two possible scenarios which could account for these observations. Both assume a dust cloud was generated in northwest Australia and then advected over the IOR. In Scenario 1, the lower radiance values in the coastal regions result from dissipation of the dust source, i.e. the dust storm gradually terminates. In other words, if the dust cloud were created, isolated from its

source, and then advected over the IOR before settling could significantly alter the dust concentrations, it is conceivable such a signal may exist. Scenario 2 suggests light rainfall over the coastal region of the IOR removed some of the suspended dust particles, thereby, reducing the radiance signal. To a large extent, the 1979 spring signal over the IOR occurred in November which marks the onset of the monsoon season lending some credibility to Scenario 2.

However, details of the 1979 spring composite and the daily spring images suggest the high radiances may be due to clouds and sun glint, not aerosols. Firstly, there is an apparent inverse relationship in the 1979 spring aerosol composite between radiance counts and data density values which cannot be easily explained. Secondly, the daily spring images do not seem to support the occurrence of isolated dust events. In summary, while the climatic conditions and the 1979 spring aerosol composite suggest elevated dust concentrations might exist over the IOR, closer examination of the daily images seems to suggest the elevated radiances are closely related to the presence of clouds and sun glint with the latter being the more significant source.

The Tasman Sea Region (TSR) was identified as the final area of interest. There is empirical evidence suggesting aeolian dust transport originating in Australia is advected over the Tasman Sea (Healy, 1970; Glasby, 1971; Glasby, 1991). The climatology of southeast Australia suggests dust events are most likely to occur during the Austral summer. While an elevated radiance signal did not exist over the TSR in the fall, winter, and spring months, the 1979 summer composite indicates relatively high radiance values did occur (Figure 18). Furthermore, because the cloud cover is expected to be less extensive over the TSR in the summer months, the potential problems with cloud-masking and electronic overshoot are reduced. In addition, due to the TSR being relatively distant from the equator, the errors associated with sun glint would be reduced. Unfortunately, Figure 19 reveals the data density during the summer months is less than ideal.

Due to the inconsistency of the CZCS data set, ambiguities in aerosol analysis derived from it were inevitable. In the three regions of focus presented in this research,

there was climatological evidence which supported the apparent aerosol signals. In all cases, there was insufficient information to unequivocally resolve these uncertainties. However, in some instances, the 1979 CZCS aerosol climatology provided further support to existing theories concerning general aerosol sources and distributions. In particular, the results of this research are in agreement with the established theory of aeolian dust transport from Australia over the Tasman Sea. Because this theory is largely founded on empirical evidence, the corroborative nature of the CZCS data set is encouraging.

Since aerosols are important players in the earth's global radiation budget, the effectiveness of global climate models is partly dependent on the ability to accurately quantify and characterize global aerosol distributions. The secondary goal of this research was to further evaluate the feasibility of conducting large scale aerosol analysis with space-borne ocean color sensors. Again, because of the sporadic nature of the CZCS data coverage, the ability to perform large scale analysis was diminished. However, the results of this research do provide further evidence which seems to be in agreement with expected aerosol distributions in the Australasian region. On the other hand, it also raises some questions about the reliability of the CZCS atmospheric correction algorithm in cloudy and equatorial regions. Therefore, while this study supports the continued use of space-borne ocean color radiometers as a viable scientific option for gathering a global aerosol climatology, it also suggests there may be reason to further investigate the effectiveness of the CZCS cloud-masking algorithm.

REFERENCES

Abbott, M. R., and D. B. Chelton, 1991: Advances in passive remote sensing of the oceans. U.S. National Report to International Union of Geodesy and Geophysics 1987-1990, *Contributions in Oceanography. Am. Geophys. Union*, 571-589.

André, J. M., and A. Morel, 1989: Simulated effects of barometric pressure and ozone content upon the estimate of marine phytoplankton from space. *J. Geophys. Res.*, **94**, 1029.

Andreae, M. O., 1991: Biomass burning: its history, use, and distribution and its impact on environmental quality and global climate. *Global Biomass Burning*, J. S. Levine, Ed., MIT Press, 3-21.

Carder, K. L., W. W. Gregg, D. K. Costello, K. Haddad, and J. M. Prospero, 1991: Determination of Saharan dust radiance and chlorophyll from CZCS imagery. *J. Geophys. Res.*, **96**, 5369-5378.

Charlson, R. J., and M. J. Pilat, 1969: Climate: the influence of aerosols. *J. Appl. Met.*, **8**, 1001.

--------, S. E. Schwartz, J. M. Hales, R. D. Cess, J. A. Coakley, Jr., J. E. Hansen, and D. J. Hofmann, 1992: Climate forcing by anthropogenic aerosols. *Science*, **256**, 423-455.

Crutzen P. J., and M. O. Andreae, 1990: Biomass burning in the tropics: impact on atmospheric chemistry and biogeochemical cycles. *Science*, **250**, 1669-1678.

Deschamps, P. Y., M. Herman, and D. Tanre, 1983: Modeling of the atmospheric effects and its application to the remote sensing of ocean color. *Appl. Opt.*, 22, 3751-3756.

Dignon, J., and J. E. Penner, 1991: Biomass burning: a source of nitrogen oxides in the atmosphere. *Global Biomass Burning*, J. S. Levine, Ed., MIT Press, 370-375.

Durkee, P. A., D. R. Jensen, E. E. Hindman, and T. H. Vonder Haar, 1986: The relationship between marine aerosols and satellite detected radiance. *J. Geophys. Res.*, **91**, 4063-4072.

--------, F. Pfeil, E. Frost, and R. Shema, 1991: Global analysis of aerosol particle characteristics. *Atmos. Environ.*, **25A**, 2457-2471.

Feldman, G., N. Kurwing, C. Ng, W. Esaias, C. McClain, J. Elrod, N. Maynard, D. Endres, R. Evans, J. Brown, S. Walsh, M. Carle, and G. Podesta, 1989: Ocean color: availability of the global data set. *EOS*, **70**, 634-641.

Gentilli, J., W. J. Maunder, and U. Radok, 1971: *World Survey of Climatology for Volume 13, Climates of Australia and New Zealand*, J. Gentilli, Ed., Elsevier Publishing Company, 53-115.

Glasby, G. P., 1971: The influence of aeolian transport of dust particles on marine sedimentation in the South-west Pacific. *J. Royal Society of New Zealand*, **1**, 285-300.

--------, 1991: Mineralogy, geochemistry, and origin of Pacific red clays: a review. *New Zealand J. Geol. and Geophys.*, **34**, 167-176.

Gordon, H. R., D. K. Clark, J. W. Brown, O. B. Brown, R. H. Evans, and W. W. Broenkow, 1983a: Phytoplankton pigment concentrations in the Middle Atlantic Bight: comparison between ship determinations and Coastal Zone Color Scanner estimates. *Appl. Opt.*, **22**, 20-36.

--------, J. W. Brown, O. B. Brown, R. H. Evans, and D. K. Clark, 1983b: Nimbus 7 CZCS: reduction of its radiometric sensitivity with time. *Appl. Opt.*, **22**, 3929-3931.

--------, and D. J. Castaño, 1987: Coastal Zone Color Scanner atmospheric correction algorithm: multiple scattering effects. *Appl. Opt.*, **26**, 2111-2122.

--------, and D. J. Castaño, 1989: Aerosol analysis with the Coastal Zone Color Scanner: a simple method for including multiple scattering effects. *Appl. Opt.*, **28**, 1320-1326.

--------, 1993: Radiative transfer in the atmosphere for correction of ocean color remote sensors. *Ocean Colour: Theory and Applications in a Decade of CZCS Experience*, V. Barale and P. M. Schlittenhardt, Eds., Kluwer Academic Publishers, 33-37.

Griggs, M., 1975: Measurement of the atmospheric aerosol optical thickness over water using ERTS-1 data. *J. Air Pollut. Control Ass.*, **25**, 622-626.

Hansen, J. E., and A. A. Lacis, 1990: Sun and dust versus greenhouse gases: an assessment of their relative roles in global climate change. *Nature*, **346**, 713-719.

Healy, T. R., 1970: Dust from Australia - a reappraisal. *Earth Sci. J.*, **4**, 106-116.

Heicklen, J., 1976: *Atmospheric Chemistry*, Academic Press, 406 pp.

Hooker, S. B., C. R. McClain, and A. Holmes, 1993: Ocean color imaging: CZCS to SeaWiFS. *Marine. Tech. Soc. J.*, **27**, 3-15.

Houghton, H. G., 1985: *Physical Meteorology,* MIT Press, 442pp.

Milliman, J.D., and R. Meade, 1983: World-wide deliver of river sediment to the oceans. *J. Geol.*, **91**, 1-21.

Mueller, J. L., 1988: Nimbus-7 CZCS: electronic overshoot due to cloud reflectance. *Appl. Opt.*, **27**, 438-440.

National Research Council, 1993: *Protecting Visibility in National Parks and Wilderness Areas,* L. R. Paulson, Ed., National Academy Press, 446 pp.

Pandis, S. N., S. E. Paulson, J. H. Seinfeld, and R. C. Flagan, 1991: Aerosol formation in the photooxidation of isopropene and beta-pinene. *Atmos. Environ.*, **25**, 997-1008.

Patterson, E. M., C. S. Kiang, A. C. Delany, A. F. Wartburg, A. C. Leslie, and B. J. Huebert, 1980: Global measurements of aerosols in remote continental and marine regions: concentrations, size distributions, and optical properties. *J. Geophys. Res.*, **85**, 7361-7376.

Penner, J. E., R. E. Dickinson, and C. A. O'Neill, 1992: Effects of aerosol from biomass burning on the global radiation budget. *Science*, **256**, 1432-1433.

--------, R. J. Charlson, J. M. Hales, N. S. Laulainen, R. Leifer, T. Novakov, J. Ogren, L. F. Radke, S. E. Schwartz, and L. Travis, 1994: Quantifying and minimizing uncertainty of climate forcing by anthropogenic aerosols. *Bull. Amer. Metr. Soc.*, **75**, 375-400.

Pye, K., 1987: *Aeolian Dust and Dust Deposits*, Academic Press, 334 pp.

Richards, J. A., 1986: *Remote Sensing Digital Image Analysis: An Introduction,* J. A. Richards, Ed., Springer-Verlag, 281 pp.

Rogers, R. R. and M. K. Yau, 1983: *A Short Course in Cloud Physics,* Pergamon Press, 323 pp.

Simpson, J. J., 1993: The coastal zone color scanner (CZCS) algorithm: a critical review of residual problems. *Ocean Colour: Theory and Applications in a Decade of CZCS Experience,* V. Barale and P. M. Schlittenhardt, Eds., Kluwer Academic Publishers, 117-166.

Staylor, W. F., 1990: Degradation rates of the AVHRR visible channel for the NOAA 6, 7, and 9 spacecraft. *J. Atmos. Ocean Tech.,* **7,** 411-423.

Taylor J. A., and P. R. Zimmerman, 1991: Modeling trace gas emissions from biomass burning. *Global Biomass Burning,* J. S. Levine, Ed., MIT Press, 345-350.

Taylor K. E., and J. E. Penner, 1994: Response of the climate system to atmospheric aerosols and greenhouse gases. *Nature,* **369,** 734-737.

Wallace, J. M., and P. V. Hobbs, 1977: *Atmospheric Science: An Introductory Survey,* Academic Press, 467 pp.

Warneck, P., 1988: *Chemistry of the Natural Atmosphere,* Academic Press, 554pp.

Watson, C. E., J. Fishman, G. L. Gregory, and G. W. Sachse, 1991: A comparison of wet and dry season ozone and CO over Brazil using in situ and satellite measurements. *Global Biomass Burning,* J. S. Levine, Ed., MIT Press, 115-121.

Weiss, R., R. J. Charlson, A. P. Waggoner, M. B. Baker, D. Covert, D. Thorsell, and S. Yuen, 1976: Application of directly measured aerosol radiative properties to climate models. *Radiation in the Atmosphere,* H. J. Bolle, Ed., Academic Press, 469-471.

VITA

Gregory Michael Giondomenica, son of William and Renate Giondomenica, was born May 24, 1967 in Frankfurt, Germany. In 1968, his family moved to Japan where they remained for three years. He spent the next fifteen years in the Philippines where he graduated from Wagner High School, Clark AFB in 1985. He then attended the United States Air Force Academy, Colorado Springs, Colorado from which he graduated with a B.S. in Aeronautical Engineering in 1990.

Upon graduation, Greg was commissioned a Second Lieutenant in the United States Air Force on August 3, 1990. He was then selected by the Air Force Institute of Technology (AFIT) to pursue a second undergraduate degree. After being enrolled at Texas A&M University, College Station, Texas, he received a B.S. in Meteorology in 1991. He was then assigned to Castle AFB, California where he served as a Wing Weather Officer. In 1993, he was selected by AFIT to pursue a Masters degree in meteorology.

Greg's permanent address is 3093 South King Street, Denver, Colorado 80236.